NTNU
Norwegian University of Science and Technology

Carbon Formation and Catalysis in the Conversion of Methyl Chloride and Silicon into Dimethyldichlorosilane

Collaboration with Elkem - Bluestar

Amalie Tysseland

Preface

This master's thesis was submitted to the Norwegian University of Science and Technology (NTNU) as part of the five year master's degree program Chemical Engineering and Biotechnology (Industriell kjemi og bioteknologi). The thesis work has been carried out within the Department of Chemical Engineering (IKP) between January 2018-June 2018. Professor Hilde J. Venvik has acted as the supervisor during the master's thesis while Professor Edd Blekkan has served as the co-supervisor.

Acknowledgment

The work done during this thesis has been both challenging and educational. There are several people whom have been essential to this thesis and have my deepest gratitude. First, I would like to thank my main supervisor Professor Hilde J. Venvik for guidance, knowledge and support through both the laboratory work and the writing process. Thanks to my co-supervisor Professor Edd A. Blekkan for much needed advice and support through the semester. Also, a thanks to Harry Rong and Torbjørn Røe from Elkem for support throughout this thesis.

I am eternally grateful for the support, encouragement and constant positivity from senior engineer Estelle M. Vanhaecke. Her insight and knowledge about Raman spectroscopy has been much needed throughout the process and the feedback and kind words during the writing process is something I would not have been without.

Thank you also to PhD candidate Isaac Yeboah for guidance and help with the Pyrolysis GC/MS investigation.

Lastly, I would like to thank both by friends and family for being my greatest cheerleaders and always lending a helping hand when needed. A special thanks to the lovely Silje M. Dale for help with the XRD-measurements, helpful discussions and help/feedback during the final writing process. Thanks to the brilliant Maiken Johnsgaard for constant encouragement, kind words and feedback/help during the final writing process. Frida P. Danmo also deserves a shout out for help with XRD experiments and countless lovely coffee break discussions. Lastly, a big thanks to my amazing mom and dad for feedback and advice on this thesis as well as also supporting me throughout everything I do.

Trondheim, 13. June 2018

Amalie Tysseland

Abstract

The Direct Process is the most prominent method for producing dimethyldichlorosilane, and is a copper-catalyzed reaction between solid silicon and methyl chloride gas. The process faces several complications such as the carbon formation during the synthesis, which causes both economical and efficiency problems. This thesis is part of a preliminary investigation into the carbon species which are formed in the Direct Process. Through research, starting with characterization of the contact mass (a mixture of silicon, copper and promoters), the aim is to better understand the process and gain more knowledge about the carbon formation. Reducing the carbon formation would increase the production efficiency as well as benefit the production economically.

In this thesis eight samples of reacted contact mass, as well as a reference sample of the same metallurgical silicon which is used to create the contact mass, were investigated. Raman Spectroscopy, Thermal gravimetric analysis, Scanning electron spectroscopy, X-ray diffraction, Energy-dispersive X-ray spectroscopy, Pyrolysis GC/MS and Fourier Transform Infrared Spectroscopy were used to characterize the samples of reacted contact mass and the reference sample of silicon.

Results from Raman Spectroscopy showed that much of the carbon was formed between 4 hours (sample P1) and 21.5 hours (sample P2) and that all the carbon displayed the D peak at $1300\mathrm{cm}^{-1}$ and the G peak at $1600\mathrm{cm}^{-1}$. The GC/MS indicated that a large range of organic components with long carbon chains are present within the samples. The organic content included alcohols, amides, acids, nitriles and esters. Several experiments showed oxygen within the samples. Thermal gravimetric analysis might be unsuited for the contact mass since there are indications that the silicon oxidizes during the analysis. Further work is needed to classify both the carbon species which are formed and from which reactions the carbon species stem from. An investigation with samples extracted at small intervals between 4 hours and 21.5 hours might prove especially useful.

Sammendrag

Prosessen der silisium katalyserast med kopar og metylklorid for å produsere dimetyldiklorsilan kallast «The Direct Process». «The Direct Process» er ein komplisert reaksjon med ei rekke utfordringar som til dømes korleis karbonforbindinga dannast i reaksjonen og set seg på silisium-overflata. Denne oppgåva er ein del av innleiande forsking på «The Direct Process» og karbonforbindingane som dannast. Ved karakterisering av kontaktmassen (ei blanding av silisium, kopar og ulike promotorar) med bruk av ulike metodar kan ein betre forstå prosessen og auke kunnskapen om dei ulike karbonforbindingane. Redusering av desse forbindingane vil både kunne effektivisera produksjonen av dimetyldiklorsilan og redusere kostnadane.

Som ein del av denne masteroppgåva vart åtte prøvar med reagert kontaktmasse og éin referanseprøve av metallurgisk silisium undersøkt. Undersøkingane vart utført med Ramanspektroskopi, termogravimetrisk analyse (TGA), sveipeelektronmikroskop, røntgendiffraksjon, energidispersiv spektroskopi, Pyrolyse GC/MS og Infraraud spektroskopi.

Resultata frå undersøkinga med Ramanspektroskopi viste at mykje av karbonet dannast mellom den første prøven, tatt ut av reaktoren etter fire timar, og den andre prøven, tatt ut etter 21.5 timar. Alle Ramanspektra frå prøvane med reagert kontaktmasse inneheldt D-topp (Ramanskift på 1300 cm^{-1}) og G-topp (Ramanskift på 1600 cm^{-1}). Resultata frå GC/MS eksperimentet viste at ulike organiske forbindingar var til stade i prøvane. Nesten alle dei organiske forbindingar bestod av lange karbonkjeder med funksjonelle grupper frå alkoholar, amid, nitrilar, esterar og syrer. Fleire av instrumenta påviste oksygen i alle prøvane. TGA av referanseprøven indikerte at silisiumet oksiderte under eksperimentet. Noko som vidare kan indikera at metoden ikkje er optimal for karakterisering av kontaktmassen. For å betre forstå korleis karbonet i «The Direct Process» vert danna trengs det vidare arbeid. Eit viktig punkt er å teste fleire prøvar med kontaktmasse innanfor tidsintervallet mellom fire og 21.5 timar med reaksjon, sidan det verkar som hovudvekta av karbonet oppstår i dette intervallet.

List of Tables

List of Figures

Contents

1. Introduction

Since 1940 the silicone industry has revolutionized the way we live our lives[1]. Silicone based materials have now become a necessity in both our every day life and in industries such as: in the production of medicine, lubricants, insulation and many other important products. Thus, the demand for silicones keeps growing each year. This is mostly due to their heat resisting nature and rubber-like texture. The silicone material industry is today a multi-billion global industry, due to the high demand for silicone based products and the good economic benefits of producing both silicone products and their precursors.

Every year, companies world wide use large amount of resources on research in order to optimize and/or create new methods of synthesizing silicones[2]. However, there are many processes involving silicones which can and should be improved upon. The synthesis of methylchlorosilanes, a high demand silicone precursor, from methyl chloride gas and silicon is one such process[3]. The synthesis of methylchlorosilanes is often refereed to as the Direct Process or even Müller-Rochow synthesis, after it's inventors, Dr. Eugene G. Rochow and Dr. Richard Müller[4]. The process was discovered more than 70 years ago and has since its discovery been utilized worldwide. The process is still discussed and researched today, due to its complicated and unclear reaction mechanism, and a wide range of factors which in therm influence both the effectiveness and economics of the synthesis[4].

The Direct Process is the most prominent method for producing organosilicones, and is a copper-catalyzed reaction between solid silicon and methyl chloride gas[4]. Since its discovery in the early 1940s, the synthesis has been vital for the silicone industry and is today the preferred industrial method for producing methylchlorosilanes. Many studies have tried to identify the reaction mechanism and every year a great deal of work is put into trying to isolate at which conditions dimethyldichlorosilane yields are the highest. There are

several other products which can be produced by The Direct Process, but dimethyldichlorosilane is the product most often desired. The process faces several complications such as the carbon formation during the synthesis, which causes both economical and efficiency problems [5–7].

It should also be noted that early studies into the process was plagued with problems due to unknown impurities in both the silicon and copper, which in turn could have had a grave impact on the general properties of the contact mass. This has most likely colored our understanding of the synthesis and might be one of the main reasons why the synthesis is still not fully understood [8].

1.1   Motivation

In this master's thesis the direct process of dimethyldichlorosilane has been studied through several different characterization techniques. This thesis is part of a preliminary investigation into the carbon species which are formed in the Direct Process. Through research, starting with characterization of the contact mass (a mixture of silicon, copper and promoters), the aim was to better understand the process and gain more knowledge about the carbon formation. Reducing the carbon formation would not only increase the efficiency of the production, but also benefit the production economically.

For this investigation eight samples of reacted contact mass, as well as a reference sample of the same metallurgical silicon which is used to create the contact mass, were investigated. The contact mass was investigated with Raman spectroscopy, Pyrolysis-GC/MS, TGA, XRF, FT-IR, S(T)EM, EDX and XRD.

The master's thesis work is a collaboration with Elkem-Bluestar and all samples were provided by Elkem Silicone Materials in Trondheim.

2. Theory

2.1 The Direct Process

The Direct Process is, as stated earlier, the copper-catalyzed reaction of silicon with organic chlorides by which organochlorosilanes are formed. The main interests for the process is the productions of methylchlorosilanes from chloromethane and then especially the production of dimethyldichlorosilane. Dimethyldichlorosilanes are as of today the product with largest commercial applications. The general reaction of silicon with organic chlorides over copper is given in Equation 2.1

$$2\,RCl\,(g) + Si\,(s) \xrightarrow{\ Cu\ } (R)_x SiCl_{4-x}(g) \tag{2.1}$$

where x=1-4 and R=CH_3,C_2H_5 or C_6H_5[4].

The main low-boiling products and their boiling points from the reaction between methyl chloride and silicon are given in Table 2.1. Yields of upwards of 90 % of the wanted product is not uncommon, but there are also usually several by-products that can be isolated during the reaction. Hydrocarbons and hydrogen are both possible by-products alongside the low-boiling products shown in Table 2.1. Previous studies have found as much as 24 different hydrocarbon by-products for the synthesis[9].

Table 2.1: The main low-boiling products from the reaction between methyl chloride and silicone.

Compound	Formula	Boiling point [°C]
Tetramethylsilane	$Si(CH_3)_4$	26.5
Trimethylchlorosilane	$Si(CH_3)_3Cl$	57.9
Dimethyldichlorosilane	$Si(CH_3)_2Cl_2$	70.3
Methyltrichlorosilane	$Si(CH_3)Cl_3$	66.4
Methyldichlorosilane	$Si(CH_3)HCl_2$	40.7
Dimethylchlorosilane	$Si(CH_3)_2HCl$	34.7
Trichlorosilane	$SiHCl_3$	31.8
Tetrachlorosilane	$SiCl_4$	57.6

A number of unwanted high-boiling silanes, polysilanes and siloxanes are sometimes formed in the reaction alongside the low-boiling by-products. The large amount of possible by-product mean that the synthesis can be unpredictable and hard to reproduce with the same exact products each time. The reaction rate as well as the nature of the products depend on a large number of different factors, including the nature and purity of the starting materials (silicon, promoters and copper), the preparation of the contact mixture, the temperature within the reactor, the pressure within the reactor, which type of reactor is used, and the degree of conversion for the silicon and organic chloride. The varying factor and the large amount of products yielded during the synthesis means that the Direct Process is a complicated and sometimes unpredictable synthesis. It should be mentioned that the reaction mechanism is still not truly understood especially when it comes to what the active species and sites within the reaction is. The reaction mechanism is further discussed in the next section [10].

2.1.1   Reaction Mechanism

The reaction mechanism for formation of methylchlorosilanes by the Direct Process is still an area of ongoing research, and even though the process has been studied for several decades, the level of knowledge regarding the mechanism is unsatisfactory[4].

In this section, only the reactions of methyl chloride with silicon over the copper catalyst will be discussed since this is the most economical relevant reaction and also the reaction which has the most reliable scientific data[11].

The first mechanism for the reaction was proposed by E.G Rochow and D.T. Hurd in 1945[12]. They proposed that the copper catalyst cleaves the methyl chloride and then forms methyl copper and copper(I)chloride. The methyl groups could then react with the silicon and the copper(I)chloride would be reduced by the elemental silicon in a highly exothermic reaction which in turn yields Si–Cl and Cu. The full mechanism proposed by Rochow and Hurd is given in Equations 2.2 - 2.6.

$$2\,Cu + CH_3Cl \xrightarrow{\text{ca} \cdot 250\,°C} CuCl + CuCH_3 \qquad (2.2)$$

$$Si + CuCl \longrightarrow Cu + (Si-Cl)\ \text{active intermediate} \qquad (2.3)$$

$$(Si-Cl) + CH_3 \longrightarrow (CH_3SiCl) \qquad (2.4)$$

$$\text{or possibly } (Si-Cl) + CuCH_3 \longrightarrow (CH_3SiCl) + Cu \qquad (2.5)$$

$$\text{or } (Si-Cl) + CuCl \longrightarrow (SiCl_2) + Cu \qquad (2.6)$$
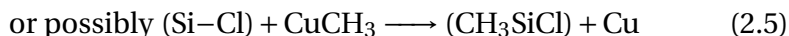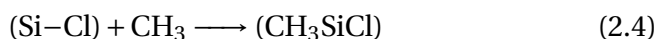
The surface compound, CH_3SiCl, can then be further methylated by the chlorinated intermediate, which remains on the surface, until all four silicon valences are satisfied and the compound is desorbed for the surface[8].

However, this mechanism does not explain why the synthesis of dimethyldichlorosilane is still possible at low temperature well below the needed temperature for Equation 2.2. The mechanism has also been criticized due to the lack of explanation for the favorization of dimethyldichlorosilane production during the reaction. The observed production of tetramethylsilane further contradict the mechanism proposed by Rochow and Hurd. These, and many more contradictions

were presented by Voorhoeve and several others in the early studies of the Direct Process[11].

Approximately ten years after Hurd and Rochow proposed their mechanism a new hypothesis for the mechanism in the Direct Process was proposed. The hypothesis proposed that the Direct Process should be treated as a heterogeneous catalytic process in which chemisorption of the organic halide on the surface of the contact mass is an important step. The suggestion was that an intermetallic compound, which was present in the silicon-copper mixture, was a key feature in the production of dimethyldichlorosilane. This was proposed by several studies including studies done by V. Bažant in 1966[6]. He proposed that the first step was a dissosative adsorption in which the methyl group becomes attached to the copper and chlorine, while chlorine attaches itself to the silicon as shown in Equation 2.7.

$$Si-Cu + CH_3Cl \longrightarrow \begin{array}{c} Cl\,\text{---}\,CH_3 \\ \vdots \qquad \vdots \\ Si\,\text{-----}\,Cu \end{array} \qquad (2.7)$$
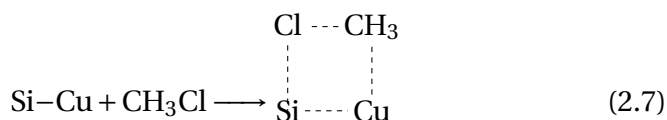
The positively charged methyl group then migrates to the silicon. The mechanism which Klebanskii and Fiktengol[13,14] proposed is similar to Bažant's. They also based their mechanism on the organic halide undergoing dissociative chemisorption, but the mechanism is governed by the polarity of the adsorbent and the adsorbate. The organic halide is polarized to $R^{\delta+}$ - $X^{\delta-}$ by it dipole moment and the substrate is polarized to $Cu^{\delta+}$ - $Si^{\delta-}$ by the ionic forces of the intermetallic Cu-Si lattice. The adsorption then takes place as shown in Equation 2.8.

$$Cu^{\delta+} - Si^{\delta-} + R^{\delta+} - X^{\delta-} \longrightarrow \begin{array}{c} X\,\text{-----}\,R \\ \vdots \qquad \vdots \\ Cu\,\text{-----}\,Si \end{array} \qquad (2.8)$$
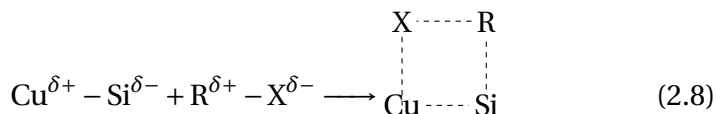
The importance of chemisorption on the Si-Cu interface is supported by the experimental observation that copper must be present as a Si-Cu alloy for the selective formation of diorganodihalosilane[11].

2.1.2 Copper and the Active Phase

Several different conflicting hypotheses about the active center of the Direct Process exist in the literature today. It is believed that the catalytic activity of copper stems from its ability to form binary intermetallic compounds. This means that the metallic copper itself is not an active catalyst in the Direct Process as one first might think. Voorhoeve[10] have discussed the significance of the Cu_3Si intermetallic compound and also shown that the compound was present in all reaction mixture which produced methylchlorosilanes. Falconer[15] proposed that Cu_3Si itself was not active, but would become active as chlorine attached itself to the silicon on the surface. Lieske[16] showed that Cu_3Si had a minor role as a catalytic active species. However he found that it could play a role as a precursor for the formation of the active Cu-Si surface species.

The copper undergoes complete metamorphosis and transport reaction by solid diffusion and is therefore not viewed as a catalyst in the classical sense. The copper used in the Direct Process is actually often viewed as a catalyst precursor since it seems to necessary to produce the actual active phase[4]. Veer[17] found in a study that copper was the diffusing element when starting from Cu-Si diffusion couples. Due to the way copper easily diffuses in silicon, verses the way silicon diffuses in copper, points to the fact that copper diffuses through silicon to from the Cu_3Si^3 phase. Frank *et al.*[18] found when investigating the composition of silicon and the Cu_3Si that Si-Cl bonds were present in the contact mass after the reaction is started. This made them conclude that the active sites are those where silicon is bound to chlorine.

2.1.3 Contact Mass

The contact mass and its preparation has, as mentioned earlier, a high impact on the reaction. The contact mass can be prepared in several ways, where the easiest preparation is to mix silicon powder, the copper powder, and the promoters. Other method include introducing copper in the form of copper(I)chloride, as copper oxide or as an Cu_3Si alloy. The contact mass is then reacted with chloromethane.

However, the formation of methylchlorosilanes does not happen right away. There is a induction period before methylchlorosilanes are produces. The induction period can vary in length, but it has been observed that methane, hydrogen and carbon (deposited on the surface) is produced in this period. These products are believed to be the result of cracking of methyl chloride on the free copper[11]. After the induction period the starting period occurs where the methylchlorosilane formation starts with low selectivity, based on dimethyldichlorosilane[4].

2.1.4 Promoters

Through the years many types of promoters have been tested for the Direct Process in hopes of better controlling the selectivity and reaction rate. However, it has been found that only aluminium, zinc, phosphorus, and to some degree tin, are of importance as additives to the process. Aluminium is always present as a promoter when technical grade silicon is used and has been shown to lead to a higher production rate when resent in the right form and right amount[8]. Zinc has been found to be one of the most suitable promoters and is today almost always used. However, if the zinc concentration in the contact mass is too high, sticky phases can occur in the reactor which in turn increases the cracking reaction of chloromethane and thereby reduces the reactivity and selectivity[19] of the process. Tin has also to some extent been used as a promoter usually in combination with metallic copper. Tin is believed to further enhance diffusion between silicon and active Cu-Si sites, but acts as a poison if used at too high concentrations[19]. In later years phosphorus has been introduced to the catalytic system either by selecting raw materials which contain phosphorus, adding it to the contact mass, or by adding it to the chloromethane feed. The addition has lead to improved selectivity, reduction of coke formation and reduction of high boiling fractions[20].

2.2   Carbon Formation

Catalytic deactivation is a known problem in most industrial catalytic processes. The loss of catalytic activity and selectivity can lead to great hurdles and large expenses for any industrial process and unfortunately the Direct Process is no exception[21].

It is impossible to completely stop catalyst decay, but by classifying the deactivation and investigating the mechanisms behind the deactivation, one hopes to avoid, and or postpone the most drastic consequences of deactivation and thereby enhance the life time of the catalyst[21].

While the mechanisms of catalyst deactivation may be complicated, and often differ from process, to process and catalyst to catalyst, a classification system where the deactivation's are grouped into six different mechanisms are often used. The categories are: poisoning, fouling, thermal degradation, vapor formation, vapor-solid/solid-solid reactions and attrition/crushing. The following section will focus on the underlying theory behind fouling, coking and carbon deposition and dive further into the specific deactivation of the copper catalyst used in the Direct Process[21].

Deactivation due to coke formation on the surface of the catalyst is one of the most common causes of catalyst deactivation. For any catalytic reaction with carbon containing molecules in oxygen depleted atmospheres, there is a possibility for coke formation, especially if the process is carried out at reasonably high temperatures[22]. The formation of carbonaceous residues happens due to side reactions on the catalytic surface. The carbonaceous residue is usually refereed to as either carbon or coke. However, the definition of carbon and coke can be hard to distinguish as they are often somewhat arbitrary and by convention related to their origin. Carbon is often labeled as the product when CO is disproportional high in a reaction while coke is classified as the product that stems from decomposition or condensation of hydrocarbons on a catalyst surfaces. The cokes form can vary from high molecular weight hydrocarbons to carbons such as graphite depending on the process conditions[21].

The deactivation influence of coke on a catalyst depends on the nature of the coke, the structure of the coke, the morphology of the coke, and where on the catalyst surface the coke is deposited. If the coke is deposited mostly on the carrier surface and not on the

active sites of the catalyst, the catalyst can handle much more coke formation before the activity starts to decline, than if the coke is mainly deposited on the active sites. It has also been proposed that the catalytic reactions which experience carbon and coke formation and be categorized as either coke sensitive or coke insensitive, similar to Boudart's classification of structure sensitive or structure insensitive reactions. It is due to this classification that Menon put forth that the structure and location of a coke could be more important than its quantity when measuring the cokes effect on the catalytic activity[23].The mechanism of coke formation also varies with the catalyst type e.g. whether it is a metal, metal oxide or sulfides. Only the formation on metal catalyst are discussed in this section.

There are three main ways that the coke or carbon can effect a metal catalyst. The carbon may chemisorb strongly as a monolayer or physically adsorbed in multilayers and thereby block the reactants access to the metal surface sites, the carbon could totally encapsulate the metal particle and deactivate the particle, and lastly, the carbon can plug micro and/or mesopores and thereby blocking access for the reactant to the crystallites inside these pores[21]. There are many different structures of carbonaceous solids, from near amorphous structures to highly crystalline structures, that all might accumulate on a metal surface. The carbonaceous solids are often placed into three main classes: amorphous, filamentous and graphitic platelets[23]. However, it is important to note that not all carbon/coke structures result in a loss of catalytic activity[21].

2.2.1   Carbon Formation in The Direct Process

Side reactions during the Direct reaction leads to the formation of carbonaceous residue on the surface of the copper-silicon particles[6]. This can cause severe reduction of the selectivity of desired product, dimethyldichlorosilane, by blocking surface sites which are active for silane formation[5]. It has also been discussed that the carbon deposition on the contact mass might hamper the diffusion of copper into the silicon and therefore contribute to the deactivation of the reaction[7]. The coke formation can in some cases make it necessary to

continually remove spent silicon particles from the industrial fluidized bed reactors and replace them with fresh feed stock (contact mass) to continue the production[10].

Frank *et al.*[18] found that both graphitic carbon and carbide was present on the surface of the contact mass after reaction. They also found that graphitic carbon had a concentration as high as 85 % on the surface without reducing the selectivity or silane formation. This might indicate that the active sites are only present on a fraction of the surface, and therefore large amount of carbon species can be present on the contact mass without blocking the active sites. Furthermore, they found that the graphite concentration was larger at higher temperature which indicates that the activation energy for graphite is higher than for silane formation. They believed that the surface graphite may be formed from carbide and that Zn might promote the conversion of carbide to graphite.

Several studies have proposed the hypothesis that significant coking happens when metallic copper is exposed to methyl chloride even at low temperatures[18,24,25] (473 K). Kolster *et al.* found that methyl chloride readily decomposed over pure copper, and between the temperatures 273 and 473 K, formed both surface carbon and hydrogen[5].This lead to the theory that coke formation occurs more rapidly over bulk copper than over silicon or Cu_3Si. This means that a higher amount of metallic copper in the contact mass could lead to more coking during the synthesis.

Thermal decomposition of methyl chloride in the induction period, when the distribution is mainly described by the reaction of copper with methyl chloride, due to hot spot in the reactor, can be another source of carbon formation[26].

Another study found that nonmetallic aluminum impurities in the silicon mass could have a negative effect on the Direct Process. Not only does the impurities lower the selectivity for $(CH_3)_2SiCl_2$, but the study also proposed that they could promote the decomposition of methyl chloride and thereby carbon formation[27]. Lastly, the study

in which more carbon phases were recorded for a sample containing high levels of calcium can be mentioned. However, the study offers no explanation as to why the calcium should promote carbon formation, only that it occurred[28].

2.3   Characterization

In this section some theoretical background information on the different instrument used for characterization of the contact mass is given. It should be mentioned that very few previous studies on the Direct Process have been done with these instrument. A study done by T. J. Wessel and D. G. Rethwisch[24] even reported difficulties in analyzing the mass loss in thermal gravimetric analysis (TGA) due to oxidation of the silicon. There are some previous literature where scanning electron microscopy (SEM) and transmission electron microscopy (TEM) have been used, but never before have a scanning (transmission) electron microscope (STEM) with the possibility to investigate the surface structure on nanoscale been used. Even though Raman spectroscopy is often implemented in carbon investigations there are little too no literature about the use of Raman spectroscopy to investigate the contact mass in the Direct Process.

2.3.1   Thermal Gravimetric Analysis

Thermal Gravimetric Analysis (TGA) is done by measuring the mass variation of a sample versus either time or temperature in a controlled atmosphere with the help of a temperature program. The technique can help determine reactions related to mass loss such as drying, reduction, degradation etc. or reaction related to mass gain such as wetting, oxidation, adsorption etc. The analysis does not take mass conservative phenomena into account, but is still a useful tool, especially when coupled with other techniques, to reveal mass conservative changes.

Several parameter can affect the signal recorded in the measurements: for example increasing the mass of the sample raises the reaction temperature, or increasing the scanning rate can also increase the temperature. Therefore the mass and the scanning rate

should be kept equal in order to compare results. The derivative of the thermogravimetric signal can yield more accurately mass variations and give information on the kinetics of the phenomenon[29].

2.3.2 Differential Scanning Calorimetry

Differential Scanning Calorimetry (DSC) is a temperature-programmed method where the difference in the heat flow (or thermal power) is measured between a sample and a reference. The heat flow is then measured versus time or temperature in a controlled atmosphere. As the system is heated, as set by a predetermined temperature program, a signal which is proportional to the heat flow between the furnace and the sample and reference is recorded. The enthalpy changes or reaction rates of the system can also be recorded. The resulting thermogram for the recording can present steps or peaks, either endothermic or exothermic.

The equation for the thermogram from the DSC is based on Equation 2.9 which show the expression for the heat flows of the reference (r) and the sample (s).

$$\frac{dq_r}{dt} = C_r \frac{dT_r}{dt} \quad and \quad \frac{dq_s}{dt} = C_s \frac{dT_s}{dt} + \frac{dh}{dt} \tag{2.9}$$

where C_r and C_s are the heat capacity for the reference and sample filled crucible at constant pressure, respectively, and $\frac{dh}{dt}$, the absorbed thermal power resulting from the change in the sample. The heat flow is also related to the difference in temperature via the thermal resistance of the thermocouple as shown in Equation 2.10.

$$\frac{dq}{dt} = \frac{dq_s}{dt} - \frac{dq_r}{dt} = -\frac{T_s - T_r}{R} \quad or \quad R\frac{d^2q}{dt^2} = -\frac{dT_s}{dt} + \frac{dT_r}{dt} \tag{2.10}$$

The temperature for the reference crucible, T_r , and the furnace temperature, T , can be considered very close since the reference crucible is inert. This means that also the derivation of the temperature should be similar and therefore, $\frac{dT_r}{dt} \cong \frac{dT}{dt}$. The equation for the DSC thermogram can then be written as[29]:

$$\frac{dq}{dt} = (C_s - C_r)\frac{dT}{dt} + \frac{dh}{dt} - C_s R \frac{d^2 q}{dt^2} \tag{2.11}$$

2.3.3   X-Ray Fluorescence

The elemental analysis technique known as X-ray fluorescene (XRF) spectrometry is based on the principle that when an atom is excited by an external energy source it will emit X-ray photons which have and characteristic energy and wavelength. When a photon with energy larger than the binding energy of an atoms inner electron orbital hits an atom part of the photons energy can be absorbed with a certain probability (photoelectric absorption). This lead to the ejection of the atomic electron from its position and the atom is now ionized.

The ionized atom will then try to return to its original state either through the emission of other photoelectrons or by transferring an electron from one of the outer orbital to fill the vacancy in the inner orbital. The difference in energy as the electron is transferred from its initial to its final state is then given off in the form of an X-ray photon (Characteristic X-ray). The first effect is called the Auger effect while the second effect is the atom undergoing fluorescence. In XRF spectrometry the photon given off during fluorescence is detected, and by measuring its energy, one can determine the element and specific electronic transition from which the photon originated[30]. There are, in other words, two competing effects for the internal rearrangement of an atom. A ratio, which is called the fluorescent yield, takes the number of vacancies resulting in the production of characteristic X-ray photons and divides them on the total number of vacancies created in the excitation process. The ratio increases with increasing atomic number.

Since the emission of characteristic X-rays only involves the inner electron shells it is possible to detect the elemental composition of a sample, whether the elements are present in their pure forms, or as compounds. However, this makes the measurements of elements with low Z values difficult for the XRF, and usually elements which are smaller than sodium is not detected[31].

2.3.4 Gas Chromatography - Mass Spectrometry

Gas Chromatography was first introduced by James and Martin in 1952. The principle behind the GC is that a sample is introduced in a heated inlet or injector and then separated based on their volatility in a specially prepared column. A carrier gas, also called the mobile phase, is used to transfer the sample from the injector, through the column and into the detector or mass spectrometer. The most common column used in GC today are capillary tubes with a stationary phase coated on the inner wall. The determination of the different compounds are done by measuring the distribution of each component between the mobile phase and the stationary phase. A compound that spends a short amount of time in the stationary phase will elude, quickly while the remaining components in the carrier gases flown into detector or mass spectroscopy.

The configuration of the gas chromatograph can vary, but a typical set up for a gas chromatograph-mass spectrometer is shown in Figure 2.1. Typical features of gas chromatographs are ovens that heat the individual injectors, the column, each detector and the transfer line to mass spectrometer. The column and injector ovens can be controlled by temperature programming during separation, making it possible to increase the temperature at a regular rate.

For a GC/MS apparatus the actual GC/MS interface is the section which starts at the column exit in the gas chromatograph and extends to the ion source of the mass spectrometer. The mass spectrometer ionizes the eluate from the gas-phase from the GC column and forms positive charged molecular ions. In GC/MS most all ions which are formed have a single charge except for aromatic hydrocarbons which
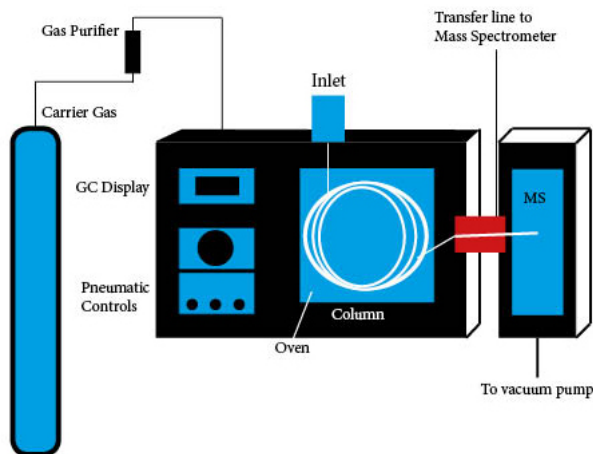
Figure 2.1: A typical set up for a gas chromatograph-mass spectrometer instrument showing how the carrier gas, the column, the oven and mass spectrometer is connected.

form double charged ions when subjected to electron ionization. Since the abundance of the double charged ions are very low compared to single charge ions of the same mass the m/z values of ions in GC/MS is considered to be the mass of the ion. The mass spectrometer then separates the ions according to their mass-to-charge-ratio values (m/z). The ions are then accelerated out of the ion source with constant energy into a m/z analyzer. The data that is collected during the GC/MS analysis are known as mass spectra and are acquired one after another at a constant rate. The coordinates for each mass spectral peak represent the m/z value and abundance of an ion with the corresponding m/z value[32].

2.3.5 Scanning Electron Microscopy

A key technique for the characterization of both catalyst and material is the use of different electron microscopy imaging. Electron microscopy offers different observation modes based on the desired information one needs. All electron microscopy uses the interaction between accelerated electrons and an arbitrary sample, under vacuum conditions. The interaction between the electrons and sample causes

the emissions of various particles or radiation. The emissions is then collected using different detectors, and by combining different signals and analyzing them, the sample can be characterized. The observation modes which can be used is the scanning and/or transmission electron microscopy known as SEM, TEM and STEM and different variations of these modes.

The different signals created from the electron-matter interaction yields different information about the sample. As the electrons from the high-energy beam interacts with the sample undergoes both inelastic and elastic scattering. This leads to the emissions of electrons, X-rays and light (photons). The emissions can be both low energy emissions such as secondary electrons and Auger electrons and high energy emissions such as backscattered electrons. The electron microscopy can use the low-energy transitions of a few electrons volts to characterize defects and transitions of around 1 keV in Auger spectrometry and even high energy transitions (E_0 - Δ E) which can be used for the micro analysis of energy losses. The different signals which can be derived from the electron-material interaction within a bulk sample is shown in Figure 2.2.
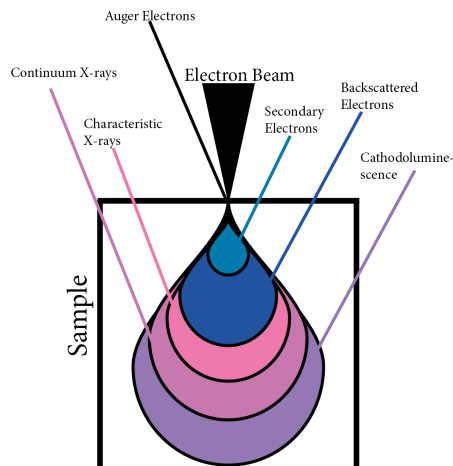
Figure 2.2: Illustration of the different signals which can be derived from the electron-material interaction within a bulk sample which can then be used to characterize samples with a electron microscope.

There are several signals which are used for chemical analysis such as X-ray photons which is used to conduct quantitative or semi-quantitative mapping of element distribution that can be measured using energy-dispersive spectrometry (EDS) or wavelength-dispersive spectrometry (WDS). Inelastic transmitted electrons, Auger electrons and Inelastic transmitted electrons, are all signal which can yield information through chemical analysis of a sample[33].

The scanning electron microscope is a instrument which is often used for the characterization of heterogeneous materials and their surfaces. The principle behind the characterization is that the area of a sample is examined using a thin focused high-energy electron beam. The electron beam can be both stationary, or scan over the surface. As the beam hits the sample surface there are several types of signals created, as detailed earlier in this section. A typical set up for the scanning electron microscope is shown in Figure 2.3.[34]
The electron gun in the set up usually uses a electron source of tungsten filament,a LaB_6, a Schottky emitter or a tungsten field-emission tip.
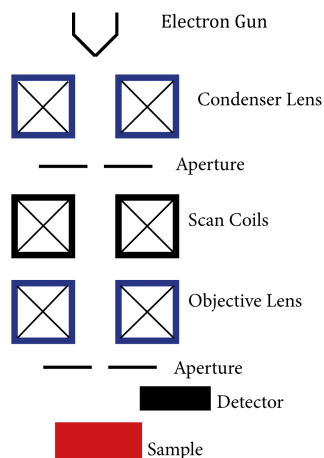
Figure 2.3: The different part which a microscope in a general scanning electron microscope (SEM) consist of.

In this project the type of electron microscope used was a scanning electron microscope, with attached bright field and dark field detec-

tors which allows for transmission measurements. The first STEM was constructed by von Ardenne in 1938 by adding scanning coils to a TEM. The STEM uses the fine-probe scanning technique of a SEM with a thin sample, but while the SEM records the secondary electrons to create an image, the STEM records the electrons that emerge from the opposite side of the specimen. In other word the transmission measurement in the STEM is done by collecting the electrons that are transmitted through the specimen and scattered within a certain angular range, determined by the inner and outer diameters[35].

2.3.6 Energy-Dispersive X-ray Spectroscopy

As mentioned earlier in this section, the electron-material interaction within a bulk sample gives of x-ray photones which can me used in energy-dispersive X-ray spectroscopy, called EDX or EDS for short. The EDX makes us of the characteristic X-rays that result from electron transitions between inner orbits within an atom. Since each characteristic X-ray correspond to a specific element the EDX can detect which elements are present in a sample[36]. As shown in Figure 2.2 the characteristic X-rays are emitted from under the surface of a sample meaning that the EDX is not a surface exclusive analytic method. An EDX is generally more useful for heavier elements, especially when the content of the element is small[37]. This is due to the fact that as the vacancy in the inner shell is created by the electron beam and then filled by an electron from an outer shell the extra energy is emitted as a characteristic X-ray, but another event can also take place. This is when the extra energy is transferred to another electron thereby creating and ejecting an Auger electron. Since the production of auger electron is more likely for lower atomic numbers and production of characteristic X-rays is more likely for higher atomic numbers, EDX analysis is more suitable for heavier element which higher atomic numbers[38].

2.3.7 X-ray Diffraction

X-ray diffraction (XRD) is a rapid analytical technique which can be used for phase identification of a crystalline material, which means that the unit cell symmetry and dimensions can be determined.

When X-rays interact with a crystalline material, the X-rays are scattered by planes of atoms within the material. Diffraction happens when the scattered X-ray undergo constructive and destructive interference. The diffraction of X-rays by crystals can be described by Bragg's Law, Equation 2.12, but most materials are not single crystals and therefore more complicated descriptions and calculations are needed.

$$n\lambda = 2sin\theta \tag{2.12}$$

In a crystalline powder the small crystallites are randomly oriented within a sample. To gain the diffraction data, monochromatic X-rays are directed onto a sample. Within the X-ray diffractometer the sample and detector are rotated while the intensity of the diffracted X-rays are recorded. When the angles of the incident and diffracted X-rays satisfies the Bragg Equation, constructive interference occurs and a peak in intensity is recorded by a detector.

2.3.8   Raman Spectroscopy

Raman Spectroscopy is a nondestructive spectroscopic technique which can be used to study solid, liquid, and gaseous samples by taking advantage of the phenomenon known as Raman scattering. The phenomenon was discovered in 1928 by Sir Chandrasekhra Venkata Raman. In Raman spectroscopy a samples is irradiated by an intense laser usually in the UV-visible (v_0) region.The scattered light can then be observed in the direction perpendicular to the incident beam. The observed light consist of two types of scattering, Rayleigh scattering and Raman scattering. Rayleigh scattering is strong and has the same frequency as the incident beam (v_0) while Raman scattering is comparably very weak and the frequencies can be detonated as $v_0 \pm v_m$, where v_m is a vibrational frequency of a molecule. The $v_0 - v_m$ lines are also called the Stokes lines while the $v_0 + v_m$ lines are called anti-Stokes lines. Figure 2.4 shows the Rayleigh and Raman scattering process.
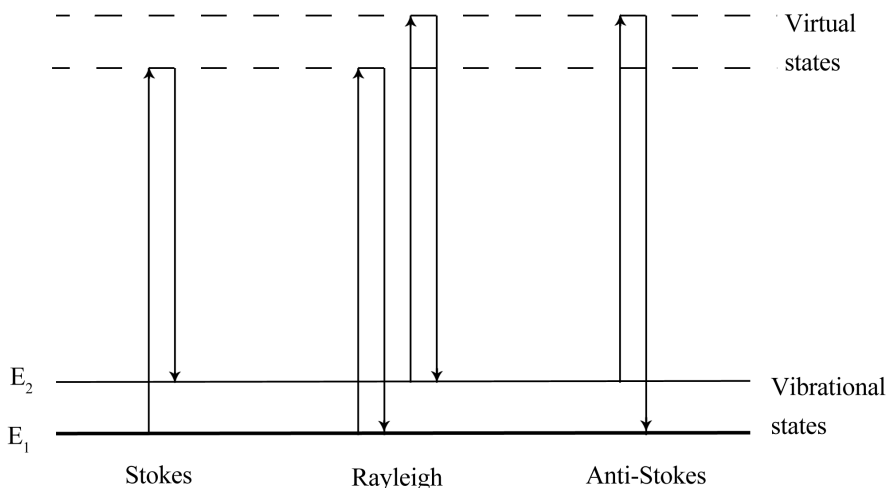
Figure 2.4: A scheme of the Rayleigh, Stokes and anti-Stokes scattering, where the lowest line correspond to the lowest energy vibrational(E_1) state and with states of increasing energy above it. The low energy (upward arrow) and the scattered energy (downward arrow) have much larger energies than the energy of a vibration[39].

In Raman spectroscopy one measures the vibrational frequency (ν_m) as a shift from the incident beam frequency (ν_0). Raman spectra are measured in the UV-visible region where the excitation as well as Raman lines appear[40]. Sometimes the sample or impurities may absorb the laser radiation and re-emit it as fluorescence band which obscures the Raman spectra.

Most Raman spectrometers consist of four major components: An excitation source, a sample illumination and collection system, a wavelength selector, and a detection and computer control/processing systems[39].

2.3.9   Fourier Transform Infrared Spectroscopy

FT-IR spectroscopy is based on the principle that molecular vibrations can absorb infrared radiation in range the of the electromagnetic radiation. Infrared radiation can be defined as electromagnetic radiation with frequencies between 14300 and 20 cm^{-1} where one can divide the frequency range into three regions; the near region, the mid region and the far IR region. The mid region is usually the region studied since most organic matter has molecular vibrations between 400 cm^{-1} and 4000cm^{-1}.

In FT-IR spectroscopy the radiation between two beams interfere to create a interferogram. The mathematical process of Fourier-transformation is then applied to the interferogram, and thereby enhancing the quality of the IR spectra while minimizing the time required to obtain the data. The mathematical definition of forward continuous Fourier transform is shown in Equation 2.13.

$$F[f(t)] = \int_{-\infty}^{\infty} e^{-2\pi i s t} f(t) dt \qquad (2.13)$$

where $s = \frac{n}{T}$ when $T \rightarrow \infty$ and T is the period of the function.

The IR spectra is collected by using an interferometer before the Fourier transform applied and the spectrum obtained. The analytic results obtained are associated with a database of characteristic electromagnetic radiation energies or absorption wavelengths. The spectrum can then be analyzed with the help of tables which correlate the frequencies of vibration bands with functional groups.

The spectrum is a collection of the absorbed radiation by the sample, which is then converted into energy of molecular vibration and then correlates to the energy of a specific molecular vibration. Each peak in spectrum corresponds to a frequency of a vibration of part of the sample. Each vibration has a unique frequency which depends on the strength of the chemical bond between atoms and the mass of each atom. A common set-up for the FT-IR spectroscope interferometer is shown in Figure 2.5[41].
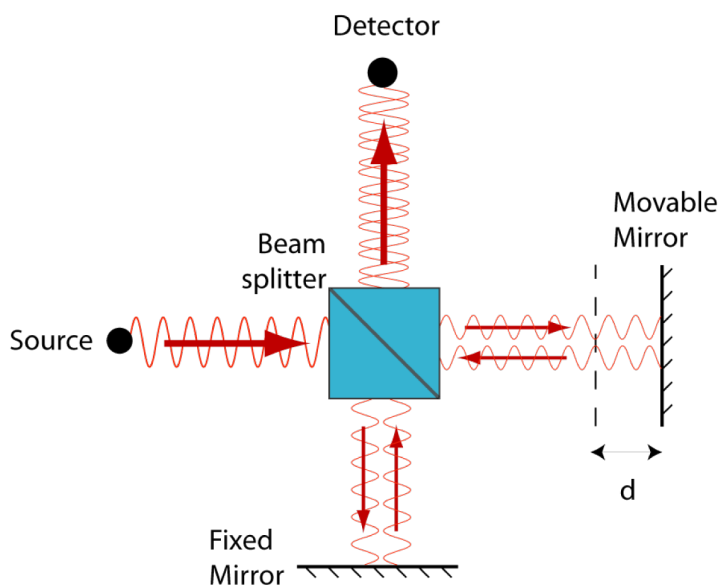
Figure 2.5: A common set-up for the fourier transform infrared (FT-IR) spectroscope interferometer which is used when obtaining the FT-IR spectrum[42].

3. Materials and Methods

In this master's thesis nine solid samples were obtained from Elkem Silicon Materials. The nine solid samples consisted of one main series of five samples, here referred to as the P-series, where the samples were labeled P1, P2, P3, P4 and P5. Two older samples, which were also investigated as part of the subject TKP4580 Chemical Engineering, Specialization Project in the fall of 2017, labeled EL1 and EL2. One catastrophe sample which should contain large amount of carbon species labeled C1 and lastly a reference sample, referred to as REF which silicon which is used to make the contact mass.

3.1 Sample Information

The contact mass samples are a mixture of metallurgical silicon promoted with zinc and tin as well as the catalyst; copper(I)chloride. The main series, P-series, was extracted from a fluidized bed experiment conducted at 4 bar and 300 °C. Chlorormethane and argon was fed into the reactor at a rate of 285 mL/min and 10 mL/min. P1-P4 was extracted at 4 hours, 21.5 hours, 27.5 hours and 46 hours respectively. This was done by inserting and opening a small cylinder containing inert gas at ambient pressure into the fluidized bed. The last sample of the P-series, P5, was extracted at 51 hours after termination of the experiment. The contact mass was cooled in an inert atmosphere before the P5 sample was extracted. The two older samples, EL1 and EL2, are both samples of contact mass from a terminated experiments at similar conditions to the P-series where the contact mass was cooled in inert atmosphere before extraction.

3.2   Thermal Gravemetric Analysis

Thermal gravemetric analysis of the samples were done with a Netzsch STA 449C Jupiter TGA/DSC which was coupled with a Netzsch Aerlos QMS 403C MS so as to simultaneously preform mass spectrometry. During the thermal gravemetric analysis both mass loss and heat exchange for each sample was recorded, while the amount of CO_2 and H_2O produced was recorded by the mass spectrometry by configuring the Netzsch Aerlos QMS 403C MS to record the amount of molecules with the molar mass of 44 g/mole and 18 g/mole .

A standard temperature program was used for all measurements. The program was started at 35°C and ended at 800°C with an increase in temperature of 10°C/min. The atmosphere for each experiments was either an oxidizing atmosphere with 25 ml/min of pure Ar and 75 ml/min of air (20% O_2), or an inert atmosphere with 100 ml/min of pure Ar. Some samples where dried in air overnight in a Termax oven at 100 °C prior to the thermal analysis so one could compare the dried and not dried measurements and thereby reducing the H_2O recorded due to during during the thermal analysis.

3.3   Scanning (Transmission) Electron Microscopy and Energry-Dispersive X-Ray spectroscopy

The topography of each sample was investigated by a Hitachi S-5500 S(T)EM by applying a voltage of 10kV and a current of 5-7A. A elementary distribution analysis (EDX) of each samples was also done by using the Hitachi S-5500 with a voltage of 15kV and current of 20A. The STD 5500 holder was used for both measurements and the samples where placed onto the holder by mixing each sample with ethanol,dropping it on the sample holder and letting the mixture dry before inserting the sample holder into the Hitachi .

3.4   Raman Spectroscopy

In order to study the Raman spectra of each sample a Horiba Jobin
Yvon LabRAM HR800 spectrometer was used together with the soft-
ware Labspec 6. Most spectres was obtained by using a x50LWD
objective, a 632 nm laser and continuous scans in the range 200-
3000cm^{-1}. The filter was set at 100% and the grating at 600 while the
hole setting where at a 100.

The P5 sample was also investigated with a 325nm laser with a
x40NUV objective in the range of 100-2000 cm^{-1} and a 1800 grating,
200 hole and with the x100LWD objective together with the 632nm
laser in the range 200-3000cm^{-1}. The filter was set between 33%-67%
and the grating at 600 while the hole setting were at a 100.

3.5   X-ray Diffraction

Preliminary X-ray diffraction investigations were done on the con-
tact mass by running samples through a D8 Focus DaVinci X-ray
Diffractometer, where Cu Kα radiation was used to investigate the
composition and purity of the samples in Bragg-Brentano geometry.
θ - 2θ scans were recorded within the 2θ range of 5°-80°, with a
divergence slit of 0.2mm, step size of 0.0143 at 0.3 seconds per step
and a scan time of 27 minutes.

Sample preparation was done by muddling the sample by hand
before mixing it with ethanol. The suspension of sample and ethanol
was then dropped onto the sample holder and left to dry in air before
the experiment was started. For determining the resulting peaks,
all diffractograms were searched and matched with scans from the
PDF-4+ database (International Centre for Diffraction Data) using
Bruker AXS DIFFRACT.EVA (Version 5) software.

3.6   X-Ray Fluorescence

A wavelength dispersive X-ray fluorescence (WDXRF) apparatuses
(Supermini200, Rigaku) was used to determine the composition of
each sample.

For the sample preparation boric acid was used as a binder to-
gether with a small amount of the sample to created the pellets for
the instrument measurement. The sample and binder was blended
together and muddled by hand to create a homogeneous powder. The
powder was then introduced into a pellet die so that a 40 mm of diam-
eter pellet could be pressed. The pellet was then pressed for 4 minutes
at 7 bar by a press machine. After the introduction of the pellet to
the sample retainer, the pellet was covered with polypropylene film (6
μm).

3.7   Pyrolysis GC/MS

To detect any organic decomposition products from the samples
a Single-Shot Pyrolyzer "PY-3030S" from Frontier lab was used to
preform pyrolysis GC/MS measurements. The flash pyrolysis was
used for all sample at a furnace temperature of 500°C. The gas from
the flash pyrolysis was then let in a Agilent 7820A gas chromatograph
equipped with an Ultra ALLOY® capillary column to be separated and
further analyzed by a an Agilent 5977 MSD.

3.8   Fourier Transform Infrared Spectroscopy

Fourier Transform infrared (FT-IR) radiation spectroscopy was done
with a Bruker Tensor II with a cube corner interferometer within the
wavenumber range of 600 - 4000 cm^{-1}. A KBr beam splitter was used
with a 2mm aperture setting, a scanner velocity of 15KHz and a MIR
source setting.

4. Results

The following chapter contains the results of laboratory work done as part of this master's thesis. All different characterizations techniques used are presented here. Due to small amount of sample mass not all samples could be investigated by all techniques. Especially thermal gravimetric analysis and fourier transform infrared (FT-IR) spectroscopy which both require larger amount of sample mass could not be used on all samples.

4.1 Surface Morphology and Composition

The morphology of the P-series of reacted contact mass, P1 (4 hours), P2 (21.5 hours), P3 (27.5 hours), P4 (46 hours) and P5 (51 hours), and the morphology for the reference sample, REF, is shown in Figure 4.1 - Figure 4.6. The morphology of each sample is heterogeneous, but the following SEM micrographs are a selection of topology which represents the all over structure within the sample unless anything else is stated. For Figures 4.1-4.6 the morphology of each samples is shown with similar magnification. All structures shown in the following figures where found at several spot through the samples.
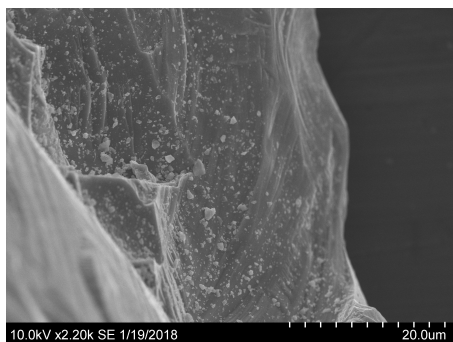
Figure 4.1: SEM micrograph of the surface morphology of the reference sample, REF, taken at a voltage of 10kV and current of 5A.
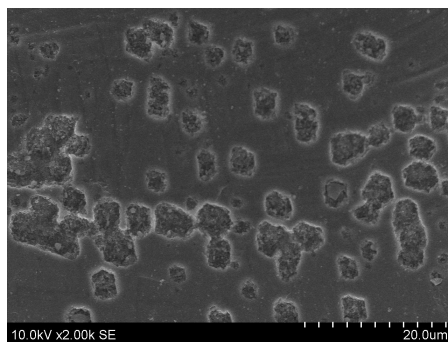
Figure 4.2: SEM micrograph of the surface morphology of the reacted contact mass from the P1 sample, extracted after 4 hours, taken at a voltage of 10kV and current of 7A.
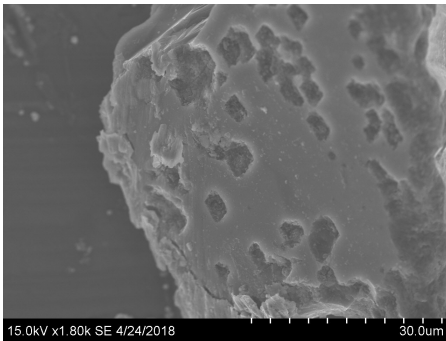
Figure 4.3: SEM micrograph of the surface morphology of the reacted contact mass from the P2 sample, extracted after 21.5 hours, taken at a voltage of 10kV and current of 7A.
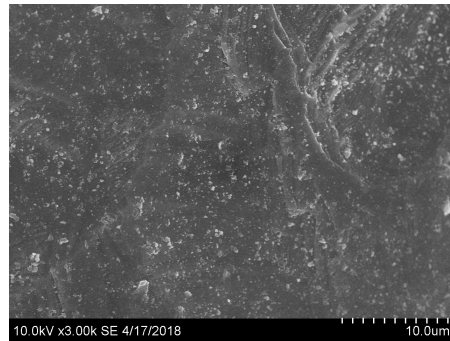
Figure 4.4: SEM micrograph of the surface morphology of the reacted contact mass from the P3 sample, extracted after 27.5 hours, taken at a voltage of 10kV and current of 7A.
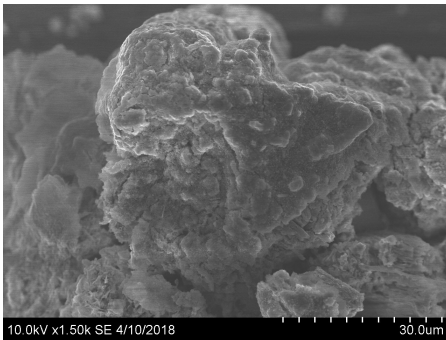
Figure 4.5: SEM micrograph of the surface morphology of the reacted contact mass from the P4 sample, extracted after 46 hours, taken at a voltage of 10kV and current of 7A.

Figure 4.6: SEM micrograph of the surface morphology of the reacted contact mass from the P5 sample, extracted after 51 hours after termination, taken at a voltage of 10kV and current of 7A.

The surface morphology shown in Figure 4.7 and Figure 4.8 where only found in samples P4 and P5. However, several particles with the same structure was found in both sample P4 and in sample P5. In the SEM micrographs one can clearly see several large solid looking particle in between the very porous structure of a larger particle.
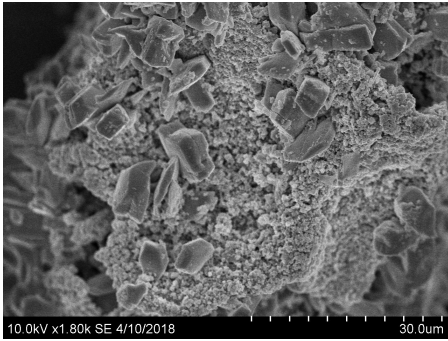
Figure 4.7: SEM micrograph of the reacted contact mass from the P5 sample, extracted after 51 hours after termination, taken at a voltage of 10kV and current of 7A showing nonporous particles within a porous structure.
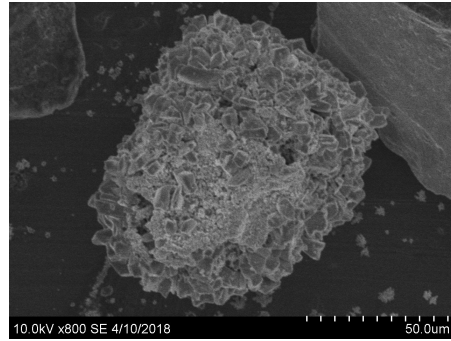
Figure 4.8: SEM micrograph of the reacted contact mass from the P4 sample, extracted after 46 hours, taken at a voltage of 10kV and current of 7A showing nonporous particles within a porous structure.

Figure 4.9 and Figure 4.10 show two small particles with a crystal like structure. The small particles where present both on their own and deposited on larger particles. The crystal like structures where present in all sample within the P-series (P1, P2, P3, P4, P5).
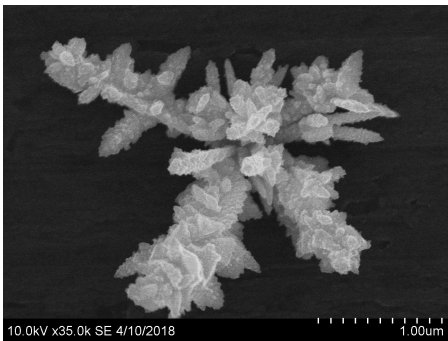
Figure 4.9: SEM micrograph of the reacted contact mass from the P4 sample, extracted after 46 hours, taken at a voltage of 10kV and current of 7A showing a crystal-like structure with a large amount of copper present in its composition.
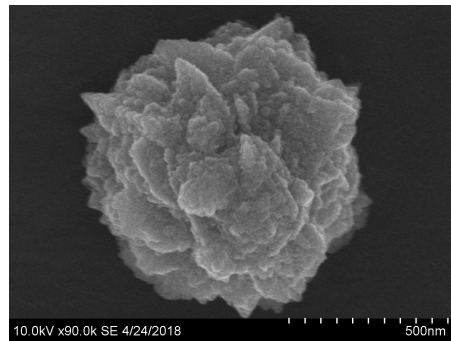
Figure 4.10: SEM micrograph of the reacted contact mass from the P2 sample, extracted after 21.5 hours, taken at a voltage of 10kV and current of 7A showing a crystal-like structure with a large amount of copper present in its composition.

The structure shown in Figure 4.9 was found in the P4 sample while the structure shown in Figure 4.10 was found in the P2 sample. The crystal like shapes consisted of mainly copper, more information about their composition are given in the EDX section.

Figures 4.11 - 4.16 show how the surface structure of each sample change from the sample REF (silicon), until after termination of the reaction, sample P5. Again the surface morphology shown Figures 4.11 - 4.16 were found in several particles within each sample. The micrographs show the samples at similar magnifications and are a closer look at the porous/reacted areas of each sample. One can clearly see that reaction pits are formed already at the fourth hour, at which sample P1 was extracted and that the samples become more porous and structured as the reaction continues.
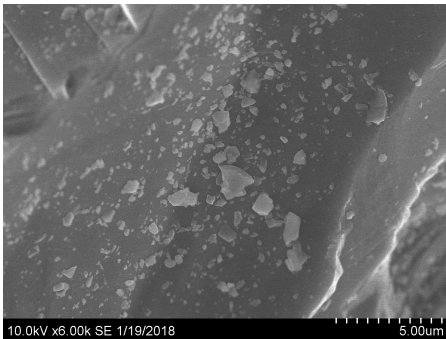
Figure 4.11: SEM micrograph of the surface morphology of the reference sample, REF, at a voltage of 10kV and current of 5A.
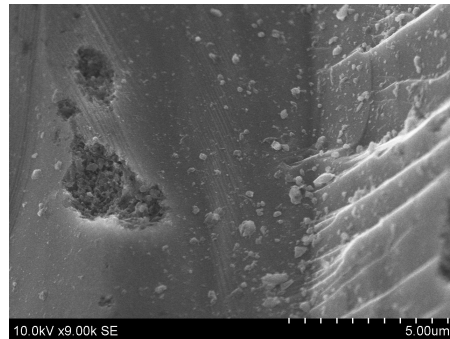
Figure 4.12: SEM micrograph of the surface morphology of the reacted contact mass from the P1 sample, extracted after 4 hours, taken at a voltage of 10kV and current of 7A.
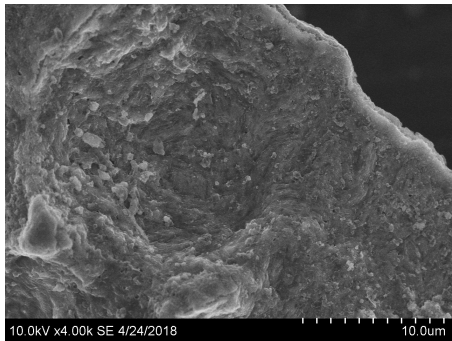
Figure 4.13: SEM micrograph of the surface morphology of the reacted contact mass from the P2 sample, extracted after 21.5 hours,taken at a voltage of 10kV and current of 7A.
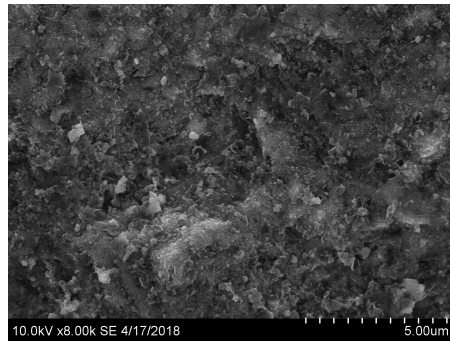
Figure 4.14: SEM micrograph of the surface morphology of the reacted contact mass from the P3 sample, extracted after 27.5 hours, taken at a voltage of 10kV and current of 7A.
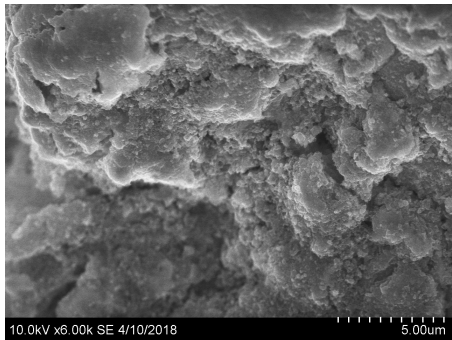
Figure 4.15: SEM micrograph of the surface morphology of the reacted contact mass from the P4 sample, extracted after 46 hours, taken with a voltage of 10kV and current of 7A.
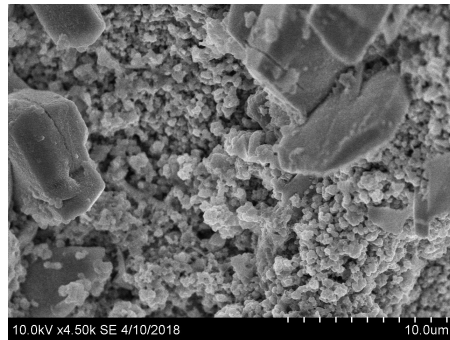
Figure 4.16: SEM micrograph of the surface morphology of the reacted contact mass from the P5 sample, extracted after 51 hours after termination, taken at 10um magnification at a voltage of 10kV and current of 7A.

The reaction pits found by the SEM in sample P1 was further studied by EDX. Figure 4.17 shows the composition of some of the reaction pits discovered within sample P1. The pits seem to be richer in both copper and oxygen. This was also seen in several other spots where the surface morphology of a sample had changed due to reaction, forming structured pits within the sample. All reaction pits in all samples showed inrichement in copper, and sometimes also oxygen, with some silicon depletion with in reaction pits. This correspond to previous results found by H.Ehrich *et al.*[43].
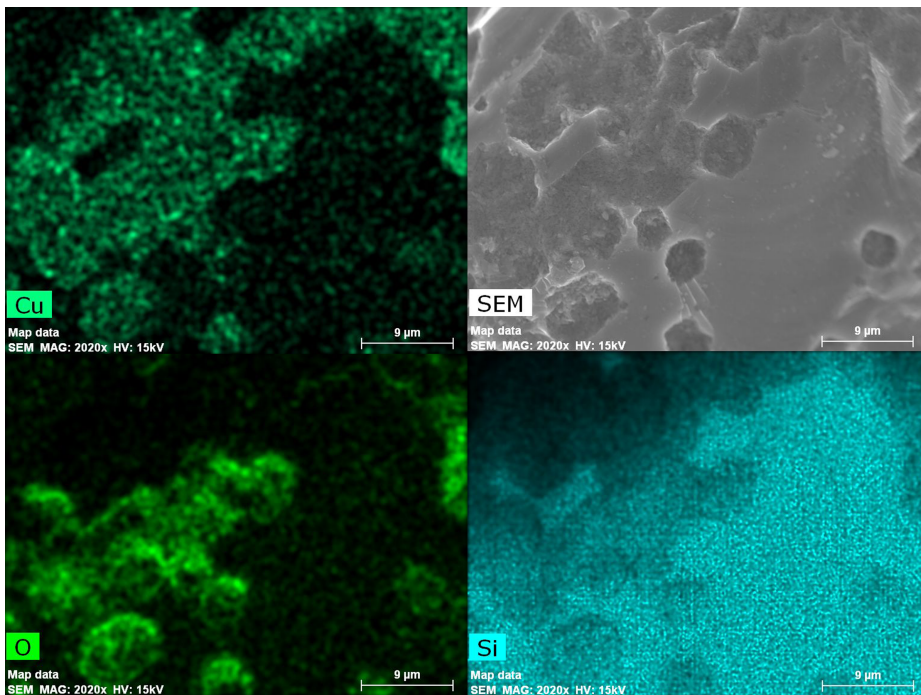
Figure 4.17: SEM micrographs showing the distribution of copper, oxygen and silicon measured by EDX in the P1 sample, extracted at 4 hours, measured with a voltage of 15kV and current of 20A.

The crystal structures found in the P-series were tested in EDX, where the composition of the crystals were measured to be mainly copper with some silicon, oxygen, carbon and aluminum. The aluminum might mainly stem from the sample holder since the sample holder

consists of mainly aluminum. Figure 4.18 shows the result from the EDX of one of theses crystal structures.
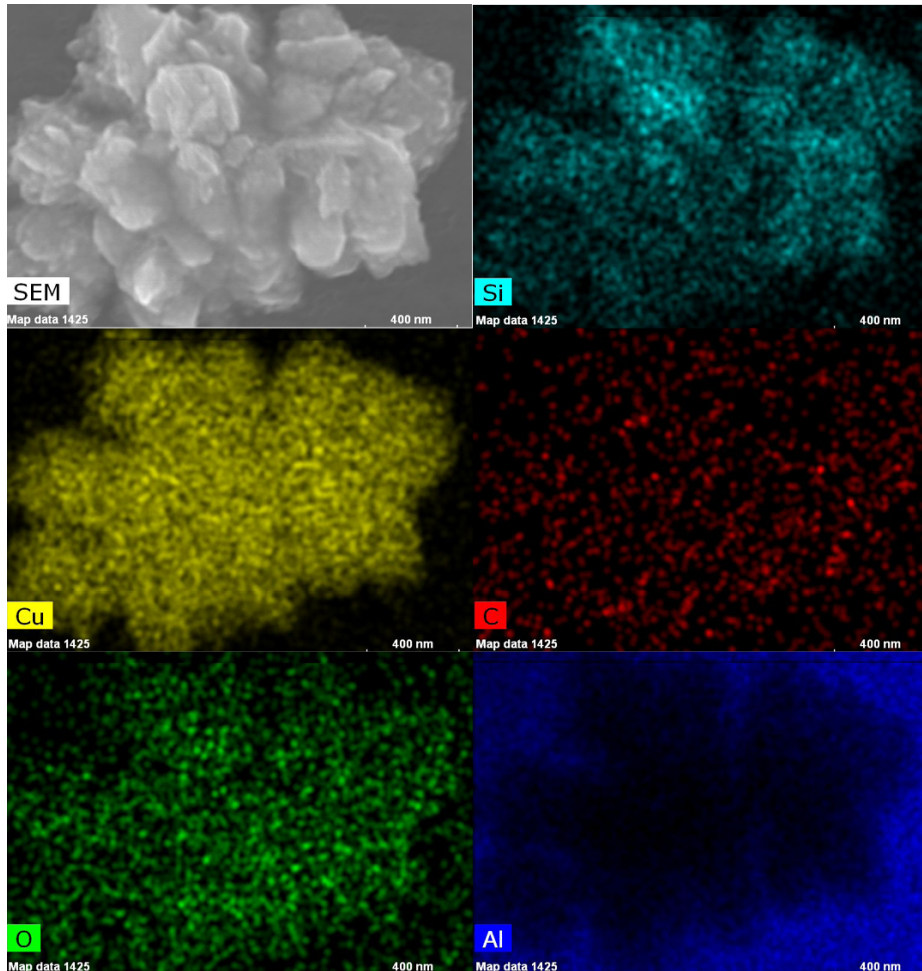
Figure 4.18: SEM micrographs showing the distribution of silicon, copper, carbon, oxygen, aluminum measured by EDX on a crystal structure found in the P2 sample,extracted at 21.5 hours, measured with a voltage of 15kV and current of 20A.

Figure 4.19 shows more of the reaction pits shown in Figure 4.17, but this time for the sample P2. Here the distribution of carbon and chlorine is shown as well as the distribution of copper, silicon and oxygen. The copper seems to be most prevalent within the reaction pits and the oxygen is especially prevalent in the reaction pits for the P2 sample.

The carbon seem to be distributed quite evenly over the surface with some brighter spot corresponding to spot with high density of copper and/or oxygen. The chlorine is in higher concentrations where there is lower concentrations of silicon.
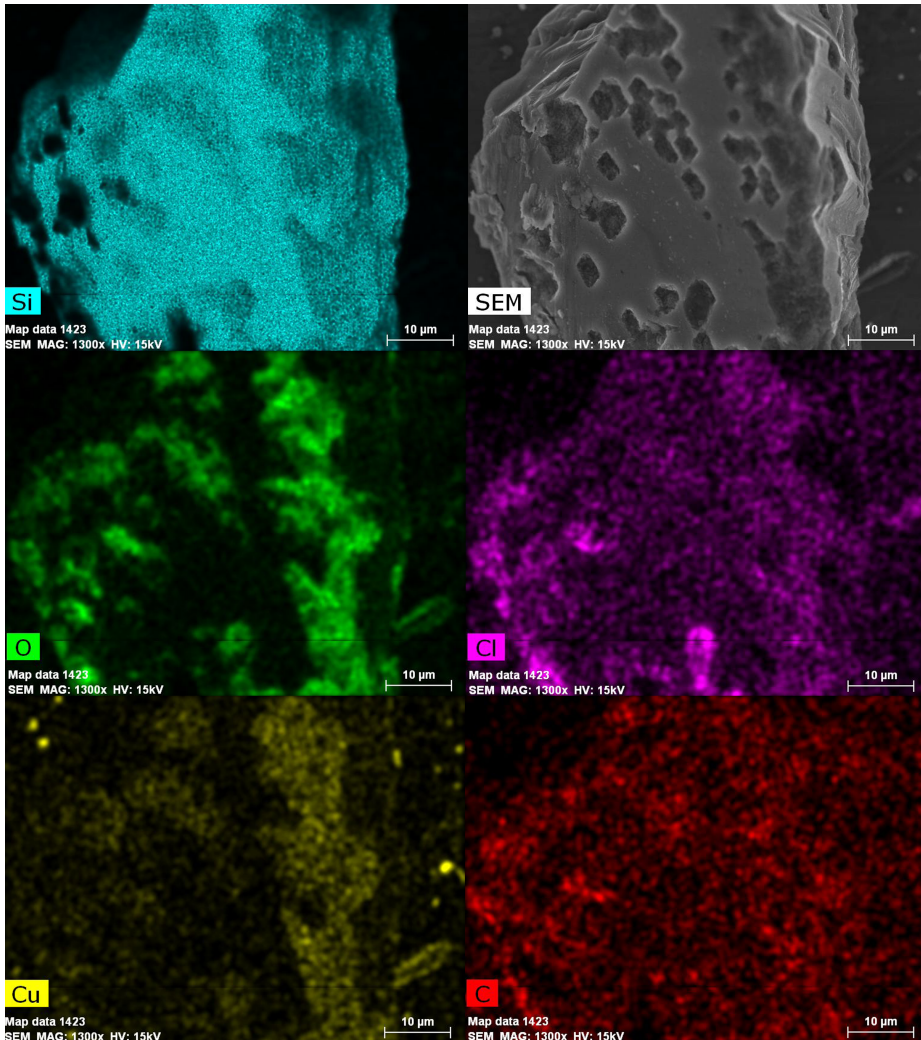
Figure 4.19: SEM micrographs showing the distribution of silicon, oxygen, chlorine, copper and carbon measured by EDX in the P2 sample, extracted at 21.5 hours, measured with a voltage of 15kV and current of 20A.

In sample P4 the carbon and oxygen showed even more of the correlation which was indicated within the reaction pits of the P2 sample. Even though both carbon and oxygen is distributed through out the P4 sample there are light spot in both distribution maps which corresponds well to each other. Figure 4.20 shows the oxygen and carbon distribution of carbon and oxygen within a particle form the P4 sample.
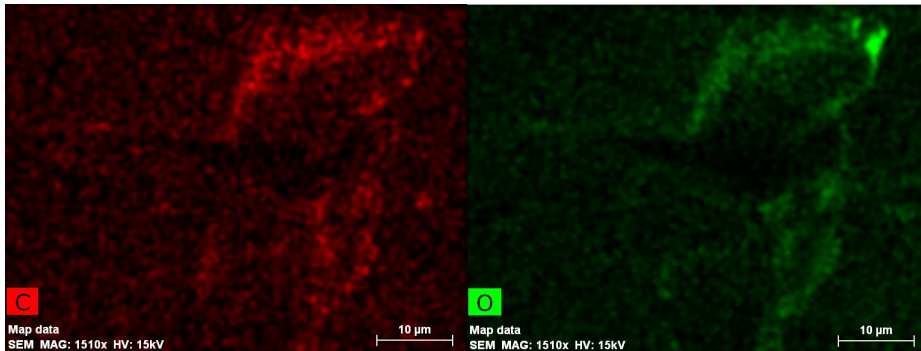
Figure 4.20: SEM micrographs showing how the distribution of carbon and oxygen are related in the P4 sample, extracted at 46 hours. The distribution was measured by EDX with a voltage of 15kV and current of 20A.

For the reference sample, REF, silicon, copper, oxygen, tin, carbon and aluminum was measured with the EDX. However not all points measured for the REF sample showed copper. Especially the points taken at lower magnifications did not show any copper present. When copper was present, it was evenly distributed over the surface. No zinc was detected in the reference sample, REF, but was found to be present in some of the P-series samples. The EDX result for the REF sample is shown in Figure 4.21
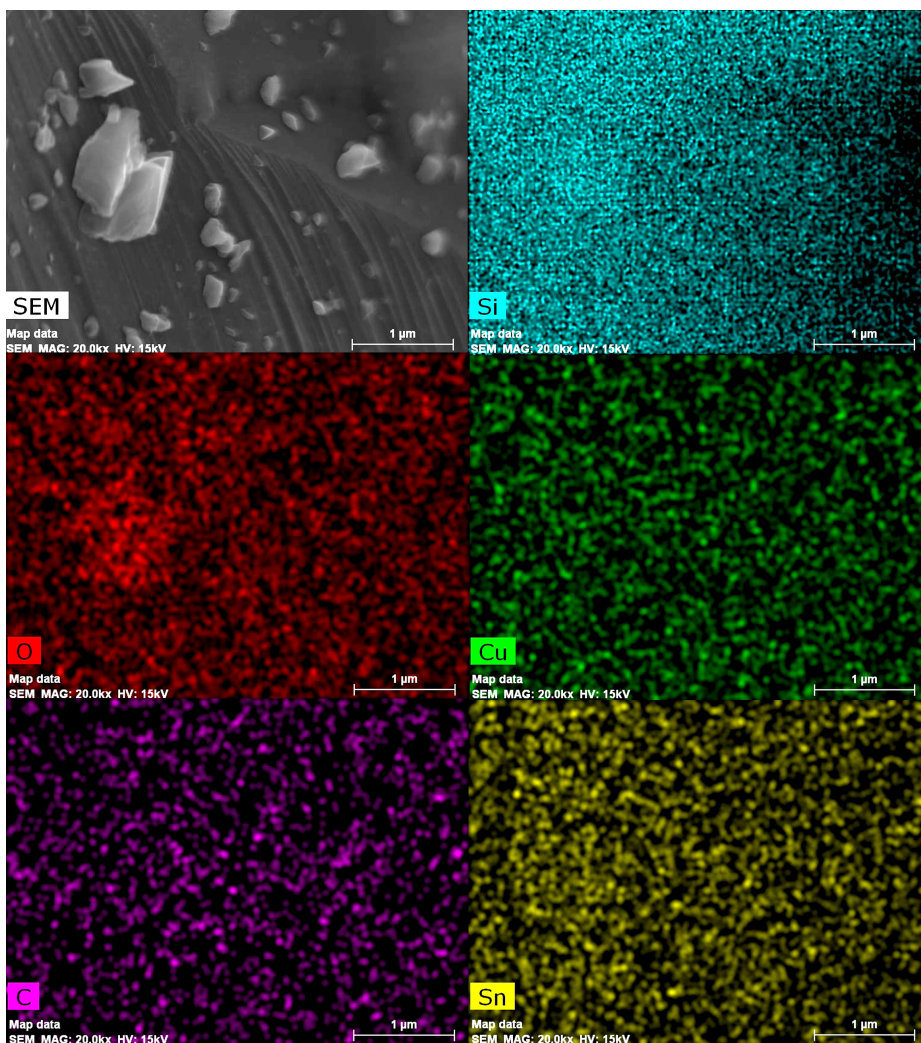
Figure 4.21: SEM micrographs showing the distribution of silicon, oxygen, copper, carbon and tin measured by EDX in the reference sample, REF, , measured with a voltage of 15kV and current of 20A.

4.2   Raman Spectroscopy

To achieve the Raman spectrum for each of the nine samples, several points on each sample were measured with the Raman spectroscope. The average spectrum for each sample was then determined from these points and plotted by using MATLAB. Only the spectra from investigation in the visible light region is shown in this section.

The spectra for the P-series were collected in Figure 4.22. The spectra have been modified so that the highest peak (518 cm^{-1}) had the same intensity for all samples within the P-series (P1, P2, P3, P4 and P5). This was done to better compare the other peaks of much lower intensity from sample to sample. The high intensity peak at 518 cm^{-1} has also been cut to better show the smaller peaks in each spectrum. Lastly, each spectra has been offset along the y-axis at an arbitrary starting value.
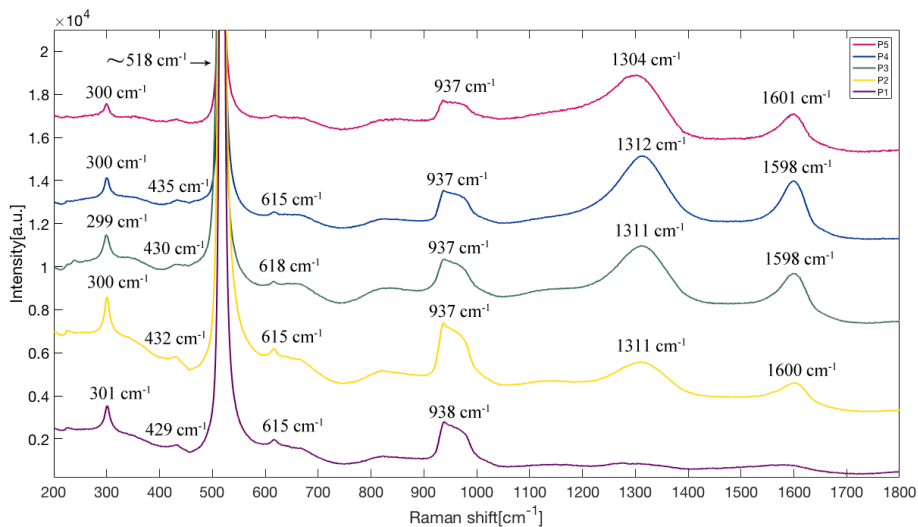
Figure 4.22: Raman spectra obtained for the P-series in visible light with a 632 laser. Each spectrum has been modified so the peak at 518 cm^{-1} has the same intensity for all samples. Each spectrum has been offset along the y-axis.

The peak around 1300 cm^{-1} is related to the D1-Band which is due to the breathing vibrational mode of six-membered rings. The peaks

around 1600 cm^{-1} is related to the G-Band which is due to the relative motion of sp2 hybridized C atoms[44]. The other five peaks observed can all be related to the silicon. The peaks at around 300 cm^{-1}, 435 cm^{-1}, 519 cm^{-1}, 615 cm^{-1} and 940 cm^{-1} and there respective intensity and shape all correspond to a standard silicon Raman spectra. Studies done by T. Kallel *et al.*[45] and several others[46–48] show the same peak for silicon in their studies. According to B. Graczykowski *et.al*[47] the phononic silicon modes to which the peaks at 300 cm^{-1}, 435 cm^{-1}, 519 cm^{-1}, 615 cm^{-1} and 940 cm^{-1} could correspond to are 2TA, TO, 2LA and 2TO. Where TA stands for transverse acoustic , TO stands for transverse optic and LA stands for longitudinal acoustic.

Figure 4.23 shows the average spectra of the P5 sample before and after TGA measurements, and after being grounded in order to achieve a more homogeneous sample sample.
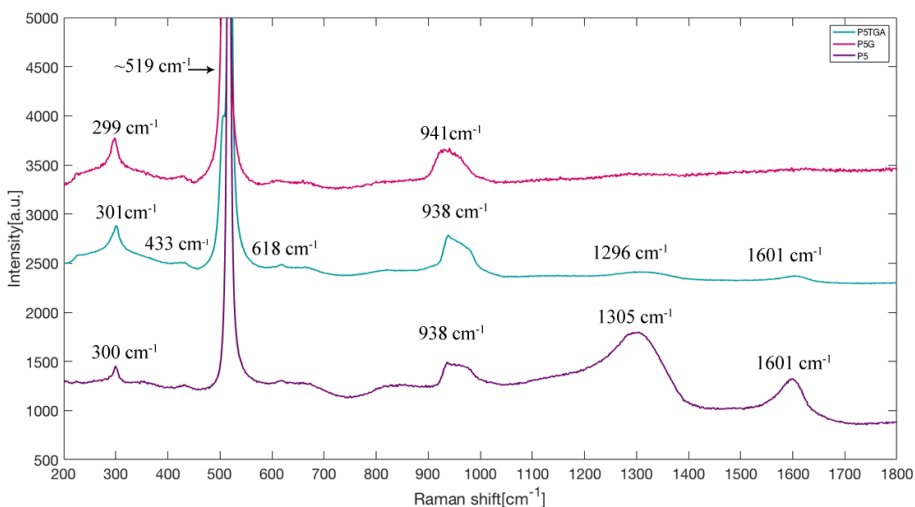
Figure 4.23: Raman spectra obtained for the P5 sample, the P5 sample after TGA and a muddled P5 sample in visible light with a 632 laser. Each spectrum has been modified so the peak at 519 cm^{-1} has the same intensity for all samples. Each spectrum has been offset along the y-axis.

The spectra have been modified so that the highest peak (519 cm^{-1}) had the same intensity for all samples. This was done to better compare the other peaks of much lower intensity from sample to

sample. The high intensity peak at 519 cm^{-1} has also been cut to better show the smaller peaks in each spectrum. Lastly, each spectra has been offset along the y-axis at an arbitrary starting value. The figure shows the average spectra of the P5 sample before and after TGA measurements, and after being grounded in order to achieve a more homogeneous sample.

Figure 4.24 compares the average measurement of P4, EL1, EL2 and the reference sample, REF. The spectra have been modified so that the highest peak (517 cm^{-1}) had the same intensity for all samples. This was done to better compare the other peaks of much lower intensity from sample to sample. The high intensity peak at 517 cm^{-1} has also been cut to better show the smaller peaks in each spectrum. Lastly, each spectrum has been offset along the y-axis at an arbitrary starting value.
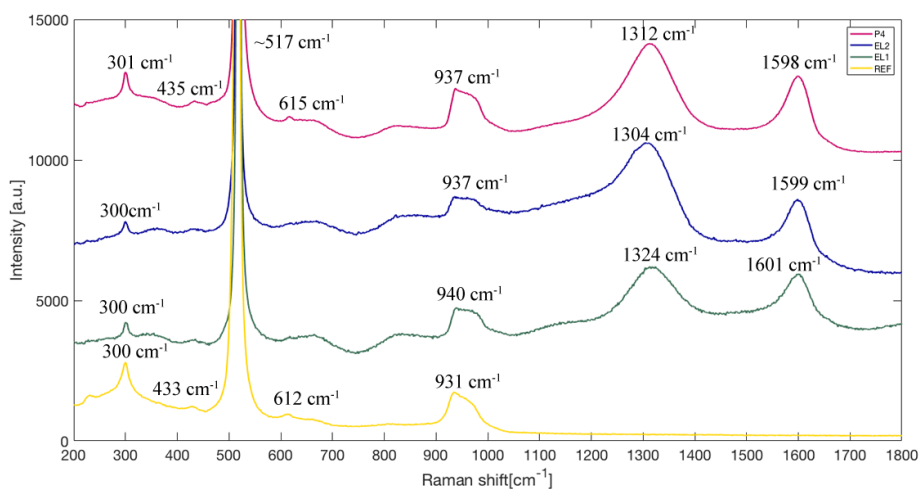
Figure 4.24: Raman spectra obtained for the P4 sample, the EL1 and EL2 sample as well as the the REF sample in visible light with a 632 laser. Each spectrum has been modified so the peak at 517 cm^{-1} has the same intensity for all samples. Each spectrum has been offset along the y-axis.

To better understand the composition of the carbon species the ID (intensity of the D peak)/IG (intensity of the G peak) ratio was calculated. The ratio was calculated by dividing the peak height of the D peak, found at around 1310 cm^{-1}, on the peak height of the G peak, found at around 1600 cm^{-1}. The peak height were found by MATLAB and were taken at the points marked in Figures 4.22-4.24. Table 4.1 shows the calculated ratios for the P-series (excluding sample P1), EL1 and EL2.

Table 4.1: The intensity ratio between the D-Band (~1300cm^{-1}) and G-band (~1600cm^{-1}) found by Raman spectroscopy for each sample.

Sample [#]	D-Band [a.u.]	G-Band [a.u.]	ID/IG Ratio
EL1	3763	3661	1.0279
P3	6790	5795	1.1717
EL2	5667	4821	1.1755
P2	6610	5564	1.1880
P5	2930	2457	1.1925
P4	7036	5870	1.1986

The spectrum achieved from the investigation of sample P5 within the UV region with the 325 nm laser is given in Appendix A.3. The investigation of sample P5 in the visible light region with the x100LWD objective is also given in Appendix A.3.

4.3 Thermal Gravimetric Analysis

4.3.1 NaHCO$_3$ Sample

NaHCO$_3$ was used to test the TGA and calculate the peak area ratio of CO$_2$ and H$_2$O which was to be used as a response factor when calculating the H/C ratio of samples P2, P4, P5 and C1. Figure 4.25 shows the mass loss and heat exchange for the NaHCO$_3$ in standard atmosphere (75ml/min Air and 25ml/min Argon).
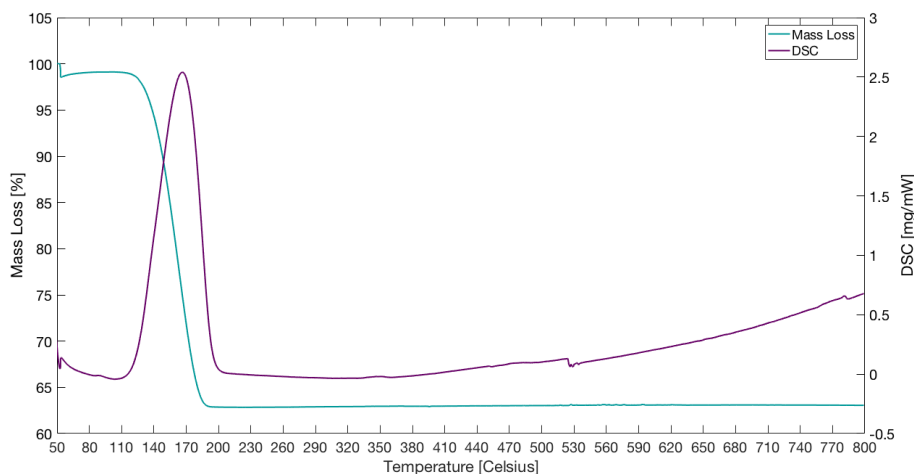
Figure 4.25: The mass loss[%] and heat exchange[mg/mW] for a test sample of NaHCO$_3$, in standard atmosphere (75ml/min Air and 25ml/min Argon) without pre-drying.

There is a clear mass loss of nearly 40 % which correspond to an sharp endothermic peak in the same temperature interval. The mass loss and heat exchange correlates to the formation of CO$_2$ and H$_2$O in the same temperature region.

The mass spectrum for NaHCO$_3$ measuring compounds with the molar mass of 44g/mol (CO$_2$) and 18 g/mol (H$_2$O) is shown in Figure 4.26. The mass spectrum was used to find the peak areas of CO$_2$ and H$_2$O by using the trapz function in MATLAB to calculated the area under each curve. The trapz function is a Trapezoidal numerical integration via the trapezoidal method. This method approximates the

integration over an interval by breaking the area down into trapezoids with more easily computable areas [49].
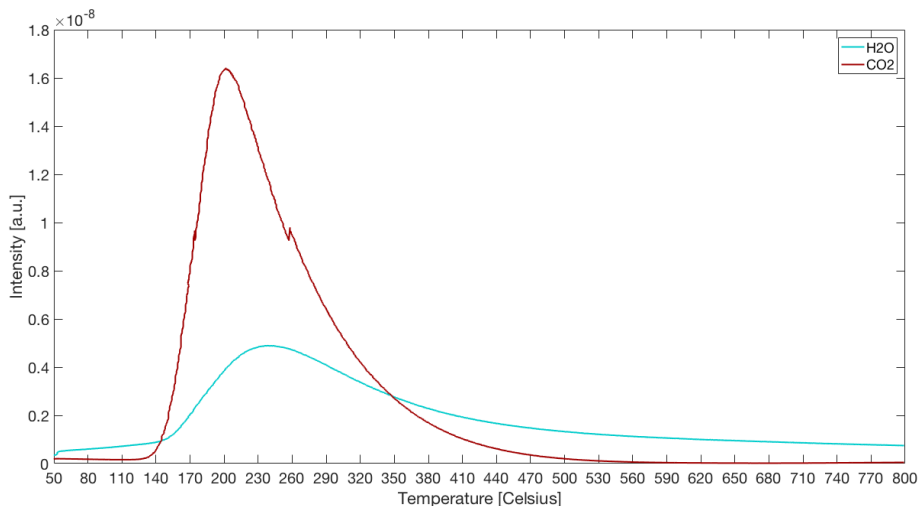
Figure 4.26: The mass spectrum measuring the formation of molecules with a molar mass of 44 g/mol (CO_2) and 18 g/mol H_2O for a test sample of $NaHCO_3$ in standard atmosphere (75ml/min Air and 25ml/min Argon) without pre-drying.

4.3.2   P-Series and Sample C1

In Figures 4.27-4.30 the mass loss and heat exchange for samples P2, P4 and P5 from the P-series as well as the mass loss and heat exchange for the C1 sample are shown. Since the amount of sample mass for the P-series was very low not all sample were tested in the TGA. The TGA is a destructive technique and requires large amounts of sample mass compared to the other characterization techniques. All samples were measured in standard atmosphere and without pre-drying in air.

For the P-series samples the mass loss is hard to quantify since the changes are very small (<0.2). There is also mass fluctuates within each sample instead of a continuously mass loss as seen in the $NaHCO_3$. In sample P2 the mass difference is almost zero, while P4 has several sharp peaks where the mass jumps up and down. However, the fluctuation in P4 is very small with the highest peak just under 100 % and the lowest peak point at just under 99.8 %.
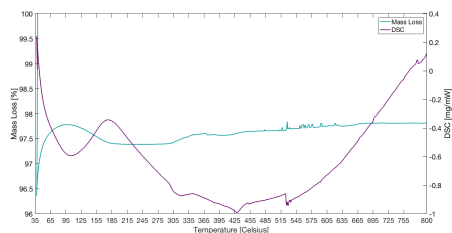
Figure 4.27: The mass loss[%] and heat exchange[mg/mW] for the P2 sample of reacted contact mass, extracted at 21.5 hours, in standard atmosphere (75ml/min Air and 25ml/min Argon) without pre-drying.
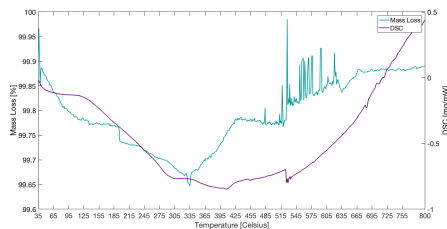
Figure 4.28: The mass loss[%] and heat exchange[mg/mW] for the P4 sample of reacted contact mass, extracted at 46 hours, in standard atmosphere (75ml/min Air and 25ml/min Argon) without pre-drying.
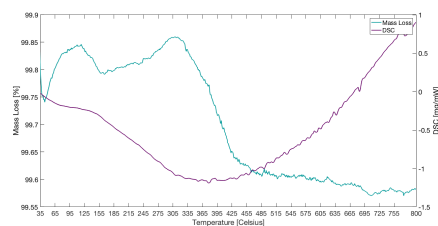
Figure 4.29: The mass loss[%] and heat exchange[mg/mW] for the P5 sample of reacted contact mass, extracted at 51 hours after termination of the experiment, in standard atmosphere (75ml/min Air and 25ml/min Argon) without pre-drying.
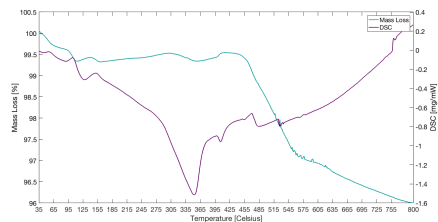
Figure 4.30: The mass loss[%] and heat exchange[mg/mW] for the C1 sample of reacted contact mass, extracted after termination of the experiment, in standard atmosphere (75ml/min Air and 25ml/min Argon) without pre-drying.

Of the P-samples only P5 has a clear mass loss interval at around 320 °C until 450 °C. The mass loss is quite small with only a 0.23% difference for P5. All P-sample have a similar heat exchange curve with the lowest point around 400 °C for P5 and P4, while the lowest point for P2 is found at around 430 °C.

The sample C1 has the largest mass loss in the temperature interval 450 °C - 580 °C where it loses approximately 2.5 % mass. The sample also has a clear exothermic peak at 350 °C with an intensity of 1.5 mg/mW.

The mass spectra for CO_2 and H_2O are shown in Figure 4.31 - 4.34. All spectra have peaks for CO_2 around the temperature interval 275 °C- 515 °C. P2 has the widest peak while P4 has the most narrow peak for CO_2. P5 also has an extra peak for CO_2 from 35 °C until 275 °C. The sample C1 has the most intense CO_2 peak of all the samples.
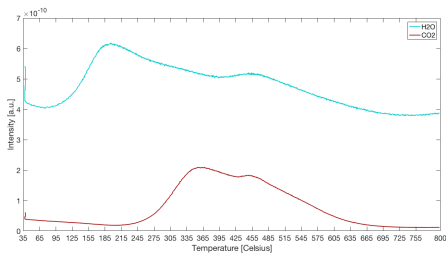
Figure 4.31: The mass spectrum measuring the formation of molecules with a molar mass of 44 g/mol (CO_2) and 18 g/mol H_2O for sample P2 in standard atmosphere (75ml/min Air and 25ml/min Argon) without pre-drying.
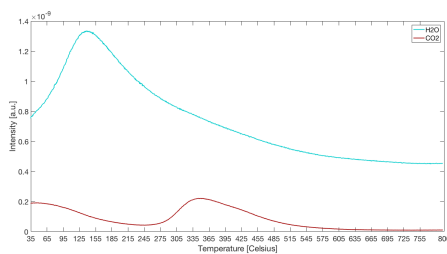
Figure 4.32: The mass spectrum measuring the formation of molecules with a molar mass of 44 g/mol (CO_2) and 18 g/mol H_2O for sample P4 in standard atmosphere (75ml/min Air and 25ml/min Argon) without pre-drying.
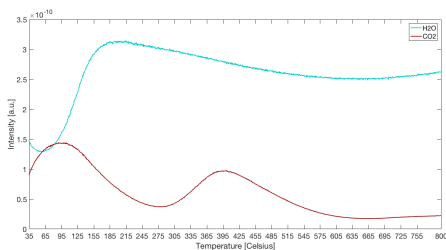
Figure 4.33: The mass spectrum measuring the formation of molecules with a molar mass of 44 g/mol (CO_2) and 18 g/mol H_2O for sample P5 in standard atmosphere (75ml/min Air and 25ml/min Argon) without pre-drying.
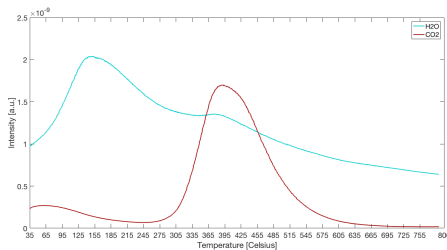
Figure 4.34: The mass spectrum measuring the formation of molecules with a molar mass of 44 g/mol (CO_2) and 18 g/mol H_2O for sample C1 in standard atmosphere (75ml/min Air and 25ml/min Argon) without pre-drying.

The H_2O peaks are harder to distinguishes, but all samples have peaks in low temperature ranges (<200°C) which are most likely related to drying. Sample P2 and C1 also have a secondary H_2O peak at higher temperatures which appears around the same temperature as the CO_2 peak.

The peak area for H_2O and CO_2 was calculated by using the trapz function in MATLAB. Equation 4.1 was then used to calculated the ratio of hydrogen to carbon in the samples. For sample P5 only the second CO_2 peak was taken into consideration since it is unlikely that CO_2 was formed at the low temperatures of the first peak.

$$\frac{Area_{H2O}}{Area_{CO2}} \cdot RF \qquad (4.1)$$

where RF is the response factor for the TGA found by running a standard sample of $NaHCO_3$ and dividing the resulting peak area of CO_2 on the peak area measured for H_2O. The response factor was found to be 2.15. The resulting H/C ratios are given in Table 4.2

Table 4.2: The Table show the H/C ratio for the samples P2, P4, P5 and C1. The ratio was calculated for the mass spectroscopy done on each sample.

Sample	Ratio
P2	5.44
P4	4.79
P5	2.53
C1	2.93

4.3.3 Sample EL1 and Sample EL2

Figure 4.35 shows the mass loss and the heat exchange for the sample EL1 while Figure 4.36 shows the mass loss and heat exchange for sample EL2. A mass loss of about 1 % from 35 °C until 260 °C and a mass loss of around 1.5% from 260 °C until 430 °C can be seen in sample

EL1. The mass loss for sample EL2 is more continues and the sample has a total mass loss of about 0.8 %. In sample EL1 there is a exothermic peak with an intensity of 1.5 mg/mW at 322 °C while the heat exchange in sample EL2 is more similar to P2, P4 and P5 with the lowest values around 425 °C and no clear exothermic peak.
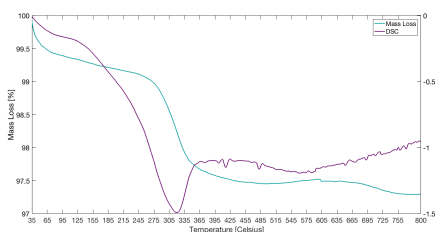
Figure 4.35: The mass loss[%] and heat exchange[mg/mW] for the EL1 sample of reacted contact mass, extracted after termination of the experiment, in standard atmosphere (75ml/min Air and 25ml/min Argon) without pre-drying.
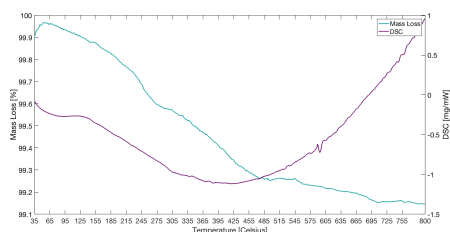
Figure 4.36: The mass loss[%] and heat exchange[mg/mW] for the EL2 sample of reacted contact mass, extracted after termination of the experiment, in standard atmosphere (75ml/min Air and 25ml/min Argon) without pre-drying.

Both runs where done at standard conditions without drying. The mass loss and heat exchange figures for all other conditions can be found in Appendix A.1.

4.3.4 Reference Sample

Figure 4.37 shows the mass loss and heat exchange of the reference sample, REF, in standard atmosphere without pre-drying. An increase in mass for the sample can clearly be seen in Figure 4.37. The increase in mass was recorded in all thermal gravemetric analysis done with the reference sample, REF, both in inert atmosphere and in standard atmosphere as well as with and without pre-drying in air.

The mass accumulated for the REF sample was approximately 0.8%, 0.4%, 0.25% and 0.14% for measurements done in: standard atmosphere, standard atmosphere with pre-drying, inter atmosphere and inter atmosphere with pre-drying.
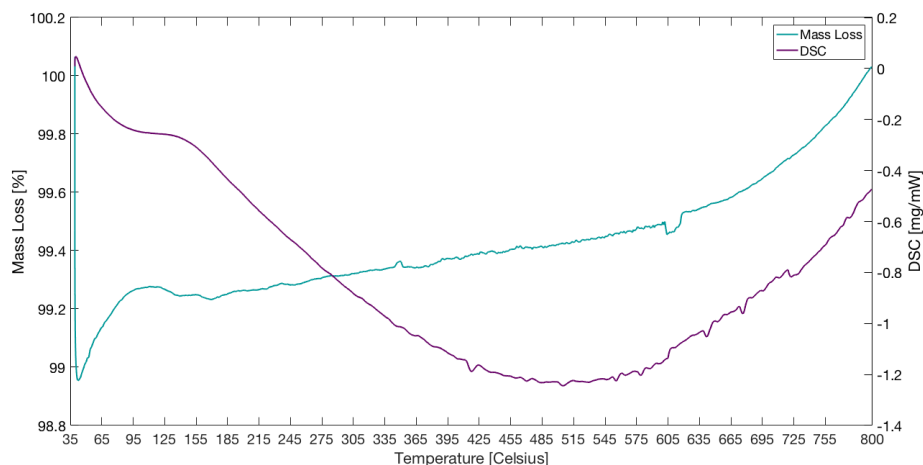
Figure 4.37: The mass loss[%] and heat exchange[mg/mW] for the reference sample, REF, in standard atmosphere (75ml/min Air and 25ml/min Argon) without pre-drying.

Figures showing mass loss and heat exchange for inert atmosphere (100ml/min argon) with and without pre-dryin and standard atmosphere (75ml/min air and 25ml/min) with pre-drying are included in Appendix A.1

4.4 Pyrolysis GC/MS

As a result of the pyrolysis GC/MS experiment several mass spectra were collected and compared to the NIST database to identify the different organic content in each sample. Only the P-series (P1,P2,P3,P4 and P5) where investigated using the pyrolysis GC/MS. Figures 4.38 - 4.42 show the different spectra for the P-series, with the most intense peaks labeled with their corresponding RT-value. The Tables 4.3-4.7 give the organic content present in each sample. Only organic content which was labeled by NIST as having a quality of 70 or higher was taken into account, as is common practice with this instrument.
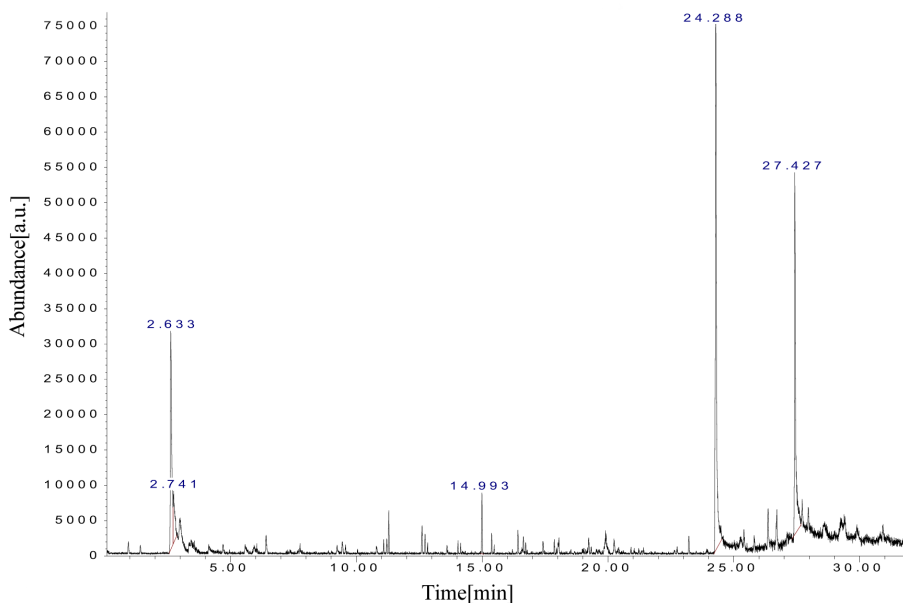
Figure 4.38: The mass spectrum obtained from the pyrolysis GC/MS experiment done at 500°C for the P1 sample, where the most clear peaks have been labeled.

For sample P1 the organic content that was found with the NIST database and its correspond abundance in the sample is shown in Table 4.3.

Table 4.3: The organic content of sample P1 that had a quality of 70 or higher with corresponding abundance and RT. The total amount of organic content is the summation of all detected content not only the content with high quality.

Organic Content	RT[min]	Abundance[a.u]
Carbon dioxide	2.633	30444
Ethanol, 2-(2-butoxyethoxy)-, acetate	14.993	8115
n-Hexadecanoic acid	24.288	75756
Octadecanoic acid	27.427	51130
Total amount		172474
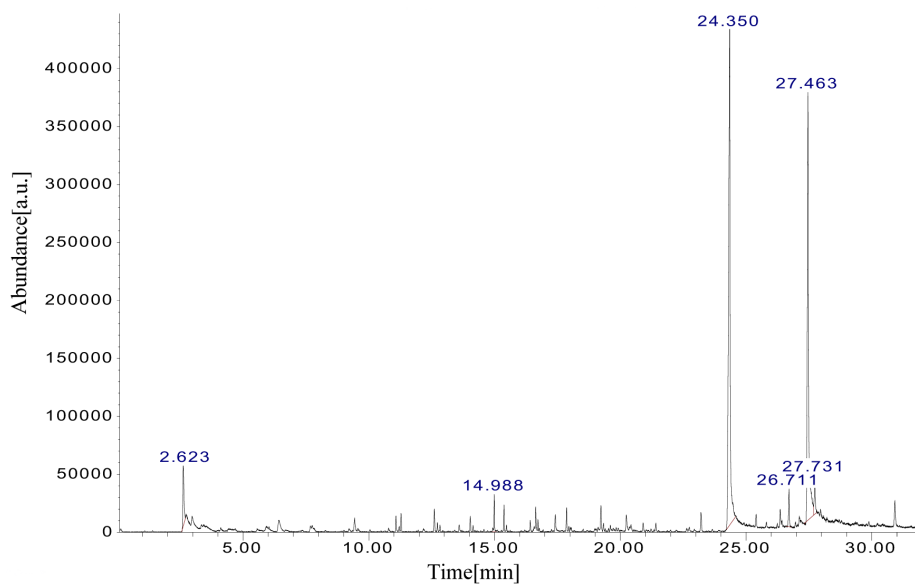
Figure 4.39: The mass spectrum from the pyrolysis GC/MS experiment done at 500°C for the P2 sample, where the most clear peaks have been labeled.

For sample P2 the organic content that was found with the NIST database and its correspond abundance in the sample is shown in Table 4.4.

Table 4.4: The organic content of sample P2 that had a quality of 70 or higher with corresponding abundance and RT. The total amount of organic content is the summation of all detected content not only the content with high quality.

Organic Content	RT[min]	Abundance[a.u]
Carbon dioxide	2.623	51607
Ethanol, 2-(2-butoxyethoxy)-, acetate	14.988	31674
n-Hexadecanoic acid	24.350	440141
Heptadecanenitrile	26.711	31396
Octadecanoic acid	27.463	368432
Total amount		956323
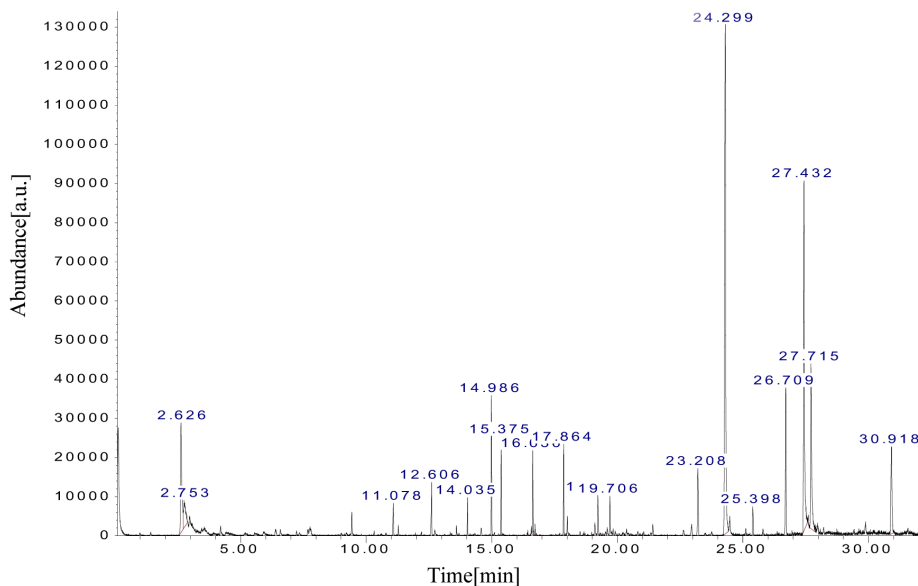
Figure 4.40: The mass spectrum from the pyrolysis GC/MS experiment done at 500°C for the P3 sample, where the most clear peaks have been labeled.

For sample P3 the organic content that was found with the NIST database and its correspond abundance in the sample is shown in Table 4.5.

Table 4.5: The organic content of sample P3 that had a quality of 70 or higher with corresponding abundance and RT. The total amount of organic content is the summation of all detected content not only the content with high quality.

Organic Content	RT[min]	Abundance[a.u]
Carbon dioxide	2.626	28056
Ethanol, 2-(2-butoxyethoxy)-, acetate	14.986	35699
5-Octadecene, (E)-	15.375	24974
n-Hexadecanoic acid	24.299	132440
Hexadecanenitrile	26.709	37672
Octadecanoic acid	27.432	89211
Hexadecanamide	27,715	41556
Tetradecanamide	30.918	22248
Total amount		537220
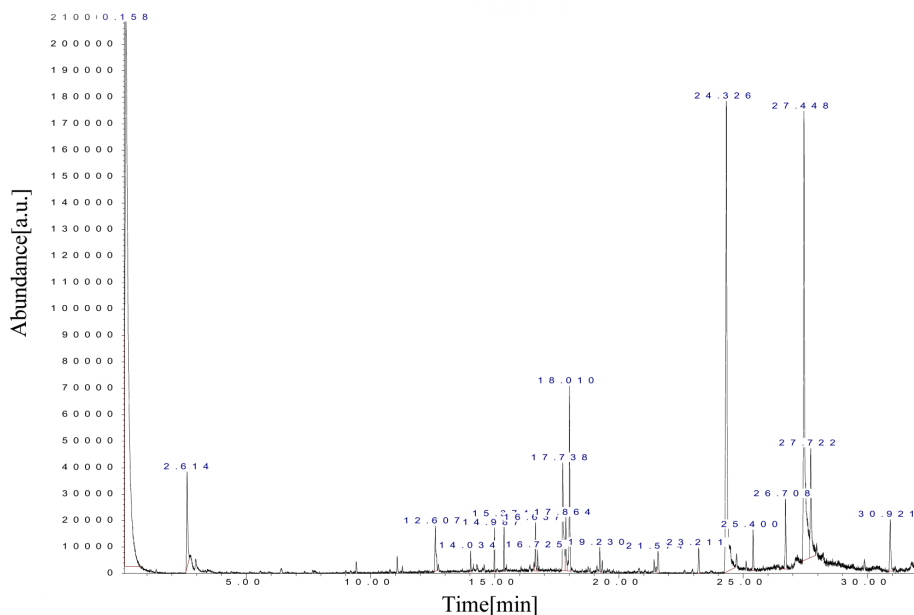
Figure 4.41: The mass spectrum from the pyrolysis GC/MS experiment done at 500°C for the P4 sample, where the most clear peaks have been labeled.

For sample P4 the organic content that was found with the NIST database and its correspond abundance in the sample is shown in Table 4.6.

Table 4.6: The organic content of sample P4 that had a quality of 70 or higher with corresponding abundance and RT. The total amount of organic content is the summation of all detected content not only the content with high quality.

Organic Content	RT[min]	Abundance[a.u]
Carbon dioxide	2.614	35570
Ethanol, 2-(2-butoxyethoxy)-, acetate	14.987	16414
9-Octadecene, (E)-	15.374	19415
Diethyl Phthalate	17.738	40267
Diethyl Phthalate	18.010	70064
n-Hexadecanoic acid	24.326	177834
Octadecanenitrile	26.708	26380
Octadecanoic acid	27.448	167962
Hexadecanamide	27.722	40424
Tetradecanamide	30.921	18665
Total amount		724962
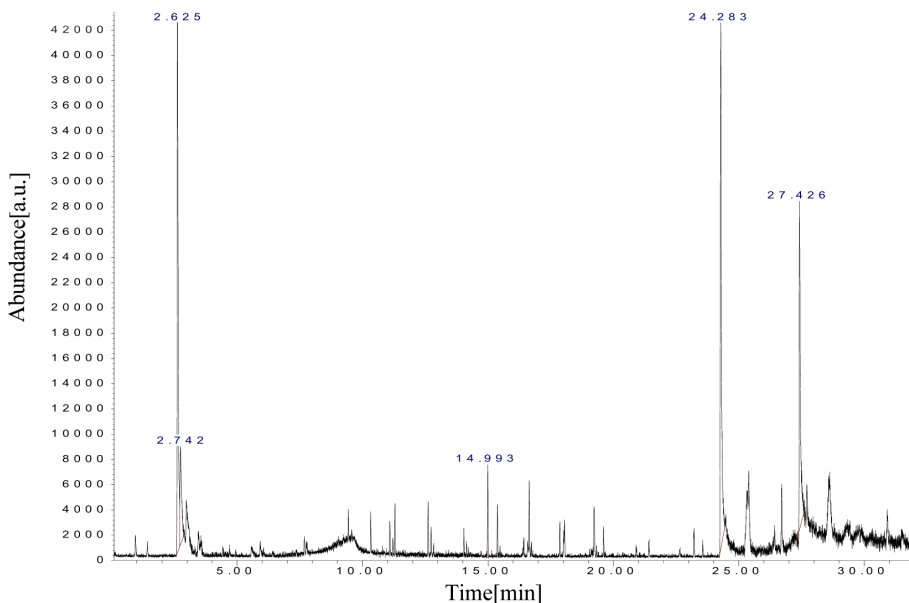
Figure 4.42: The mass spectrum from the pyrolysis GC/MS experiment done at 500°C for the P5 sample, where the most clear peaks have been labeled.

For sample P5 the organic content that was found with the NIST database and its correspond abundance in the sample is shown in Table 4.7.
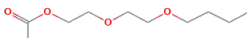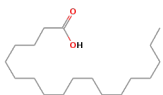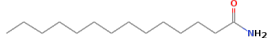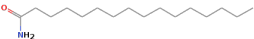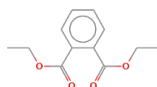
Table 4.7: The organic content of sample P5 that had a quality of 70 or higher with corresponding abundance and RT. The total amount of organic content is the summation of all detected content not only the content with high quality.

Organic Content	RT[min]	Abundance[a.u]
Carbon dioxide	2.625	42736
Ethanol, 2-(2-butoxyethoxy)-, acetate	14.993	7071
n-Hexadecanoic acid	24.283	41978
Octadecanoic acid	27.426	25605
Total amount		124939

Only content which had a quality of 70 or higher was taken into account for each sample in hopes of decrease the uncertainty in the classification of the organic content. An exception for CO_2 was made since previous knowledge indicate the presence of CO_2 species.

In Table 4.8 all organic content detected during the pyrolysis GC/MS
is given. The table shown in which sample the different organic com-
pounds are present and also shows the structure of each compound.
There are only four compound which are present in all sample while
several compound are only present in P2, P3, and P4.

Table 4.8: All organic content found in the P-series by the Pyrolysis GC/MS and the
NIST library. All organic content given in this table had a quality of 70 or higher
according to NIST library.

Organic Content	Illustration	Formula	Found In
5-Octadecene, (E)-		$C_{18}H_{36}$	P3
9-Octadecene, (E)-		$C_{18}H_{36}$	P4
Carbon Dioxide		CO_2	P1,P2,P3,P4,P5
Ethanol, 2- (2-butoxyethoxy)-, acetate		$C_{10}H_{20}O_4$	P1,P2,P3,P4,P5
Hexadecanenitrile		$C_{16}H_{31}N$	P3
Heptadecanenitrile		$C_{17}H_{33}N$	P2
Octadecanenitrile		$C_{18}H_{35}N$	P4
n-Hexadecanoic acid		$C_{16}H_{32}O_2$	P1,P2,P3,P4,P5
Octadecanoic acid		$C_{18}H_{36}O_2$	P1,P2,P3,P4,P5
Tetradecanamide		$C_{14}H_{29}NO$	P3,P4
Hexadecanamide		$C_{16}H_{33}NO$	P3,P4
Diethyl Phthalate		$C_{12}H_{14}O_4$	P4

4.5   Fourier Transform Infrared Spectroscopy

All spectra achieved by the FT-IR measurements are shown in the Figures 4.43 - 4.46. The most prominent peaks are labeled with their corresponding wavenumbers. All peaks were found to have a quite low absorbance. Due to little sample amount at the time of the FT-IR investigation only P5, P2, C1 and REF could be investigated.

For the P5 sample five peaks have been labeled at 1014 cm^{-1},1269 cm^{-1}, 2357 cm^{-1}, 3352 cm^{-1} and 3445 cm^{-1}.The abortions correspond to the functional groups Si-OR, Si-CH$_3$, Si-H and O-H for both peaks at over 3000[50].
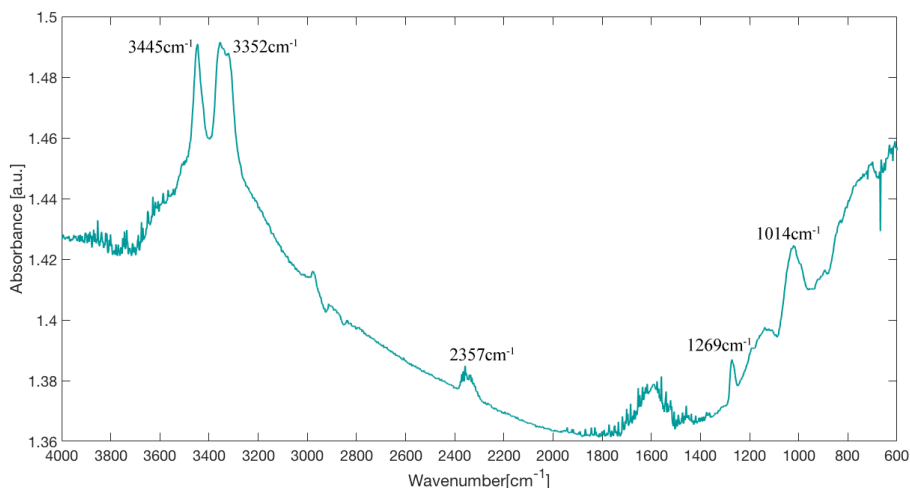
Figure 4.43: FT-IR spectrum within the wavenumber range of 600-4000cm^{-1} of the P4 sample without any noise reduction and with the most prominent peaks label with the corresponding wavenumber.

The spectrum for the C1 sample has only one clear peak at 1020 cm^{-1} even though there are several low intensity peaks that could correspond to functional groups and a shoulder peak at over 3000 cm^{-1}, only the Si-OR bond at 1020 cm^{-1} could be identified[50].
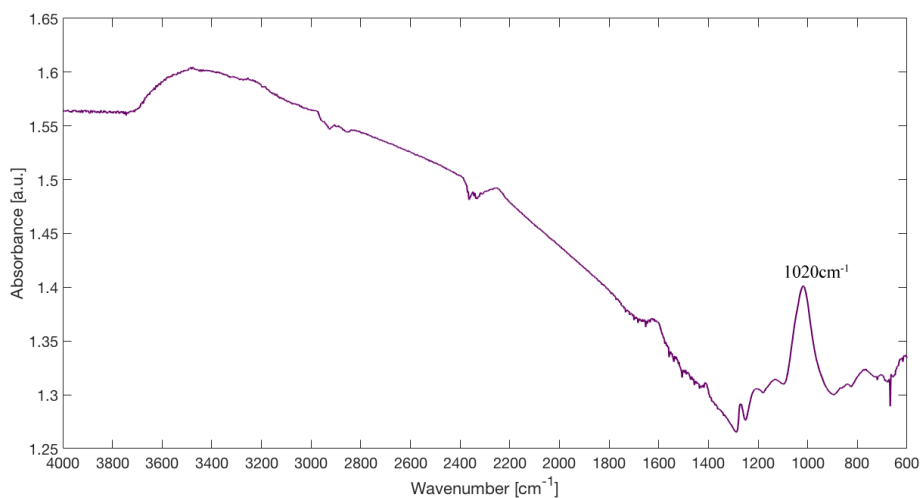
Figure 4.44: FT-IR spectrum within the wavenumber range of 600-4000cm^{-1} of the C1 sample without any noise reduction and with the most prominent peaks label with the corresponding wavenumber.

The peak at 968 cm^{-1} correspond to the Si-O stretching bond[50].
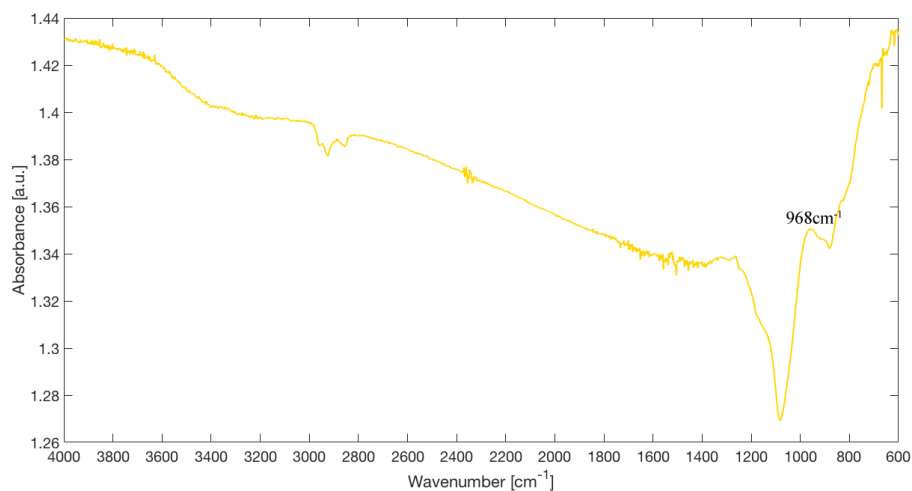
Figure 4.45: FT-IR spectrum within the wavenumber range of 600-4000cm^{-1} of the P2 sample without any noise reduction and with the most prominent peaks label with the corresponding wavenumber.

Figure 4.46 shows the spectrum for the reference sample which has to peaks both corresponding to silicon bonds. One bond for the Si-O stretching bond at $952 cm^{-1}$ and one bond for the Si-H at $2357 cm^{-1}$.[50]
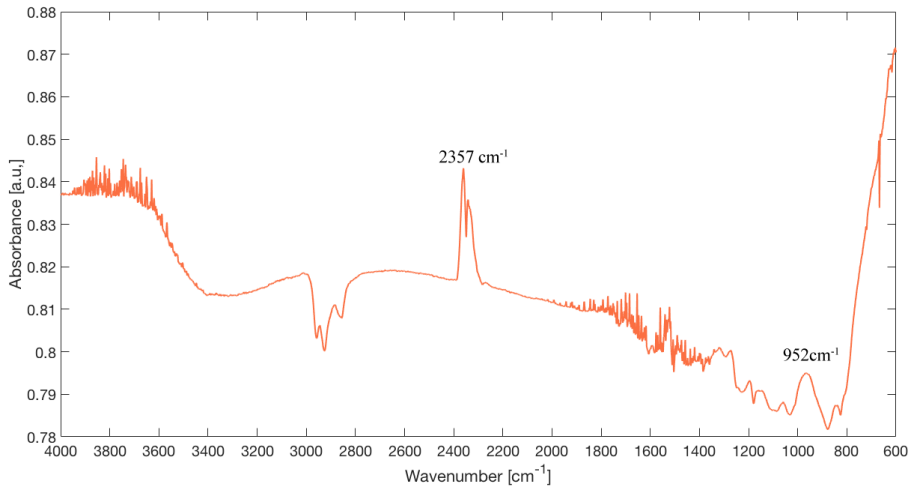
Figure 4.46: FT-IR spectrum within the wavenumber range of $600\text{-}4000 cm^{-1}$ of the REF sample without any noise reduction and with the most prominent peaks label with the corresponding wavenumber.

4.6 X-ray Diffraction

For the XRD measurements the samples EL1, EL2, P3, P4 and P5 were tested with the same program as described in Chapter 3. The results for EL1 and EL2 are shown in Figure 4.47 while the result for P3, P4 and P5 are shown in Figure 4.48. Both figures also contain the PDF (powder diffraction file) card 00-027-1402 for silicon which shows the standard peaks for silicon as a comparison to the samples.
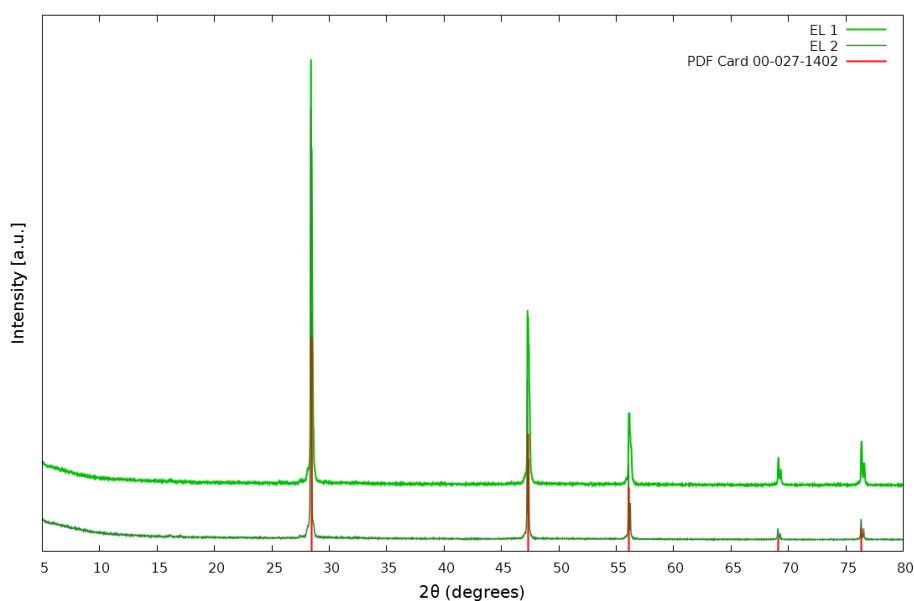
Figure 4.47: The X-ray diffractogram obtain for sample EL1 and sample EL2 in Bragg-Brentano geometry within the 2θ range of 5-80° . The largest peaks have been modified to have the same intensity for both peaks so as to make the comparison easier. Diffraction lines of Si are included as references at the bottom (red, PDF card: 00-027-1402).

The X-ray diffractograms of the El1 and EL2 samples are given in Figure 4.47, were the diffractograms have been modified so the first peak has the same intensity for both EL1 and El2. EL1 and EL2 have nearly identical patterns and one can clearly see in Figure 4.47 that both samples have peaks that corresponds to the PDF card 00-027-1402 with the larges peak at around 28° 2θ.
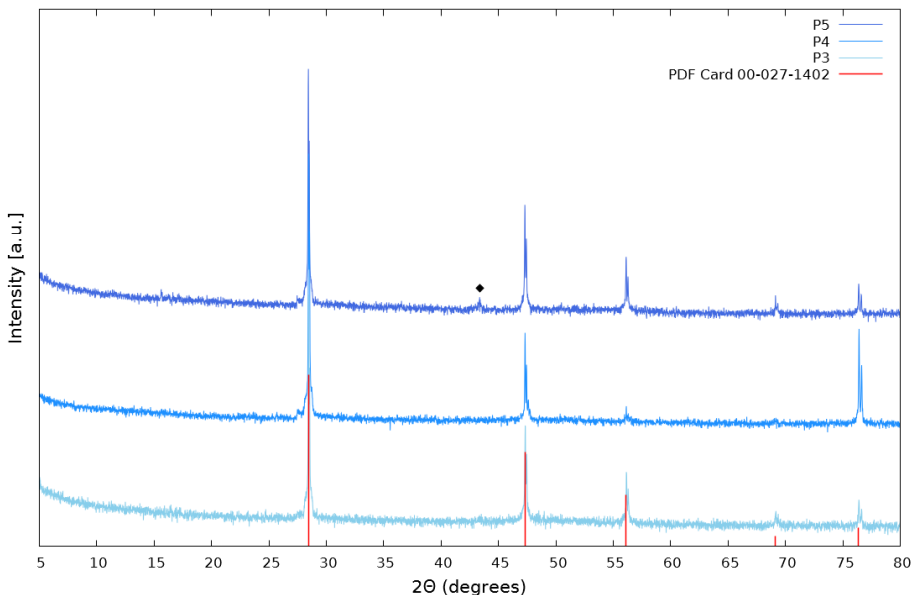
Figure 4.48: The X-ray diffraction diffractogram obtain for sample P3, sample P4 and sample P5 in Bragg-Brentano geometry within the 2θ range of 5-80°. The largest peaks have been modified to have the same intensity for both peaks so as to make the comparison easier. ♦ is assigned to a copper reflection (PDF card: 00-004-0836). Diffraction lines of Si are included as references at the bottom (red, PDF card: 00-027-1402).

The measurements for the P-samples are also very similar, but have some small variation in the peak intensity for each sample. However, the trend is very similar and also here the peak around 28 2θ degrees is more intense than the other peaks. Also Figure 4.48 have had the diffractograms modified so that the first peak has the same intensity for P3, P4 and P5.

The 28° 2θ peak correspond to the peak range for silicon(111). While the smaller peaks at around 47°, 56°, 69 ° and 77° 2θ corresponds to silicon(220), silicon(311), silicon(400) and silicon(331) respectively[51].

4.7 X-Ray Fluorescence

The results for the X-ray fluorescence (XRF) are given in the Figure A.21
in Appendix. A A silicon sample, which is used for control and calibra-
tion purpose, was tested in the XRF. This was done after last semesters
measurements (results from the specialization project TKP4580) did
not yield the desired result. The raw silicon sample was compared to
the XRF measurement done by Elkem. Due to the discrepancies be-
tween the Elkem measurement and the measurement done this year
it was decided not to precede with the XRF characterization. The high
uncertainties found both in this semester and last semester most likely
stem form the pellet preparation method described in Chapter 3.

5. Discussion

5.1 Surface Morphology

The surface investigations of the reference sample, REF, and the P-series of reacted contact mass were done to better understand how the contact mass changes as the reaction presides.

The surface morphology of the reference sample, REF, is shown in both Figures 4.1 and 4.11 at different magnifications. Both SEM micrographs show particles deposited onto the surface both on the edges of the particle, on the surface irregularities and on the plane surfaces. These particles might be silicon dust and or smaller silicon particles deposited onto the surface.

Oxygen and tin was found at all point investigated by the SEM for the REF samples. Carbon was only found at the spots that contained copper. The copper, tin and carbon are most likely just traces and impurities found within the silicon. There is a small indication in the EDX figure shown in Figure 4.21 that more oxygen is located in the same spot at the larges deposited particle/silicon dust. This might be due to a oxide layer formed on the particle and in therms might indicate that these particles are more exposed to oxidation.

The EDX measurements of sample P1 shows that even early in the reaction (4 hours) large amounts of copper is found within the reaction pits. There is still copper present all through the sample, but only in small amounts compared to the spots, which corresponds to the reaction pits on the surface. The oxygen is also present in large amount in the reaction pits while the silicon seem to have be depleted in the spots corresponding to the reaction pits. It is unknown if this is because copper migrates to these spot during reaction, or if the reaction pits are formed in these spots because they were already rich in copper.

When it comes to the distribution of carbon in the contact mass, no clear correlation can be seen from the EDX result. There are indications that carbon richer spots could be correlated to copper rich spots, and there was also some indication that oxygen and carbon was present in larger amount in the same locations (see Figure 4.20).

5.2   Raman and IR spectroscopy

For the Raman investigation Figures 4.22, 4.24 and 4.23 show that all nine samples contain similar peaks. The peak located between 517-519 cm^{-1} is found in all samples and has a much higher intensity (more than 20 times as intense) than all other peaks in the spectra. The 517-519 cm^{-1} peak is related to crystalline silicon which is usually found at 519±1 cm^{-1} [52,53]. This correlates to the crystalline structure measured with the XRD and the fact that the contact mass consists mainly of silicon.

The four other peaks before 1000 cm^{-1} are also related to the silicon in the contact mass. As mentioned in the result section the spectra measured for the nine Elkem samples all correspond to previous Raman studies of the silicon spectrum in visible light [46–48,52,53]. However, other species than silicon could be contributing to the spectra. The peaks at around 430 cm^{-1} and 615 cm^{-1} could both be related to copper species containing either oxygen or chlorine [54,55]. The EDX shows that copper, oxygen and chlorine all overlap with each other when it comes to their distribution. It is a possible that the peaks around 430 cm^{-1} and 615 cm^{-1} in the Raman spectra are influenced by oxidized or chlorinated copper.

However, the peaks also show up in the reference sample, REF, which has not been exposed to methyl chlorine meaning that chlorinated copper species could not be an influence on the peaks at around 430 cm^{-1} and 615 cm^{-1} for the REF sample. The EDX results shows that there is oxygen present in the reference sample, REF, so influences due to oxidized copper species are still a possibility. Since both peaks around 430 cm^{-1} and 615 cm^{-1} are very small, identifying them is hard. In for example sample P5, where none of the peak

are labeled in Figure 4.22, there are still small peaks/bumps in the baseline that could correspond to the peaks. They are however not prominent enough to be labeled as peaks for sure. The same can be said for samples EL1 and EL2 as well.

For the shoulder peak at around 940 cm^{-1} not only range, but the characteristic shape of the peak stays the same in all spectra. The peak is related to silicon modes/overtones and might indicate the present of Si-H in the samples[50,52]. The FTIR result indicates that both the reference sample, REF, and the P5 samples could contain the Si-H bond.

The two last peaks shown in Figures 4.22, 4.24 and 4.23 are both related to carbon species. The first peak is found at around 1310 cm^{-1} and the second peak at around 1600 cm^{-1}. The two peaks correspond to two common peaks found within the spectra of carbon species. These are the peaks for disordered graphite where a peak referred to as the D peak is located at around 1350 cm^{-1} and a peak called the G peak is located at around 1580-1600 cm^{-1}. Since both peaks are found in P2-P5 and the EL samples it would seem like the carbon species are of graphite form. Carbon with diamond structure on the other hand has only one peak at 1332 cm^{-1} which is quite sharp[44]. It has also been reported quite large amount of the diamond phase must be present for this peak to appear in a spectrum. Another peak at 1060 cm^{-1} called the T peak has been reported to be present in the UV excitation for amorphous carbon. As reported in the result section, a test in the UV-range with a 325 laser was done on sample P5. The test showed no peaks around 1060 cm^{-1} in the P5 sample[56]. However, the present of D and G peaks of varying intensity, width and position have been reported for nanocrystalline and amorphous carbons even without widespread graphitic ordering so classifying the carbon species present here from only these two peak should be done with caution[44].

Measuring the quantity from Raman spectroscopy is not possible for these samples, but by comparing the carbon peak it would seem that much of the carbon species are first formed between P1 (4 hours)

and P2 (21.5 hours), and there after between sample P2 (21.5 hours) and P3 (27.5 hours). For the peaks in the spectra for P3, P4 and P5 it is hard to see any significant difference in peak intensity for the D ($1310cm^{-1}$) and G (1600^{-1}) peak. This might indicate that not much new carbon is formed in the time interval between these samples. The difference in peak size from P1 to P2 also corresponds to the large difference in amount of organic content measured for the P1 sample and the P2 sample in the GC/MS. It should also me mentioned that compared to the main silicon peak the peaks related to the carbon modes are quite small even though carbon modes are usually very good Raman scatters. This indicates that there is very little carbon species in present in the sample P2-P5, EL1 and EL2. A result which is also indicated by the thermal gravimetric analysis.

For the the D peak and G peak the ID/IG ratio was calculated for all samples. It has been reported that an increasing ID/IG ratio is linked to increasing disorder in the carbon structure when compared with graphite. This is because the mode corresponding to the D peak is forbidden in perfect graphite and only becomes active with the Raman spectrum when there is disorder present[44]. The ratios are shown Table 4.1 and P4 is shown to have the highest ratio and therefore the highest order of disorder.

The FTIR was run to look for the O-H bond which showed up in GC/MS measurements. The O-H bond was found in the P5 sample. Unfortunately, due to lack of sample amount for both P4 and P3 these samples could not be tested in the FTIR. Sample P2 showed no clear peaks for the O-H bond in the FTIR and the only bond found in the P2 sample where the Si-O bond at 968 cm^{-1} which was present in all sample tested in the FTIR. This is unsurprising since the present of oxygen was detected both with the EDX and the fact that CO_2 was formed in the inert conditions of both the GC/MS and the TGA. However, the peaks in the FTIR are quite unclear and once again of quite low intensity, therefore the line between noise and peak is somewhat unclear. Only the clearest peaks have been labeled in the FTIR and previous knowledge of what was present in the contact mass have been taken into account when labeling the peaks.

5.3 Thermal Investigation

The thermal gravimetric analysis was done on the reacted contact mass of the P2 sample, the P4 sample, the P5 sample, the C1 sample, the EL1 sample, the EL2 sample as well as the unreacted contact mass of the REF sample. This was done to gain insight into how much carbon species were present in each sample and the H/C ratio of each sample according to the mass spectra measured in standard atmosphere. However, the result obtained in the thermal gravimetric analysis leaves much to be desired.

The mass loss for all samples fluctuated throughout the analysis and allover, very little mass loss was measured for each sample. In the REF sample no mass loss was recorded since the mass increased thought the measurement. The standard sample test of $NaHCO_3$ showed a mass loss of around 40% while the contact mass samples all had a mass loss lower than 1.5 % indicating that the allover mass loss is very low for these sample. The three most prominent mass losses happened in P5, C1, EL1 at the intervals of 330°C-450°C, 450°C-580°C and 270°C-390°C respectively. The mass losses of samples P5, C1 and EL1 are most likely related to the formation of CO_2 since CO_2 peaks occur in the mass spectra in the same temperature intervals for all samples(Figures 4.31 - 4.34) .

The sharp exothermic peak seen in Figure 4.30 for the C1 sample and in Figure 4.35 for the sample EL1 indicates that formation of CO_2 is related to the mass loss. It should be noted that the exothermic peak in C1 seem to have shifted done from the expected temperature interval (450°C-580°C) which makes it uncleared if the peak is actually only correlated to the formation of CO_2.

While most of the mass loss seems related to the formation of CO_2 the mass spectra also indicated that H_2O is formed as the samples are heated in a standard atmosphere (75ml/min Air and 25ml/min argon). It is expected that much of the H_2O measured in the mass spectra(Figures 4.31 - 4.34) stems from the samples drying and water being released from the samples as the temperature rises. This is

supported by the fact that lower mass loss was measured when the samples were dried overnight before TGA analysis, and that most water peak in the mass spectra are located at temperature below 150°C.

For the P2 sample and the C1 sample some small indication of H_2O formation at higher temperatures (>150°C) in the mass spectra. The formation of H_2O is most likely not due to water formation or drying of the samples. The formation could indicated the release of hydrogen from either C-H bond or O-H bond with in the carbon species. This would happen at higher temperature and the pyrolysis data for both sample P2 and P5 indicates that hydrogen is present in large amount in the organic content within the samples.

For the calculated H/C ratio and decreases in the ratio was seen from P2 (21.5 hours), P4 (46 hours) and P5 (51 hours) which might indicate that the ratio decreases as the reaction continues. In other word there is less hydrogen present in sample P5 than in P2.

As mentioned above accumulation of mass loss was recorded for the reference sample, REF. It was expected that this sample would have little to no mass loss and if mass loss occurred it would related to the formation of H_2O due to drying. However, the REF sample showed mass accumulation during the measurement, and even though the mass accumulation was low (0.8% in standard atmosphere without pre-drying) this might indicate that the sample is oxidizing within the TGA. Previous studies have reported that contact mass form the direct process oxides during TGA measurements[24] it is also know that silicon can oxidize even at room temperatures, and most of the contact mass consist of silicon making it prone to oxidation and interaction with oxygen. The accumulation could indicate some oxidation happening in the sample and since it is known that silicon oxidizes even at room temperature it is not fare fetch to believe that the reference contact mass that is mainly silicon could oxidize. The contact mass oxidizing under increased temperatures would mean that even though mass is lost as CO_2 and H_2O is formed, mass could simultaneously be gained through oxidation of silicon making it impossible to measure the total

mass loss of the sample with any accuracy.

5.4   Organic Content

The Organic content in each sample in the P-series was investigated with the Pyrolysis GC/MS. All organic content found in the samples are given in Table 4.8. The GC/MS was only done on the sample from the P-series(P1, P2, P3, P4, P5). Some organic content is present in all samples such as CO_2, $C_{10}H_{20}O_4$, $C_{16}H_{32}O_2$ and $C_{18}H_{36}O_2$ while several other compound are only found in one sample. Even though there is variation in the organic content found in the P-series one common factor is that most of the organic content consist of long carbon chains.

Several acids, amides, nitriles and even an ester were found to be present in the P-series. The structure of each organic compound can be complicated, one should be careful when stating with any certainty that the compounds given in Table 4.8 are present in each sample. However the presence of at the O-H bond was also found by the FT-IR spectroscopy on sample P5 which indicates that acids and alcohols could be present in this sample.

The pyrolysis measurements are done in inert conditions meaning that all the oxygen present in compound such as CO_2 must have come from the samples themselves. From the EDX result one already knows that there are oxygen present in all the samples from the P-series. By looking at how much CO_2 was measured for each sample (30 444, 51 607, 28 056, 35 570, 42 736 for P1, P2, P3, P4, P5 respectively) one sees that the P2 has the largest abundance of CO_2. The amount of CO_2 formed might indicate how much oxygen is present in the sample. No more CO_2 can be formed when no more oxygen can be released from the sample, making oxygen a limiting factor for the CO_2 formation.

Oxygen being a limiting factor in the CO_2 production is also alluded to when comparing the ratio of CO_2 to the total amount of

organic content within the sample. For P1, P2, P3, P4, P5 the fraction of CO_2 compared to the total amount or organic content found in the pyrolysis is; 0.18, 0.05, 0.05, 0.05, 0.34. Even tough the organic content increases, the CO_2 does not increase much, staying much in the same size range for the whole P-series. Even the samples that contain a lot of organic content such as P2, P3 and P4 sees little increase in CO_2 measured.

It is also notable that many organic compounds seem to disappear in sample P5. The difference between which compound is found in P2, P3 and P4 are mostly due to nitriles, alkenes and amides slightly changing the orientation and/or length of the carbon chain which can be explained by carbon chain growth and/or slight difference in the identification of each compound trough the NIST library. From sample P4 to P5 however all alkenes, amides and nitriles disappear. The P5 sample is the contact mass that is left after the reaction is terminated which could have impacted the carbon species. The extraction method and cooling were both done in inert condition according to Elkem so this should not have impacted the organic content drastically.

The pyrolysis uses very little sample mass (0.5mg - 1mg) and the contact mass is a very non-homogeneous sample. It could therefore be that the alkenes, amides and nitriles are still present in P5, but was not detected in the small amount of contact mass investigated here.

5.5   Crystalline Structure

X-ray diffraction was done on both the EL (1 and 2) samples from last falls project, and the P3, P4 and P5 samples from the P-series. Silicon peaks were detected in all five samples while one copper peak was detected for the P5 sample. The peaks corresponding to silicon(111), silicon(220), silicon(311), silicon(400) and silicon(331) were present in all samples indicating that the structure for silicon is similar in these five samples. There are some small variation in the intensity of each peak from sample to sample. Figures 4.47 and 4.48 have been altered so that the silicon(111) peak is at the same intensity to easier compare

the intensity of the smaller peaks. For the EL samples the intensity is quite similar, but some of the EL2 peak are of lower intensity than the corresponding peaks in EL1. In the sample from the P-series the intensity for P5 and P3 is very similar while P4 has almost no silicon(400) peak and a lower intensity for the silicon(311) peak.

Previously studies[19] have shown that Cu_3Si peaks and Cu_5Si peaks where both found by XRD analysis. The peaks where found in the range of 43° - 51°, but no corresponding peaks where found in the samples measured here. A small peak at just over 43° can be seen for P5 which correspond to the copper peak found in previously literature[19] and in the PDF card 00-004-0836 for copper which places the standard x-ray diffraction for copper(111) at 43.64°. The peak is however very small, but the intensity for all copper peak are very low. This might also indicate that a longer scan time could yield the Cu_3Si peaks found in previous studies. The base line for these XRD measurement are quite noise, but a longer scan at a smaller range could eliminate some of the noise, making it possible to the the Cu_3Si peaks. It should also be mentioned that the measurement were done on a suspension mixture of the contact mass and ethanol. This mean that very little contact mass was tested and running a sample of only contact mass might also yield more peaks related to copper. However, this was not possible due to lack of sample amount.

The shoulder peaks found at 27.5° is a result of background noise from the instrument.

6. Conclusion

A series of five samples of reacted contact mass extracted at 4 hours, 21.5 hours, 27.5 hours, 46 hours and after termination (51 hours) as well as three samples (EL1, EL2, C1) of reacted contact mass extracted after termination were investigated using Thermal gravimetric analysis, Scanning electron microscopy, Energy-dispersive X-ray spectroscopy, Gas Chromatography - Mass spectrometry, Raman Spectroscopy, X-ray diffraction and Fourier transform infrared spectroscopy. A sample of unreacted contact mass,sample REF, was also investigated using TGA, SEM, EDX, Pyrolysis-GC/MS, Raman, XRD and FT-IR and the result for both the reacted and unreacted contact mass was compered.

It was found that thermal gravimetric analysis was difficult due to oxidation of the contact mass, small amount of mass loss and large uncertainties in the mass spectrometry. The instrument also seems to work best with higher sample amount which is hard to work with when the sample amount is very limited. The SEM showed how reaction pits are formed early in the reaction, since they were present in sample P1 (4 hours) and how the contact mass continued to change its surface morphology becoming more structured and porous as the reaction continued. The SEM also showed how crystal structures of mainly copper are formed in the contact mass during reaction.

The EDX showed a correlation between were the copper is located and were the oxygen is located within a sample. It also showed small indications that the location of carbon could be related to the location of oxygen within a sample. The EDX investigation showed how the copper was located within the reaction pits in large quantities. The EDX also showed how silicon became depleted within the reaction pits.

The Raman investigation indicated that there are small amount of carbon species in all present in the contact mass (except for the

73

REF sample and the P1 sample). This was shown by the low intensity of the carbon related peaks compared to the main silicon peak at 517-519 cm^{-1}. Furthermore the investigation indicated that most of the carbon was formed in the time interval between P1 (4 hours) and P2 (21.5 hours). The ID/IG ratio also indicated that P4 had the carbon species with most disorder.

The Pyrolysis-GC/MS further indicated oxygen present in the sample as CO_2 was measured even though no air is present within the instrument. Several different organic compound were found such as acids, amids and nitriles, the common factor for all compound were that hey consisted of long carbon chains. The O-H bonds found here were also found in the FTIR for sample P5. For the GC/MS a jump in organic content was seen between sample P1 and P2 which might indicate that much of the carbon is formed in this time interval which corresponds with what was found in the Raman. However, very little organic content was found in P5 compared in P4 which was not seen for the Raman investigation.

7. Further Work

There is still several aspects of the contact mass that needs to be further investigation for the carbon formation to be better understood. So far the use of TGA has proven very tricky and might have to be replaced with another instrument or all together left out of the investigation. Determination if the silicon actually oxidizes within the TGA would be a start, but also finding an instrument with higher mass loss sensitivity might be key for further investigation

Further investigation on which carbon species are formed by running more FTIR to investigate the O-H bond and other bond related to the carbon species could yield important information. Running more Pyrolysis-GC/MS especially at other temperature would also prove useful to gain insight into the accuracy of the organic compound found during GC/MS.

So far the EDX and SEM investigation has proven useful, but managing to quantify the compounds in the EDX would prove to be very useful especially to determine when, and how much of, the carbon is formed. Measuring the oxygen content within each sample would also be useful. More insight into the structure could also be gain from running longer XRD scans since the scan run this time was quite short. Again, if more sample mass was available a full powder investigation could be possible instead of suspending the sample in ethanol as was done this time. This made the sample amount tested in the XRD very little which might have limited what was possible to measure especially regarding the different copper species and phase.

The P-series use in this thesis was a good starting point, but in further investigation much more sample amount for the earlier extracted sample are needed. The limiting sample amount proved the investigation quite difficult and many experiment could only be conducted once on sample P1-P4 and some could not be conducted at all one these samples due to lack of samples. This is especially troubling

since there seems to be some differences between the contact mass extracted during the experiment run and the contact mass tested after termination.

Lastly, a new series were there are several extractions preformed between 4 hours and 21.5 hours might prove useful since there are indication that much of the carbon is formed in this time interval. In this investigation that meant that figuring out what happened between sample P1 and P2 was almost impossible especially due to the large time interval.

Bibliography

[1] W.J. Ward, A.Ritzer, K.M. Carroll, and J.W. Flock. Catalysis of the Rochow Direct Process. *J. Catal.*, 100(1):240 – 249, 1986.

[2] Acmite Market Intelligence. Market report: Global silicone market. `https://www.britannica.com/science/silicone,http://www.acmite.com/brochure/Brochure-Global-Silicone-Market-Report.pdf`. Online; accessed 12-May-2018.

[3] W. F. Banholzer, N. Lewis, and W. Ward. Active site formation in the direct process for methylchlorosilanes. *J. Catal.*, 101(2):405–415, 1986.

[4] W. Kalchauer and B. Pachalay. Müller–Rochow synthesis: The direct process to methylchlorosilanes. In *Handbook of Heterogeneous Catalysis*. VCH Verlagsgesellschaft mb, 2008.

[5] R. J. H Voorhoeve, J. A. Lips, and J. C. Vlugter. Mechanism and Kinetics of the Metal-Catalyzed Synthesis of Methylchlorosilanes I. The Synthesis of Methylchlorosilanes in a Fluid Bed. *J. Catal.*, 3(5):414 – 425, 1964.

[6] V. Bazant. Direct synthesis of organohalogensilanes. *Pure Appl. Chem.*, 13(1-2):313 – 327, 1966.

[7] W. Luo, G. Wang, and J. Wang. Surface morphology and catalytic activity of the MCS beds in organosilane synthesis. *Chem. Eng. Commun.*, 193(6):754 – 763, 2006.

[8] M. P. Clarke. The direct synthesis of methylchlorosilanes. *J. Organomet. Chem.*, 376(2-3):165 – 222, 1989.

[9] P. J. Launer. Hydrocarbon By-Products from the Rochow Direct Process for Methylchlorosilanes. *J. Chem. Eng. Data*, 11(4):621 – 622, 1966.

[10] R. J. H. Voorhoeve. General principles of the direct synthesis of methylhlosilanes and other organohalosilanes. In *Organohalosilanes, Precursors to Silicones.*, pages 120–146. Elsevier publishing company, Amsterdam, 1967.

[11] R. J. H. Voorhoeve. Mechanism of the copper-catalyzed reactions bewteen silicon and organic halides. In *Organohalosilanes, Precursors to Silicones.*, pages 244–280. Elsevier publishing company, Amsterdam, 1967.

[12] D. T. Hurd and E. G. Rochow. On the Mechanism of the Reaction between Methyl Chloride and Silicon-Copper. *J. Am. Chem. Soc.*, 67(7):1057–1059, 1945.

[13] A. L. Klebanskii and V. S. Fikhtengolts. Studies on the synthesis of organo-silicon compunds. 2. comparative activity of varying types of masses used for synthesis of methyl chlorosilanes. (engl. transl.). *Russ, J. Gen. Chem.*, 27, 1957.

[14] A. L. Klebanskii and V. S. Fikhtengolts. Investigation in the field of synthesis of organo-silicon compounds. 1. on the mechanism of the reaction between chlorous methyl and silicon in the presence of copper. (engl. transl.). *Russ, J. Gen. Chem.*, 26, 1956.

[15] T. C. Frank, K. B. Kester, and J. L. Falconer. Catalytic formation of silanes on copper-silicon alloys. *J. Catal.*, 91(1):44 – 53, 1985.

[16] H. Lieske, H. Fichtner, I. Grohmann, M. Selenina, W. Walkow, and R. Zimmermann. Characterization of Rochow contact masses by catalytic results, XRD, chemisorption and XPS. *Silicon for the Chemical Industry I, Geiranger*, 1992.

[17] F. A. Veer, B. H. Kolster, and W. G. Burgers. Diffusion in the Cu_3Si phase of the copper-silicon system. *Trans. Metall. Soc. AIME*, 242, 1968.

[18] T. C. Frank, K. B. Kester, and J. L. Falconer. Surface Analysis of Methylchlorosilane Formation Catalysts. *J. Catal.*, 95(2):396–405, 1985.

[19] L. N. Lewis, Y. Gao, R. Bolon, V. Ravikumar, and M. D'Evelyn. Surface analysis of MCS beds. *Silicon for the Chemical Industry IV*, Geiranger-Norway, 3-5. June, 1998.

[20] W. J. Ward, L. N. Lewis, and J. M. Bablin. Exploring the effects of phosphorus in the direct process with a fixed bed reactor. *Silicon for the Chemical Industry V*, Tromso,Norway May 29. - June 2., 2000.

[21] C. H. Bartholomew. Mechanisms of catalyst deactivation. *Appl. Catal. A Gen.*, 212(1-2):17 – 60, 2001.

[22] D. L. Trimm. Catalyst design for reduced coking (review). *Appl. Catal.*, 5(3):263 – 290, 1983.

[23] P. G. Menon. Coke on catalysts-harmful, harmless, invisible and beneficial types. *J. Mol. Catal.*, 59(2):207 – 220, 1990.

[24] T. J. Wessel and D. G. Rethwisch. Deactivation of CuSi and CuZnSnSi Due to Coke Formation during the Direct Synthesis of Methylchlorosilanes. *J. Catal.*, 161(2):861–866, 1996.

[25] J. R. Anderson and B. H. McConkey. Reactions of methyl chloride and of methylene chloride at metal surfaces: Ii. *J. Catal.*, 11(1):54 – 70, 1968.

[26] K. Bohmhammel, G. Roewer, I. Röver, and J. Acker. Basic reactions and mechanism of processes related to the direct synthesis. *Silicon for the Chemical Industry VII*, MS Trollfjord, Tromsø-Bergen,Norway, 2004.

[27] C. S. Kuivila, R. H. Zapp, O. K. Wilding, and C. A. Hall. The control of the methylchlorosilane product distribution from rochow direct process. *Silicon for the Chemical Industry III*, Sandefjord, Norway, June 18-20, 1996.

[28] G. J. Hutchings R. W. Joyner P. Beahan, K. H. Brookes, H. M. Rong, and G. J. Tatlock. Surface characterisation of intermetallic inclusions in silicon. *Silicon for the Chemical Industry II*, Loen- Norway, 8-10 juni, 1994.

[29] A. Mekki-Berrada and A. Auroux. Thermal methods. In *Characterization of Solid Materials and Heterogeneous Catalysts: From Structure to Surface Reactivity*, pages 747–852. Wiley-VCH Verlag GmbH & Co. KGaA, Weinheim, Germany, 2012.

[30] E. Margui and R. V. Grieken. *X-Ray Fluorescence Spectrometry and Related Techniques:An Introduction.* Momentum Press, 2013.

[31] R. Jenkins. X-ray fluorescence analysis. *Anal. Chem.*, 56(9), 1984.

[32] D. Sparkman, Z. E. Penton, and F. G. Kitson. Mass Spectrometry Instrumentation. In *Gas Chromatography and Mass Spectrometry: A Practical Guide*, pages 15–88. Elsevier, Amsterdam, 2011.

[33] J. Ayache, L. Beaunier, J. Boumendil, G. Ehret, and D. Laub. The different observation modes in electron microscopy (SEM, TEM, STEM). In *Sample Preparation Handbook for Transmission Electron Microscopy*, pages 33–57. Springer, New York, NY, 2010.

[34] J. Hjelen. *Scanning Elektron-Mikroskopi.* SINTEF, Avdeling for metallurgi Metallurgisk Institutt, NTH, 1986.

[35] R. F. Egerton. Physical principles of electron microscopy, an introduction to TEM, SEM, and AEM. *Springer US*, pages 125 – 153, 2005.

[36] Y. Leng. X-ray spectroscopy for elemental analysis. In *Materials Characterization : Introduction to Microscopic and Spectroscopic Methods*, pages 191–220. John Wiley & Sons, Incorporated, 2. edition, 2013.

[37] D. Shindo and T. Oikawa. *Energy Dispersive X-ray Spectroscopy. In: Analytical Electron Microscopy for Materials Science.* Springer Japan, 2002.

[38] B. Hafner. Energy dispersive spectroscopy on the sem: A primer. `http://www.charfac.umn.edu/instruments/eds_on_sem_primer.pdf`. Online; accessed 2-June-2018.

[39] E. Smith and G. Dent. *Modern Raman Spectroscopy: A Practical*

Approach. John Wiley & Sons, Ltd, England, 2005.

[40] J. R. Ferraro, K. Nakamoto, and C. W. Brown. *Introductory Raman Spectroscopy.* Elsevier, second edition, 2003.

[41] E. Moore. *Fourier Transform Infrared Spectroscopy (FTIR) : Methods, Analysis, And Research Insights.* Nova Science Publishers, 2016.

[42] `http://www.arcoptix.com/pdf/Fourier%20transform%20spectrometer%20tutorial.pdf`.

[43] H. Erich, D. Born, J. Richter-Mendau, K. Richter, and H. Lieske. Surface and catalytic studies on various rochow contact masses bedses. *Silicon for the chemistry industry III*, Sandefjord-Norway, 18-20. June:247–258, 1996.

[44] A. C. Ferrari and J. Robertson. Interpretation of raman spectra of disordered and amorphous carbon. *Phys. Rev. B*, 61:14095–14107, 2000.

[45] T. Kallel, M. Dammak, J. Wang, and W. M. Jadwisienczak. Raman characterization and stress analysis of AlN:Er^{3+} epilayers grown on sapphire and silicon substrates. *Mater. Sci. Eng. B.*, 187:46 – 52, 2014.

[46] M. Khorasaninejad, J. Walia, and S. S. Saini. Enhanced first-order raman scattering from arrays of vertical silicon nanowires. *Nanotechnology*, 23(27), 2012.

[47] B. Graczykowski, A. El Sachat, J. S. Reparaz, M. Sledzinska, M. R. Wagner, E. Chavez-Angel, S. Volz Y. Wu, Y. Wu, F. Alzina, and C. M. Sotomayor Torres. Thermal conductivity and air-mediated losses in periodic porous silicon membranes at high temperatures. *Nat. Commun.*, 8(415), 2017.

[48] S. Khachadorian, H. Scheel, A. Colli, A. Vierck, and C. Thomsen. Temperature dependence of first- andsecond-order raman scattering in silicon nanowires. *Phys. Status Solidi B*, 247(11-12):3084–3088, 2010.

[49] MathWorks. Trapz. `https://se.mathworks.com/help/matlab/ref/trapz.html#responsive_offcanvas`. Online; accessed 2-June-2018.

[50] G. Socrates. *Infrared and Raman Characteristic Group Frequencies Tables and chartes.* Wiley, 3 edition, 2001.

[51] M. C. Morris, H. F. McMurdie, E. H. Evans, B. Paretzkin, J. H. de Groot, and C. R. Hubbard. Standard X-ray diffraction powder patterns:ection 13. data for 58 substances. *University of North Texas Libraries*, page 35, 1976.

[52] P. A. Temple and C. E. Hathaway. Multiphonon raman spectrum of silicon. *Phys. Rev. B*, 7(8):3685–3697, 1973.

[53] T. Sekine K. Uchinokurau and E. Matsuura. Critical-point analysis of the two-phonon raman spectrum of silicon. *J. Phys. Chem. Solids*, 35(2):171–180, 1974.

[54] R. L. Frost and P. A. Williams. Raman spectroscopy of some basic chloride containing minerals of lead and copper. *Spectrochim. Acta A*, 60(8):2071 – 2077, 2004.

[55] Y. Deng, A. D. Handoko, Y. Du, S. Xi, and B.S. Yeo. In situ raman spectroscopy of copper and copper oxide surfaces during electrochemical oxygen evolution reaction: Identification of Cu^{III} oxides as catalytically active species. *ACS Catal.*, 6(4):2473–2481, 2016.

[56] A. C. Ferrari. Raman spectroscopy of graphene and graphite: Disorder, electron-phonon coupling, doping and nonadiabatic effects. *Solid State Commun.*, 143(1-2):47–57, 2007.

A. Additional Results

A.1 Thermal Gravimetric Analysis

The following section show the mass loss, heat exchange and mass spectra for the reference sample, REF, the P5 sample, the EL1 sample and the EL2 sample. The P5 sample is the second run for the P5 sample where more sample mass was used.
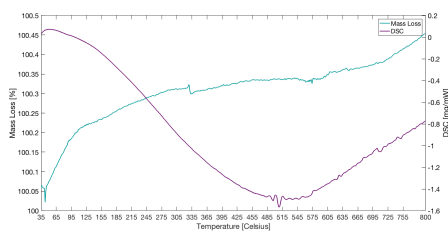
Figure A.1: The mass loss[%] and heat exchange[mg/mW] for the reference sample, REF, in standard atmosphere (75ml/min Air and 25ml/min Argon) with pre-drying overnight.
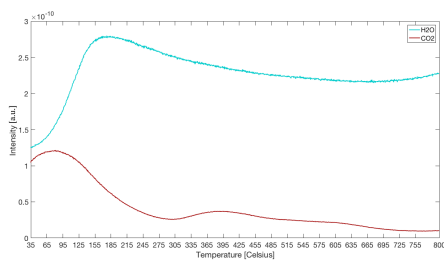
Figure A.2: The mass spectrum measuring the formation of 44 g/mol(CO_2) and 18 g/mol(H_2O) for the reference sample, REF, in standard atmosphere (75ml/min Air and 25ml/min Argon) with pre-drying overnight.
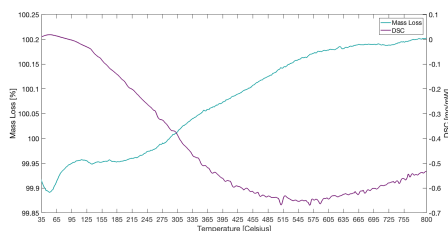
Figure A.3: The mass loss[%] and heat exchange[mg/mW] for the reference sample, REF, in inert atmosphere (100ml/min Argon) without pre-drying overnight.
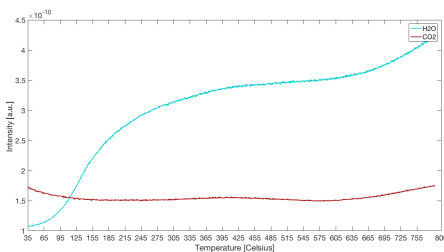
Figure A.4: The mass spectrum measuring the formation of 44 g/mol(CO_2) and 18 g/mol(H_2O) for the reference sample, REF, in inert atmosphere (100ml/min Argon) without pre-drying overnight.
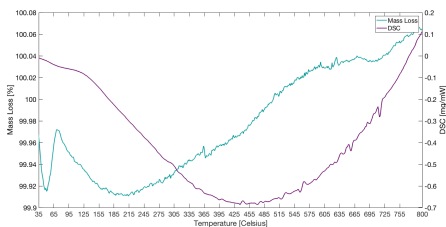
Figure A.5: The mass loss[%] and heat exchange[mg/mW] for the reference sample, REF, in inert atmosphere (100ml/min Argon) with pre-drying overnight.
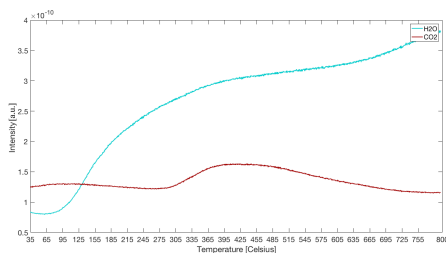
Figure A.6: The mass spectrum measuring the formation of 44 g/mol(CO_2) and 18 g/mol(H_2O) for the reference sample, REF, in inert atmosphere (100ml/min Argon) with pre-drying overnight.
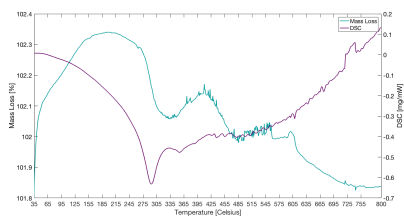
Figure A.7: The mass loss[%] and heat exchange[mg/mW] for the P5 sample of reacted contact mass, extracted at 51 hours after termination of the experiment, in standard atmosphere (75ml/min Air and 25ml/min Argon) without pre-drying.
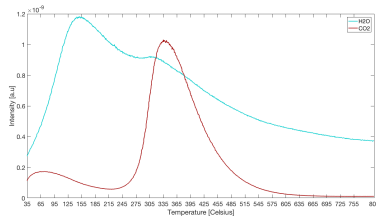
Figure A.8: The mass spectrum measuring the formation of molecules with a molar mass of 44 g/mol (CO_2) and 18 g/mol H_2O for sample P5 in standard atmosphere (75ml/min Air and 25ml/min Argon) without pre-drying.
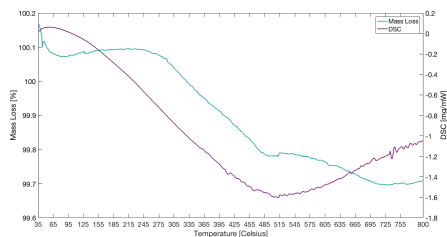
Figure A.9: The mass loss[%] and heat exchange[mg/mW] for the sample EL1 in standard atmosphere (75ml/min Air and 25ml/min Argon) with pre-drying overnight.
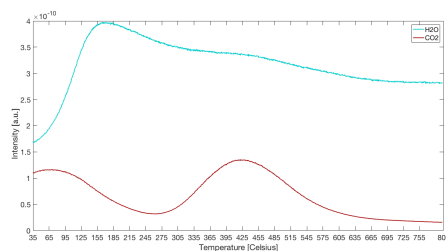
Figure A.10: The mass spectrum measuring the formation of 44 g/mol(CO_2) and 18 g/mol(H_2O) for the sample EL1 in standard atmosphere (75ml/min Air and 25ml/min Argon) with pre-drying overnight.
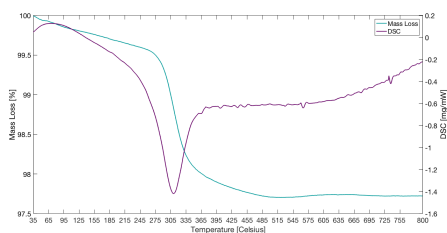
Figure A.11: The mass loss[%] and heat exchange[mg/mW] for the sample EL1 in inert atmosphere (100ml/min Argon) without pre-drying overnight.
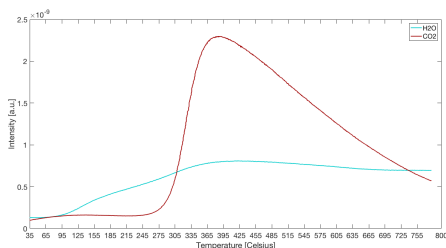
Figure A.12: The mass spectrum measuring the formation of 44 g/mol(CO_2) and 18 g/mol(H_2O) for the sample EL1 in inert atmosphere (100ml/min Argon) without pre-drying overnight.
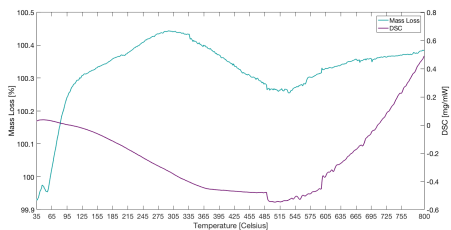
Figure A.13: The mass loss[%] and heat exchange[mg/mW] for the sample EL1 in inert atmosphere (100ml/min Argon) with pre-drying overnight.
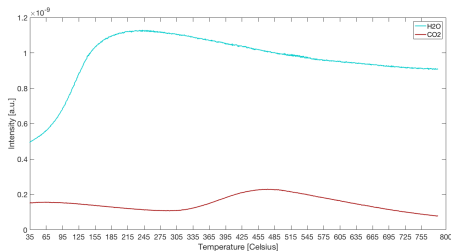
Figure A.14: The mass spectrum measuring the formation of 44 g/mol(CO_2) and 18 g/mol(H_2O) for the sample EL1 in inert atmosphere (100ml/min Argon) with pre-drying overnight
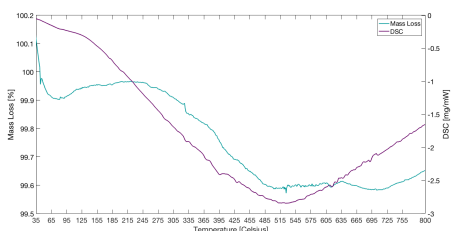
Figure A.15: The mass loss[%] and heat exchange[mg/mW] for the sample EL2 in standard atmosphere (75ml/min Air and 25ml/min Argon) with pre-drying overnight.
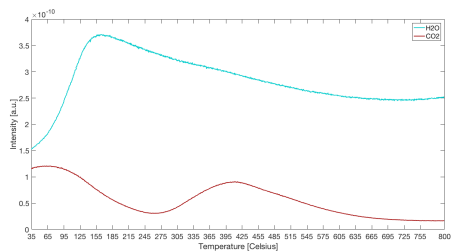
Figure A.16: The mass spectrum measuring the formation of 44 g/mol(CO_2) and 18 g/mol(H_2O) for the sample EL2 in standard atmosphere (75ml/min Air and 25ml/min Argon) with pre-drying overnight.
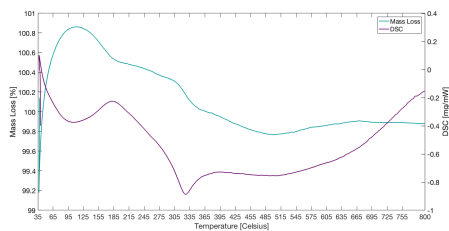
Figure A.17: The mass loss[%] and heat exchange[mg/mW] for the sample EL2 in inert atmosphere (100ml/min Argon) without pre-drying overnight.
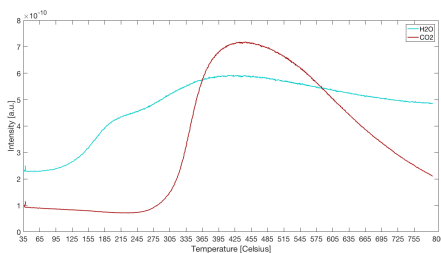
Figure A.18: The mass spectrum measuring the formation of 44 g/mol(CO_2) and 18 g/mol(H_2O) for the sample EL2 in inert atmosphere (100ml/min Argon) without pre-drying overnight.
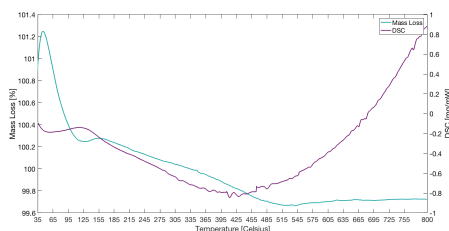
Figure A.19: The mass loss[%] and heat exchange[mg/mW] for the sample EL2 in inert atmosphere (100ml/min Argon) with pre-drying overnight.
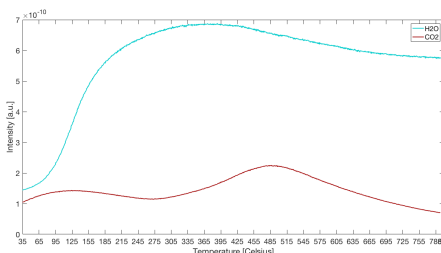
Figure A.20: The mass spectrum measuring the formation of 44 g/mol(CO_2) and 18 g/mol(H_2O) for the sample EL2 in inert atmosphere (100ml/min Argon) with pre-drying overnight.

A.2 X-ray Fluorescence

Figure A.21 show the components found to be present in the metallurgist silicon used to prepare the contact mass for the synthesis.

Component	Result	Unit	Det. limit	El. line	Intensity	w/o normal	Analyzing depth(mm)
Mg	0,6271	mass%	0,17532	Mg-KA	0,0094	0,34	0,0091
Al	1,4238	mass%	0,04615	Al-KA	0,1677	0,772	0,0138
Si	96,8637	mass%	0,15045	Si-KA	12,9672	52,5207	0,0202
K	0,5054	mass%	0,05425	K -KA	0,125	0,2741	0,0922
Ca	0,1099	mass%	0,03449	Ca-KA	0,045	0,0596	0,1245
Fe	0,3116	mass%	0,01997	Fe-KA	0,2861	0,169	0,6136
Co	0,0625	mass%	0,01677	Co-KA	0,0808	0,0339	0,7747
Ni	0,0959	mass%	0,01558	Ni-KA	0,17	0,052	0,9693

Figure A.21: Components found to be present in the metallurgist silicon which is used by Elkem to prepare the contact mass.

The results from the analysis done by Elkem AS on the same sample of silicon is shown in Table A.1.

Table A.1: Analysis done by Elkem AS on the same sample of silicon as tested in XRF in this thesis work.

Element	Unit	Mean Value	Estimated Uncertainty	Number of Results
Fe	%	0.22	0.02	8
Ca	%	00.63	0.003	7
Al	%	0.12	0.01	5
Ti	%	0.019	0.002	8
Mn	ppm	56	4	5
Cr	ppm	12	5	4
Cu	ppm	11	3	5
Ni	ppm	5	2	3
V	ppm	10	2	5
Zr	ppm	10	2	5
Co	ppm	<2	-	2
B	ppm	41	4	5
P	ppm	25	5	5
C	%	0.012	0.002	3

A.3 Raman Spectroscopy

The following section contains the Raman spectra for the P5 sample tested in UV light and with the x100LWD objective.
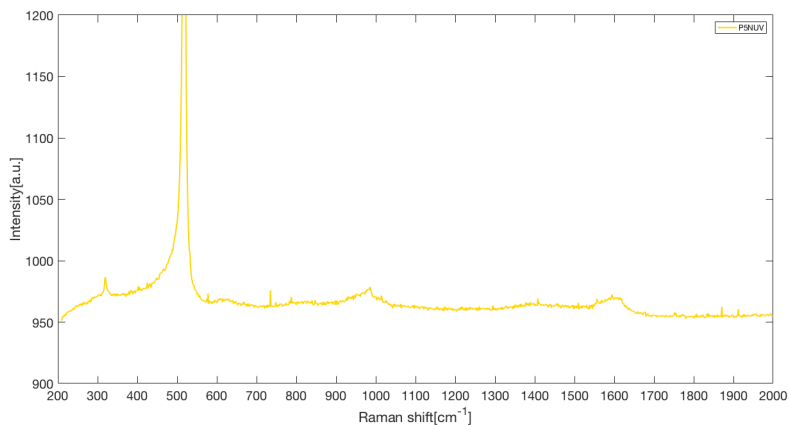
Figure A.22: Raman spectrum for the P5 sample of reacted contact mass with a 325nm laser in ultraviolet light. The largest peak has been cut to better show the smaller peak within the sample.
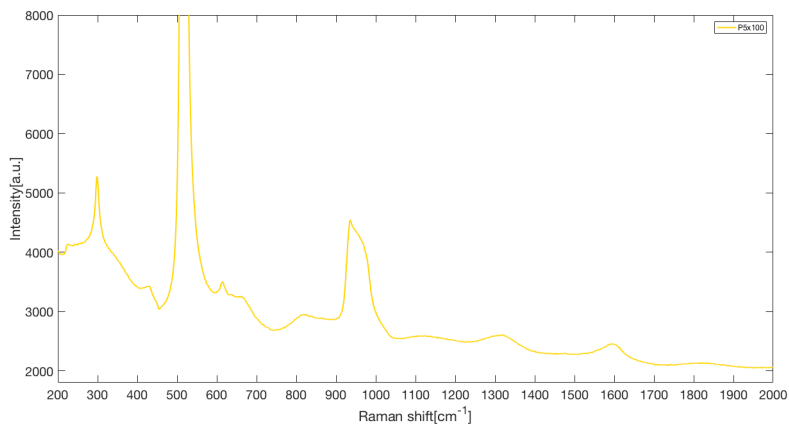
Figure A.23: Raman spectrum for the P5 sample of reacted contact mass with a 632nm laser in visible light and a x100LWD objective. The largest peak has been cut to better show the smaller peak within the sample.

B. Pyrolysis GC/MS Data

The full data result for the Pyrolysis GC/MS experiments are given in this section. The data for the P1 sample is given first, then the data for P2, P3, P4 and P5.

RT (min)	Scan number (#)	Area (Ab*s)	Baseline Heigth (Ab	Absolute Heigth (Ab	Peak Width 50% (min)	Hit Number	Hit Name	Quality	Mol Weight	CAS Number	Entry Number Library
2,633	747	1148192	30444	31398	0,056	1	Carbon dioxide	3	43,99	000124-38-9	82
						2	Carbon dioxide	3	43,99	000124-38-9	81
						3	Ethyne, fluoro-	3	44,006	002713-09-9	77
						4	Propane	3	44,063	000074-98-6	80
						5	Nitrous oxide	2	44,001	010024-97-2	84
						6	Nitrous oxide	2	44,001	010024-97-2	83
						7	Ethyne, fluoro-	2	44,006	002713-09-9	76
						8	Ethylene oxide	2	44,026	000075-21-8	75
						9	Acetaldehyde	2	44,026	000075-07-0	72
						10	Acetaldehyde	2	44,026	000075-07-0	71
						11	Ethylene oxide	2	44,026	000075-21-8	74
						12	Ethylene oxide	2	44,026	000075-21-8	73
						13	1,2-Propanediamine	1	74,084	000078-90-0	792
						14	1,2-Propanediamine	1	74,084	000078-90-0	788
						15	Propane	1	44,063	000074-98-6	79
						16	Propane	1	44,063	000074-98-6	78
						17	Tuaminoheptane	1	115,136	000123-82-0	7876
						18	2-Hexanamine, 4-methyl-	1	115,136	000105-41-9	7888
						19	Carbamic acid, monoammonium salt	1	78,043	001111-78-0	1029
						20	R-(-)-Cyclohexylethylamine	1	127,136	005913-13-3	11895
2,742	779	315182	7029	8877	0,063	1	Acetaldehyde	4	44,026	000075-07-0	72
						2	Acetaldehyde	4	44,026	000075-07-0	71
						3	(+)-2-Aminoheptane	4	115,136	006240-90-0	7884
						4	1,2-Propanediamine	4	74,084	000078-90-0	792
						5	1,2-Propanediamine	4	74,084	000078-90-0	788
						6	Tuaminoheptane	4	115,136	000123-82-0	7876
						7	Ethyne, fluoro-	3	44,006	002713-09-9	77
						8	1-Octanamine, N-methyl-	2	143,167	002439-54-5	20377
						9	Octodrine	2	129,152	000543-82-8	13019
						10	Octodrine	2	129,152	000543-82-8	13018
						11	2-Pentanamine, 4-methyl-	2	101,12	000108-09-8	4157
						12	2-Octanamine	2	129,152	000693-16-3	13027
						13	1-Propanol, 2-amino-, (S)-	2	75,068	002749-11-3	901
						14	2-Hexanamine, 4-methyl-	2	115,136	000105-41-9	7888
						15	2-Octanamine	2	129,152	000693-16-3	13026
						16	Nitrous oxide	2	44,001	010024-97-2	84
						17	Nitrous oxide	2	44,001	010024-97-2	83
						18	Carbon dioxide	2	43,99	000124-38-9	82
						19	Carbon dioxide	2	43,99	000124-38-9	81
						20	Ethyne, fluoro-	2	44,006	002713-09-9	76
14,993	4375	132281	8115	8434	0,035	1	Ethanol, 2-(2-butoxyethoxy)-, acetate	80	204,136	000124-17-4	63714
						2	Ethanol, 2-(2-butoxyethoxy)-, acetate	72	204,136	000124-17-4	63716
						3	Ethanol, 2-(2-butoxyethoxy)-, acetate	43	204,136	000124-17-4	63715
						4	2-Hexanone, 4-hydroxy-5-methyl-	42	130,099	038836-21-4	13495
						5	1,3-Dioxane, 2-methyl-	37	102,068	000626-68-6	4265
						6	4-Isopropoxy-2-butanone	25	130,099	032541-58-5	13426
						7	2-Isobutoxyethyl acetate	25	160,11	039220-44-5	31229
						8	5-Hexen-3-ol, 2,2,4-trimethyl-	25	142,136	090676-50-9	20028
						9	Propene, 3-tert-butoxy-2-(methoxymethyl)-	12	158,131	023230-86-6	30319
						10	Acetaldehyde, O-ethyloxime-	9	87,068	1000288-34-6	1897
						11	Morpholine	9	87,068	000110-91-8	1864
						12	2-Propanone, O-methyloxime	9	87,068	003376-35-0	1895
						13	Heptane, 2,3,5-trimethyl-	9	142,172	020278-85-7	19206
						14	1,2-Butanediol, 3,3-dimethyl-	9	118,099	059562-82-2	8856
						15	Decane, 1-fluoro-	9	160,163	000334-56-5	30739
						16	1-Fluorononane	9	146,147	000463-18-3	22247
						17	Oxalic acid, isobutyl nonyl ester	9	272,199	1000309-37-4	120800
						18	Butane, 1,1'-[oxybis(2,1-ethanediyloxy)]bi	9	218,188	000112-73-2	75667
						19	1-Nonen-3-ol	9	142,136	021964-44-3	19945
						20	1,2-Butanediol, 3,3-dimethyl-	9	118,099	059562-82-2	8859
24,286	7103	2560875	75756	76599	0,05	1	n-Hexadecanoic acid	98	256,24	000057-10-3	107549
						2	Tridecanoic acid	86	214,193	000638-53-9	72646
						3	Pentadecanoic acid	74	242,225	001002-84-2	95851
						4	n-Hexadecanoic acid	70	256,24	000057-10-3	107547
						5	Tetradecanoic acid	53	228,209	000544-63-8	84452
						6	Tridecanoic acid	52	214,193	000638-53-9	72648
						7	n-Hexadecanoic acid	50	256,24	000057-10-3	107548
						8	Pentadecanoic acid	47	242,225	001002-84-2	95855
						9	Tridecanoic acid	45	214,193	000638-53-9	72647
						10	Ethanone, 1-(4,5-dihydro-2-thiazolyl)-	30	129,025	029926-41-8	12837
						11	Estra-1,3,5(10)-trien-17.beta.-ol	18	256,183	002529-64-8	107688
						12	Oxalic acid, cyclobutyl heptadecyl ester	11	382,308	1000309-70-7	203491
						13	Oxalic acid, allyl pentadecyl ester	11	340,261	1000309-24-3	176817
						14	Oxalic acid, propyl tridecyl ester	11	314,246	1000309-26-6	156309
						15	Oxalic acid, cyclobutyl pentadecyl ester	11	354,277	1000309-70-5	186678
						16	Oxalic acid, allyl octadecyl ester	11	382,308	1000309-24-5	203464
						17	Oxalic acid, dodecyl propyl ester	11	300,23	1000309-26-5	144569
						18	Oxalic acid, cyclobutyl octadecyl ester	11	396,324	1000309-70-8	210293
						19	n-PROPYL NONYL ETHER	10	186,198	1000130-69-3	50326
						20	Oxalic acid, isobutyl pentadecyl ester	10	356,293	1000309-38-0	188025
27,427	8025	1663854	51130	54197	0,047	1	Octadecanoic acid	99	284,272	000057-11-4	131261
						2	Tetradecanoic acid	64	228,209	000544-63-8	84455
						3	Tetradecanoic acid	58	228,209	000544-63-8	84453
						4	Tetradecanoic acid	50	228,209	000544-63-8	84452
						5	Tridecanoic acid	50	214,193	000638-53-9	72647
						6	n-Hexadecanoic acid	47	256,24	000057-10-3	107548
						7	Pentadecanoic acid	46	242,225	001002-84-2	95855
						8	n-Decanoic acid	43	172,146	000334-48-5	39474
						9	Tridecanoic acid	38	214,193	000638-53-9	72648
						10	Dodecanoic acid	38	200,178	000143-07-7	61122
						11	Pentadecanoic acid	38	242,225	001002-84-2	95854
						12	n-Hexadecanoic acid	38	256,24	000057-10-3	107549
						13	Ethanone, 1-(4,5-dihydro-2-thiazolyl)-	25	129,025	029926-41-8	12836
						14	Ethanone, 1-(4,5-dihydro-2-thiazolyl)-	25	129,025	029926-41-8	12837
						15	n-PROPYL NONYL ETHER	11	186,198	1000130-69-3	50326
						16	Sulfurous acid, octadecyl 2-propyl ester	11	376,301	1000309-12-7	200449
						17	Oxalic acid, allyl tetradecyl ester	10	326,246	1000309-24-2	165885
						18	1-Hexadecanol, acetate	10	284,272	000629-70-9	131267
						19	3-Heptanol, 3,6-dimethyl-	10	144,151	001573-28-0	21149
						20	Oxalic acid, isobutyl tetradecyl ester	10	342,277	1000309-37-9	178452

RT (min)	Scan number (#)	Area (Ab*s)	Baseline Heigth (Ab)	Absolute Heigth (Ab)	Peak Width 50% (min	Hit Number	Hit Name	Quality	Mol Weight (amu)	Entry Number Library
2,623	744	1564393	51607	57269	0,046	1	Carbon dioxide	4	43,99	81
						2	Ethylene oxide	3	44,026	75
						3	Carbon dioxide	3	43,99	82
						4	Ethylene oxide	3	44,026	73
						5	Nitrous oxide	3	44,001	84
						6	Nitrous oxide	3	44,001	83
						7	Ethyne, fluoro-	2	44,006	77
						8	Ethyne, fluoro-	2	44,006	76
						9	Acetaldehyde	2	44,026	72
						10	Acetaldehyde	2	44,026	71
						11	Ethylene oxide	2	44,026	74
						12	Carbamic acid, monoammonium salt	2	78,043	1029
						13	1,2-Propanediamine	1	74,084	792
						14	1,2-Propanediamine	1	74,084	788
						15	Propane	1	44,063	80
						16	Propane	1	44,063	79
						17	Propane	1	44,063	78
						18	Tuaminoheptane	1	115,136	7876
						19	Benzeneethanamine, 4-fluoro-.beta.,3-dihydroxy-N-met	1	185,085	49744
						20	dl-Alanine ethyl ester	1	117,079	8495
14,989	4374	592083	31674	32255	0,029	1	Ethanol, 2-(2-butoxyethoxy)-, acetate	90	204,136	63715
						2	Ethanol, 2-(2-butoxyethoxy)-, acetate	52	204,136	63714
						3	2-[2-(2-Butoxyethoxy)ethoxy]ethyl acetate	50	248,162	100321
						4	Thiocyanic acid, ethyl ester	47	87,014	1853
						5	2-[2-[2-(2-Butoxyethoxy)ethoxy]ethoxy]ethyl acetate	47	292,189	137492
						6	(Methylthio)-acetonitrile	47	87,014	1852
						7	2-[2-[2-[2-[2-[2-(2-Acetyloxyethoxy)ethoxy]ethoxy]e	47	498,268	235018
						8	1,2-Butanediol, 3,3-dimethyl-	47	118,099	8856
						9	2-[2-[2-(2-Butoxyethoxy)ethoxy]ethoxy]ethyl a	43	336,215	173702
						10	1,3-Dioxolane-2-ethanol, 2-methyl-	43	132,079	14303
						11	3,4-Di-O-methyl-L-arabinopyranose	42	178,084	44319
						12	1,3-Dioxolane, 2-ethyl-2-methyl-	40	116,084	8181
						13	2-[2-[2-[2-[2-(2-Methoxyethoxy)ethoxy]ethoxy]	40	382,22	203137
						14	Thiophene, 2-butyltetrahydro-	38	144,097	21043
						15	4,4-Ethylenedioxy-1-pentylamine	38	145,11	21406
						16	1,3-Dioxolane, 2-methyl-2-pentyl-	38	158,131	30265
						17	Hydrazine, 1,1-diethyl-2-(1-methylpropyl)-	38	144,163	21077
						18	2-[2-[2-[2-[2-[2-(2-Acetyloxyethoxy)ethoxy]ethoxy]eth	38	454,241	227856
						19	2-Butoxyethyl acetate	38	160,11	31224
						20	4,6-Dioxadecane	32	146,131	22087
24,351	7122	19335274	440141	446435	0,062	1	n-Hexadecanoic acid	99	256,24	107549
						2	Tetradecanoic acid	90	228,209	84455
						3	Tetradecanoic acid	90	228,209	84453
						4	Pentadecanoic acid	74	242,225	95851
						5	n-Decanoic acid	70	172,146	39470
						6	Tridecanoic acid	64	214,193	72646
						7	Tridecanoic acid	64	214,193	72647
						8	n-Hexadecanoic acid	58	256,24	107547
						9	Tridecanoic acid	58	214,193	72648
						10	Pentadecanoic acid	58	242,225	95855
						11	Nonanoic acid	30	158,131	30180
						12	Estra-1,3,5(10)-trien-17.beta.-ol	25	256,183	107688
						13	Oxalic acid, allyl octadecyl ester	20	382,308	203464
						14	Oxalic acid, cyclobutyl octadecyl ester	18	396,324	210293
						15	1-Decanol, 2-hexyl-	18	242,261	95994
						16	Sulfurous acid, 2-propyl tetradecyl ester	18	320,239	161094
						17	2-Butenoic acid, 2-methoxy-3-methyl-, methyl ester	18	144,079	20720
						18	Oxalic acid, allyl tetradecyl ester	18	326,246	165885
						19	Dodecane	11	170,203	38317
						20	Tridecane	11	184,219	48832
26,712	7815	761678	31396	36167	0,037	1	Heptadecanenitrile	91	251,261	103255
						2	Octadecanenitrile	90	265,277	114921
						3	Heptadecanenitrile	87	251,261	103256
						4	Hexadecanenitrile	83	237,246	91623
						5	Pentadecanenitrile	81	223,23	80299
						6	Hexadecanenitrile	81	237,246	91624
						7	Octadecanenitrile	80	265,277	114920
						8	Hexadecanenitrile	74	237,246	91622
						9	Pentadecanenitrile	74	223,23	80298
						10	Hexadecanenitrile	68	237,246	91621
						11	Tetradecanenitrile	58	209,214	68716
						12	Pentadecanenitrile	52	223,23	80297
						13	1,1'-Bicyclohexyl, 4,4'-dimethyl-	30	194,203	56502
						14	1-Nonadecene	25	266,297	115905
						15	1,1'-Bicyclohexyl, 4-methyl-4'-propyl-	25	222,235	79571
						16	1-Azabicyclo[2.2.2]octan-3-one	25	125,084	10851
						17	Cyclopentane, 1-methyl-3-(2-methylpropyl)-	20	140,157	18070
						18	1-Octadecene	18	252,282	104184
						19	Cyclohexane, 1-ethyl-4-methyl-, trans-	18	126,141	11623
						20	2-Aziridinone, 1-tert-butyl-3-(1-methylcyclohexyl)-	15	209,178	68666
27,461	8035	13752638	368432	378867	0,053	1	Octadecanoic acid	99	284,272	131258
						2	Octadecanoic acid	99	284,272	131262
						3	Octadecanoic acid	99	284,272	131261
						4	Octadecanoic acid	98	284,272	131259
						5	Octadecanoic acid	94	284,272	131260
						6	Pentadecanoic acid	90	242,225	95851
						7	Octadecanoic acid, 2-(2-hydroxyethoxy)ethyl ester	87	372,324	198268
						8	Pentadecanoic acid	76	242,225	95855
						9	n-Decanoic acid	64	172,146	39469
						10	Tetradecanoic acid	58	228,209	84455
						11	Tetradecanoic acid	58	228,209	84452
						12	Nonane, 4,5-dimethyl-	25	156,188	28438
						13	Oxalic acid, propyl tetradecyl ester	20	328,261	167553
						14	Sulfurous acid, octadecyl 2-propyl ester	15	376,301	200449
						15	Tetradecane	11	198,235	59881
						16	Oxalic acid, cyclobutyl heptadecyl ester	11	382,308	203491
						17	Hexadecane	11	226,266	83024
						18	Octadecane, 2-methyl-	11	268,313	117646
						19	Oxalic acid, allyl octadecyl ester	11	382,308	203464
						20	Ethanol, 2-(octadecyloxy)-	11	314,318	156673
27,731	8114	947027	33073	48622	0,042	1	Octadecanamide	59	283,288	130205
						2	9-Octadecenamide, (Z)-	59	281,272	128443
						3	Pentadecanamide, 15-bromo-	59	319,151	160272
						4	Octadecanamide	59	283,288	130204
						5	Decanamide-	58	171,162	38977

956323	6	Tetradecanamide	58	227,225	83608
	7	Hexadecanamide	50	255,256	106564
	8	Heptanamide, 4-ethyl-5-methyl-	50	171,162	38995
	9	Dodecanamide	45	199,194	60440
	10	Hexadecanamide	45	255,256	106565
	11	Tetradecanamide	45	227,225	83610
	12	Carbonic acid, 2-ethoxyethyl 2,2,2-trichloroethyl ester	45	263,972	114327
	13	1,3,5-Tris(dimethyl-n-pentylsilyl)pent-1-ene	43	454,385	227954
	14	Tetradecanamide	42	227,225	83609
	15	9-Octadecenamide, (Z)-	32	281,272	128446
	16	9-Octadecenamide, (Z)-	32	281,272	128447
	17	Butanamide, 3,3-dimethyl-	27	115,1	7830
	18	3-Tetradecanol	27	214,23	72864
	19	N-(3-Methylbutyl)acetamide	22	129,115	12959
	20	Cyclohexanol, 4-methoxy-	16	130,099	13433

RT (min)	Scan number (#)	Area (Ab*s)	Baseline Heigth (Ab	Absolute Heigth (Ab)	Peak Width 50% (min)	Hit Number	Hit Name	Quality	Mol Weight	Entry Number Library
2,626	745	1008349	28056	28893	0,053	1	Nitrous oxide	5	44,001	84
						2	Nitrous oxide	5	44,001	83
						3	Carbon dioxide	3	43,99	82
						4	Carbon dioxide	3	43,99	81
						5	Ethyne, fluoro-	2	44,006	77
						6	Ethyne, fluoro-	2	44,006	76
						7	Ethylene oxide	2	44,026	75
						8	Acetaldehyde	2	44,026	72
						9	Acetaldehyde	2	44,026	71
						10	Formaldehyde	2	30,011	24
						11	Formaldehyde	2	30,011	23
						12	Formaldehyde	2	30,011	22
						13	Ethane	2	30,047	21
						14	Ethane	2	30,047	20
						15	Ethane	2	30,047	19
						16	Ethylene oxide	2	44,026	74
						17	Ethylene oxide	2	44,026	73
						18	1,2-Propanediamine	2	74,084	791
						19	Propane	1	44,063	80
						20	Propane	1	44,063	79
2,752	782	384810	6599	8709	0,091	1	Propene	16	42,047	57
						2	Propene	12	42,047	58
						3	Propane	5	44,063	79
						4	Propane	5	44,063	78
						5	Propane	4	44,063	80
						6	Methylenecyclopropane	4	54,047	151
						7	Aminocyanoacetic acid	4	100,027	3583
						8	1-Propene, 2-methyl-	2	56,063	188
						9	1-Propene, 2-methyl-	2	56,063	186
						10	1-Methylcyclopropene	2	54,047	149
						11	Ethyne, fluoro-	2	44,006	76
						12	Ethylene oxide	2	44,026	75
						13	Acetaldehyde	2	44,026	72
						14	Nitrous oxide	2	44,001	84
						15	Acetaldehyde	2	44,026	71
						16	Ethyne, fluoro-	2	44,006	77
						17	Carbon dioxide	2	43,99	81
						18	Carbon dioxide	2	43,99	82
						19	Nitrous oxide	2	44,001	83
						20	Ethylene oxide	2	44,026	74
11,078	3226	110192	8193	8269	0,022	1	5-Undecene, (E)-	64	154,172	27025
						2	Cyclopropane, 1-pentyl-2-propyl-	64	154,172	27083
						3	Cyclopropane, 1,2-dimethyl-3-pentyl-	53	140,157	18054
						4	3-Decene, 2-methyl-, (Z)-	50	154,172	27065
						5	Cyclopentane, methyl-	47	84,094	1494
						6	Trifluoroacetic acid, heptyl ester	43	212,102	71647
						7	1-Ethyl-2,2,6-trimethylcyclohexane	43	154,172	27089
						8	Cyclohexane, 1,1,2,3-tetramethyl-	43	140,157	18043
						9	Nonane, 2-methyl-3-methylene-	43	154,172	27079
						10	4-Decene, 9-methyl-, (E)-	35	154,172	27064
						11	1-Pentene, 3,4-dimethyl-	35	98,11	3357
						12	Octyl chloroformate	27	192,092	55020
						13	1-Nonanol	27	144,151	21098
						14	4-Undecene, (E)-	22	154,172	27027
						15	Dicyclopropyl carbinol	22	112,089	6505
						16	Cyclopropane, 1,1-dimethyl-	18	70,078	580
						17	4-Undecene, (Z)-	18	154,172	27033
						18	Furan, 2,3-dihydro-	14	70,042	546
						19	5-Undecene, (Z)-	14	154,172	27029
						20	2-Butenal, (E)-	14	70,042	529
12,604	3674	221065	13513	13564	0,025	1	Cyclopentane, 1,1-dimethyl-	60	98,11	3390
						2	Cyclopentane, 1,1-dimethyl-	49	98,11	3393
						3	1-Hexene, 3,5-dimethyl-	47	112,125	6706
						4	4-Pentenal, 2-methyl-	43	98,073	3198
						5	18-Nonadecen-1-amine	38	281,308	128489
						6	(S)-(+)-3-Methyl-1-pentanol	38	102,104	4482
						7	Pentane, 2-cyclopropyl-	37	112,125	6714
						8	4-Pentenal, 2-methyl-	32	98,073	3194
						9	(S)-3,4-Dimethylpentanol	32	116,12	8372
						10	1-Hexene, 3-methyl-	27	98,11	3327
						11	1-Hexene, 3-methyl-	27	98,11	3328
						12	1,2-Cyclohexanediol, cyclic sulfite, trans-	22	162,035	32429
						13	1-Pentene, 3-methyl-	16	84,094	1486
						14	1-Hexene	14	84,094	1453
						15	(Z)-2-Heptene	14	98,11	3305
						16	Ethanone, 1-cyclopropyl-	14	84,058	1430
						17	1-Hexene	14	84,094	1452
						18	Cyclopropane, 1-ethyl-1-methyl-	14	84,094	1521
						19	Pentane, 3-methylene-	14	84,094	1489
						20	Cyclopentane, (1-methylbutyl)-	10	140,157	18022
14,035	4094	106454	9742	9786	0,028	1	Cyclopentane, 1,1-dimethyl-	58	98,11	3393
						2	Cyclopentane, 1,1-dimethyl-	53	98,11	3390
						3	4-Pentenal, 2-methyl-	40	98,073	3198
						4	2-Heptene	38	98,11	3298
						5	Pentane, 2-cyclopropyl-	37	112,125	6714
						6	1-Pentene, 3-methyl-	35	84,094	1479
						7	1-Hexene, 3-methyl-	32	98,11	3327
						8	10-Azido-1-decanethiol	27	215,146	73280
						9	(Z)-2-Heptene	27	98,11	3305
						10	Cyclopropane, butyl-	22	98,11	3335
						11	Cyclobutane, 1,2-diethyl-, cis-	16	112,125	6795
						12	1-Hexene, 3,5-dimethyl-	16	112,125	6706
						13	2-Octenal, (E)-	14	126,104	11331
						14	1-Propenylaziridine	14	83,073	1293
						15	Isopropylcyclobutane	12	98,11	3336
						16	Pentane, 3-methylene-	12	84,094	1489
						17	3-Penten-2-one, (E)-	11	84,058	1417
						18	1-Butene, 3,3-dimethyl-	10	84,094	1500
						19	Aziridine, 1,-(1-butenyl)-, (Z)-	10	97,089	2999
						20	Aziridine, 1-(1-butenyl)-, (E)-	10	97,089	2994
14,986	4373	489617	35699	35778	0,022	1	Ethanol, 2-(2-butoxyethoxy)-, acetate	72	204,136	63714
						2	1,2-Butanediol, 3,3-dimethyl-	56	118,099	8859
						3	Ethanol, 2-(2-butoxyethoxy)-, acetate	50	204,136	63715
						4	1,2-Butanediol, 3,3-dimethyl-	50	118,099	8856

						#	Compound			
						5	2-[2-[2-[2-[2-(2-Methoxyethoxy)ethoxy]ethox	47	382,22	203137
						6	Ethanol, 2-(2-butoxyethoxy)-, acetate	45	204,136	63716
						7	Tetraethylene glycol, diacetate	43	278,137	125390
						8	Acetamide, N-ethyl-	43	87,068	1881
						9	2-[2-[2-[2-(2-Methoxyethoxy)ethoxy]ethoxy]eth	42	294,168	139063
						10	Thiocyanic acid, ethyl ester	40	87,014	1853
						11	3-Cyclopentylpropionamide, N,N-dimethyl-	40	169,147	37491
						12	2-Isobutoxyethyl acetate	40	160,11	31229
						13	Ethanol, 2,2'-oxybis-, diacetate	38	190,084	53400
						14	4,4-Ethylenedioxy-1-pentylamine	38	145,11	21406
						15	2-[2-[2-(2-Methoxyethoxy)ethoxy]ethoxy]ethyl a	38	250,142	101809
						16	2-[2-(2-Butoxyethoxy)ethoxy]ethyl acetate	32	248,162	100321
						17	4,6-Dioxadecane	25	146,131	22087
						18	2,7-Dimethyl-4,6-dioxanonane	25	160,146	31412
						19	Butane, 1,1'-[oxybis(2,1-ethanediyloxy)]bis-	14	218,188	75667
						20	N-Acetyl-d-galactosamine	9	221,09	78432
15,374	4487	305378	24974	25046	0,02	1	5-Octadecene, (E)-	83	252,282	104186
						2	1-Tridecene	74	182,203	47267
						3	Cyclooctane, methyl-	58	126,141	11535
						4	1-Decanol	50	158,167	29593
						5	Cetene	49	224,25	81243
						6	1-Heptanol, 4-methyl-	46	130,136	13674
						7	4-Undecene, 6-methyl-	43	168,188	36776
						8	Nonyl chloroformate	43	206,107	65525
						9	1-Decanol	38	158,167	29600
						10	Isopropylcyclobutane	30	98,11	3336
						11	Cyclopentane, 1-ethyl-2-methyl-, cis-	27	112,125	6826
						12	1-Nonene	25	126,141	11502
						13	Heptane, 2-methyl-3-methylene-	18	126,141	11602
						14	7-Oxabicyclo[4.1.0]heptane, 3-methyl-	14	112,089	6608
						15	2-Hexenal, (E)-	14	98,073	3174
						16	Cyclopropane, 1,1,2,2-tetramethyl-	11	98,11	3415
						17	2-Heptene	11	98,11	3295
						18	Pyrrolidine, 2,5-bis(imino)-	10	97,064	2951
						19	3-Hexen-2-one	10	98,073	3157
						20	1-Butene, 2,3,3-trimethyl-	10	98,11	3387
16,638	4858	281068	21326	21644	0,021	1	Cyclopentane, 1,1-dimethyl-	46	98,11	3390
						2	1-Hexene, 3-methyl-	38	98,11	3320
						3	2-Heptene, 2,6-dimethyl-	30	126,141	11550
						4	2,5-Dimethyl-1-pyrroline	30	97,089	2987
						5	7-Oxabicyclo[4.1.0]heptane	30	98,073	3252
						6	Cyclohexane, 1-ethyl-2-methyl-	25	126,141	11603
						7	Cyclohexane, 1-ethyl-4-methyl-, trans-	22	126,141	11625
						8	Cyclohexane, 1-ethyl-4-methyl-, cis-	22	126,141	11622
						9	1H-Azonine, octahydro-	22	127,136	11888
						10	trans-1,3-Diethylcyclopentane	22	126,141	11579
						11	Cyclohexanone, 2,3-dimethyl-	18	126,104	11417
						12	5-Amino-3-methylpyrazole	18	97,064	2947
						13	1-Ethyl-3-methylcyclohexane (c,t)	14	126,141	11612
						14	cis-1-Ethyl-3-methyl-cyclohexane	14	126,141	11610
						15	7-Oxabicyclo[4.1.0]heptane	14	98,073	3249
						16	Bicyclo[3.1.1]heptan-2-one, 6,6-dimethyl-, (1R)	14	138,104	17642
						17	Aziridine, 1-(2-methyl-1-propenyl)-	10	97,089	3004
						18	2,6-Octadien-1-ol, 3,7-dimethyl-, acetate	10	196,146	58031
						19	1,7-Octadiene, 2,3,3-trimethyl-	10	152,157	25442
						20	3-Penten-2-one	10	84,058	1396
17,864	5218	297978	23299	23346	0,021	1	Cyclooctane, methyl-	62	126,141	11535
						2	4-Undecene, 6-methyl-	50	168,188	36776
						3	Cyclopentane, 1,1,2-trimethyl-	38	112,125	6787
						4	Cyclopentane, 2-ethyl-1,1-dimethyl-	35	126,141	11617
						5	Pyrrolidine, 2,5-bis(imino)-	14	97,064	2951
						6	1-Octanol	14	130,136	13630
						7	1-Hexene, 3-methyl-	14	98,11	3320
						8	Cyclopentane, (2-methylpropyl)-	14	126,141	11606
						9	1-Pentene, 3-methyl-	14	84,094	1486
						10	Cyclopentane, 1-ethyl-1-methyl-	14	112,125	6796
						11	2-Pentene, 3,4-dimethyl-	11	98,11	3352
						12	1-Pentene, 2-methyl-	11	84,094	1487
						13	Cyclopropane, 1,1-diethyl-	11	98,11	3385
						14	2-Pentene, 4,4-dimethyl-, (E)-	10	98,11	3399
						15	1-Butene, 2,3,3-trimethyl-	10	98,11	3388
						16	Cyclopropane, 1,1,2,2-tetramethyl-	10	98,11	3415
						17	Cyclohexane, 1-ethyl-2-methyl-, cis-	10	126,141	11620
						18	2-Pentene, 2,4-dimethyl-	10	98,11	3372
						19	n-Tridecan-1-ol	10	200,214	61343
						20	3-Hexen-2-one	10	98,073	3157
19,227	5618	159103	9228	9621	0,027	1	Silane, [(11-chloroundecyl)oxy]trimethyl-	50	278,183	125668
						2	3-Nonene	49	126,141	11499
						3	cis-3-Nonene	47	126,141	11506
						4	3-Nonene, (E)-	43	126,141	11513
						5	1-Pentene, 3-methyl-	38	84,094	1486
						6	2,5-Dimethyl-1-pyrroline	38	97,089	2987
						7	3-Heptene, 2,6-dimethyl-	35	126,141	11551
						8	trans-1,2-Diethyl cyclopentane	35	126,141	11601
						9	1-Pentene, 3-methyl-	27	84,094	1477
						10	Cyclohexane, 1-ethyl-2-methyl-	27	126,141	11603
						11	Cyclohexane, 1-ethyl-4-methyl-, cis-	25	126,141	11622
						12	Cyclohexane, 1-ethyl-4-methyl-, trans-	22	126,141	11625
						13	3,5-Dimethyl-3-heptene	14	126,141	11544
						14	2-Pyrazoline, 5-ethyl-1,4-dimethyl-	14	126,116	11242
						15	Cyclohexanemethanol, 2-methyl-	14	128,12	12625
						16	Cyclohexane, 1-ethyl-4-methyl-, cis-	14	126,141	11619
						17	trans-1,3-Diethylcyclopentane	14	126,141	11579
						18	Cyclohexanemethanol, 4-methyl-, trans-	12	128,12	12641
						19	Ethanone, 1-cyclohexyl-	11	126,104	11363
						20	Ethanone, 1-(1-methylcyclopentyl)-	11	126,104	11470
19,707	5759	184960	9619	9736	0,03	1	1-Piperidinepropanenitrile	42	138,116	17459
						2	Methanamine, N-nitro-N-(1-piperidylmethyl)-	39	173,116	40727
						3	N-[Azirid-1-ylmethyl]piperidine	39	140,131	18569
						4	N-(1,3-Dioxo-1H,3H-benzo[de]isoquinolin-2-yl)-	39	337,143	174535
						5	N-(1-Cyclopropyl-ethyl)-N-phenyl-2-piperidin-1-y	38	286,205	133058
						6	Cyclohexanone, 2-propyl-	38	140,12	18706
						7	(R)-(1-Ethyl-2-pyrrolidinyl)methylamine	36	128,131	12391
						8	1H-Imidazole-2-methanol	9	98,048	3037
						9	3H-Pyrazole, 3,4-diamino-	9	98,059	3024
						10	1,3-Cyclopentanedione	9	98,037	3096

						#	Compound			
						11	4H-1,2,4-Triazol-3-amine, 4-methyl-	9	98,059	3028
						12	But-3-en-1-ynyl methyl sulfide	9	98,019	3129
						13	2-Pyrrolidone-5-carboxylic acid, N-methyl, meth	9	157,074	29373
						14	(R)-1-Ethyl-2-pyrrolidinecarboxamide	9	142,111	19547
						15	1-Piperidineethanamine	9	128,131	12361
						16	Propan-1-one, 1-(1-adamantyl)-3-(1-piperidyl)-	9	275,225	123620
						17	Piperidine, 4-chloro-1-methyl-	9	133,066	14643
						18	dl-.alpha.-Methylglutamic acid	9	161,069	31675
						19	Acethydrazide, 2-(1-piperidyl)-N2-(2,3(1H)-dihyd	9	286,143	132540
						20	4-Hydroxyimino-but-2-enoic acid, ethyl ester	9	143,058	20216
23,21	6787	369364	16513	16634	0,035	1	Undecanenitrile	40	167,167	35925
						2	Thiazolidin-4-one, 5-(2-furfurylideno)-2-imino-	38	194,015	56855
						3	2-Cyclopenten-1-one, 2-pentyl-	35	152,12	25170
						4	2-Cyclopenten-1-one, 2-pentyl-	35	152,12	25171
						5	2,2-Dimethyl-1-aza-spiro[2.4]heptane	27	125,12	10917
						6	1,1'-Bicyclohexyl, 4,4'-dimethyl-	25	194,203	56502
						7	Aziridine, 1-(2-methyl-1-propenyl)-	22	97,089	3004
						8	4-Piperidinamine, N,1-dimethyl-	12	128,131	12376
						9	Cyclohexane, 1-(cyclohexylmethyl)-2-methyl-, tr	12	194,203	56520
						10	Dodecanenitrile	12	181,183	46429
						11	1H-Imidazole, 1,2-dimethyl-	11	96,069	2769
						12	Cyclohexane, 1-ethyl-2-methyl-, cis-	10	126,141	11620
						13	N-n-Propylmaleimide	10	139,063	17781
						14	Cyclohexane, 1-ethyl-2-methyl-	10	126,141	11603
						15	1H-Pyrazole, 1,3-dimethyl-	10	96,069	2761
						16	Sulfurous acid, cyclohexylmethyl heptadecyl es	10	416,332	217596
						17	Oxalic acid, cyclohexylmethyl nonyl ester	10	312,23	154594
						18	Pyridine, 2-acetamido-6-hydroxy-	10	152,059	25726
						19	3,5-Dimethylpyrazole	10	96,069	2747
						20	Oxalic acid, cyclohexylmethyl octyl ester	10	298,214	142823
24,3	7107	3905910	132440	132911	0,045	1	n-Hexadecanoic acid	91	256,24	107549
						2	n-Hexadecanoic acid	91	256,24	107548
						3	n-Hexadecanoic acid	90	256,24	107547
						4	Tridecanoic acid	89	214,193	72643
						5	Tridecanoic acid	81	214,193	72648
						6	Dodecanoic acid	59	200,178	61122
						7	Tetradecanoic acid	53	228,209	84452
						8	Tridecanoic acid	53	214,193	72646
						9	Dodecanoic acid	53	200,178	61117
						10	Tridecanoic acid	53	214,193	72647
						11	Dodecanoic acid	52	200,178	61121
						12	11-Bromoundecanoic acid	50	264,072	113453
						13	1-(p-Toluidino)-1-deoxy-.beta.-d-idopyranose	43	269,126	118001
						14	Methyl-.alpha.-d-ribofuranoside	43	164,068	33910
						15	Undecanoic acid	38	186,162	50051
						16	n-Decanoic acid	38	172,146	39473
						17	n-Decanoic acid	38	172,146	39474
						18	Nonanoic acid	38	158,131	30180
						19	Tetradecanoic acid	27	228,209	84453
						20	Estra-1,3,5(10)-trien-17.beta.-ol	14	256,183	107688
25,397	7429	136170	7332	7388	0,029	1	1-Eicosyne	47	278,297	126190
						2	13-Heptadecyn-1-ol	42	252,245	104159
						3	1-Octadecyne	38	250,266	102602
						4	3-Cyclopentene-1-acetaldehyde, 2-oxo-	37	124,052	10457
						5	2-Propylcyclohexanol	37	142,136	19972
						6	1-Methyl-2-ethyl-pyrazolium bromide	35	190,011	53281
						7	1-Tetradecyne	27	194,203	56478
						8	1-Pentadecyne	27	208,219	67946
						9	1-Hexadecyne	27	222,235	79552
						10	1-Ethynyl-1-cyclooctanol	25	152,12	25132
						11	1H-Indene, octahydro-	25	124,125	10646
						12	1-Ethynyl-1-cycloheptanol	25	138,104	17542
						13	1-Tridecyne	22	180,188	45715
						14	1H-Imidazole, 2-propyl-	17	110,084	5726
						15	Cyclohexane, 1-methyl-4-methylene-	14	110,11	6027
						16	1-Ethynylcyclopentanol	12	110,073	5809
						17	1-Ethynyl-1-cycloheptanol	12	138,104	17546
						18	Cyclohexane, 1-methyl-4-methylene-	10	110,11	6028
						19	1,4-Dioxaspiro[5.5]undecan-2-one	10	170,094	38849
						20	DL-Histidine	10	155,069	27913
26,708	7814	741130	37672	37823	0,03	1	Hexadecanenitrile	72	237,246	91624
						2	Hexadecanenitrile	68	237,246	91622
						3	Hexadecanenitrile	64	237,246	91623
						4	Oxazole, 2-hexyl-5-methyl-	35	167,131	35880
						5	Aziridine, 1-(2-methyl-1-propenyl)-	15	97,089	3004
						6	Cyclohexane, 1-(cyclohexylmethyl)-2-methyl-, tr	14	194,203	56520
						7	Cyclohexane, 1-ethyl-2-methyl-	11	126,141	11603
						8	Selenopentanoic acid, 4-methyl-, O-ethyl ester	11	208,037	68155
						9	Phenol, 2-ethoxy-	10	138,068	17278
						10	Cyclohexanone, 3-butyl-	10	154,136	26707
						11	3-Heptyn-2-ol, 2-methyl-	10	126,104	11372
						12	Phenol, 4-butoxy-	10	166,099	34788
						13	3-Butene-1,2-diol, 1-(2-furanyl)-3-methyl-	10	168,079	37336
						14	Massoilactone	10	168,115	36333
						15	Pyridine, 2-acetamido-6-hydroxy-	10	152,059	25726
						16	Oxalic acid, cyclohexylmethyl octyl ester	10	298,214	142823
						17	Phenol, 2-ethoxy-	10	138,068	17280
						18	2(1H)-Pyrimidinone, 5-methyl-	10	110,048	5706
						19	4H-1,2,4-Triazole, 3,4,5-trimethyl-	10	111,08	6092
						20	11-Oxatricyclo[6.2.1.0(1,6)]undec-9-en-2-one	10	164,084	33475
27,434	8027	2334712	89211	90535	0,04	1	Octadecanoic acid	93	284,272	131258
						2	Octadecanoic acid	93	284,272	131259
						3	Octadecanoic acid	72	284,272	131261
						4	Tetradecanoic acid	64	228,209	84453
						5	Octadecanoic acid	58	284,272	131260
						6	Tetradecanoic acid	52	228,209	84455
						7	Tridecanoic acid	50	214,193	72643
						8	n-Hexadecanoic acid	49	256,24	107548
						9	Dodecanoic acid	47	200,178	61120
						10	Dodecanoic acid	43	200,178	61121
						11	Benzamide, 4-butoxy-N-[2-(2-thienyl)ethyl]-	38	303,129	147087
						12	n-Decanoic acid	35	172,146	39473
						13	11-Bromoundecanoic acid	27	264,072	113453
						14	Methyl 2,6-anhydro-.alpha.-d-altroside	27	176,068	42790
						15	N-Acetylisoxazolidine	14	115,063	7746
						16	Pentadecanoic acid	14	242,225	95855

						#	Compound			
						17	.beta.-D-Mannofuranoside, 1-O-(10-undecenyl)	14	332,22	170641
						18	Propyl 4,4-dimethyl-3-oxopentanoate	11	186,126	49865
						19	Heptacosyl acetate	10	438,444	224391
						20	Pentadecanoic acid	10	242,225	95853
27,713	8109	1274361	41556	43368	0,045	1	Hexadecanamide	80	255,256	106565
						2	Octadecanamide	80	283,288	130204
						3	Octanamide	72	143,131	20317
						4	9-Octadecenamide, (Z)-	72	281,272	128443
						5	Tetradecanamide	72	227,225	83609
						6	Tetradecanamide	72	227,225	83608
						7	Dodecanamide	59	199,194	60440
						8	Tetradecanamide	56	227,225	83610
						9	7-Nonenamide	50	155,131	28131
						10	Dodecanamide	50	199,194	60439
						11	Octadecanamide	45	283,288	130205
						12	Decanamide-	45	171,162	38977
						13	4-Cyclohexylbutyramide	42	169,147	37471
						14	Pentadecanamide, 15-bromo-	42	319,151	160272
						15	Undecanamide, 11-bromo-	42	263,088	112862
						16	Nonadecanamide	39	297,303	142051
						17	Nonanamide	38	157,147	29478
						18	9-Octadecenamide, (Z)-	38	281,272	128447
						19	9-Octadecenamide, (Z)-	38	281,272	128446
						20	13-Docosenamide, (Z)-	38	337,334	174697
30,919	9050	684281	22248	22755	0,047	1	Tetradecanamide	78	227,225	83608
						2	9-Octadecenamide, (Z)-	72	281,272	128443
						3	Octadecanamide	72	283,288	130204
						4	Tetradecanamide	64	227,225	83610
						5	Decanamide-	56	171,162	38977
						6	Hexadecanamide	56	255,256	106564
						7	Tetradecanamide	53	227,225	83609
						8	Octanamide	50	143,131	20317
						9	Dodecanamide	43	199,194	60440
						10	Dodecanamide	40	199,194	60439
						11	7-Nonenamide	38	155,131	28131
						12	Pentadecanamide, 15-bromo-	38	319,151	160272
						13	9-Octadecenamide, (Z)-	37	281,272	128445
						14	9-Octadecenamide, (Z)-	37	281,272	128447
						15	9-Octadecenamide, (Z)-	37	281,272	128446
						16	Silane, octyl-	37	144,133	21082
						17	Undecanamide, 11-bromo-	36	263,088	112862
						18	Octadecanamide	32	283,288	130205
						19	Hexadecanamide	32	255,256	106565
						20	2-Propenoic acid	9	72,021	630

RT (min)	Scan number (#)	Area (Ab*s)	Baseline Heigth (Ab)	Absolute Heigth (Ab)	Peak Width 50% (min)	Hit Number	Hit Name	Quality	Mol Weight	Entry Number Library
0,156	20	18145231	207837	210486	0,118	1	Benzene, 1,3-bis(3-phenoxyphenoxy)-	93	446,152	226479
						2	Benzene, 1,1',1'',1''',1''''-(1,3-cyclopentadiene-1,2,	53	446,203	226490
						3	Benzene, 1,1',1'',1''',1''''-(1,3-cyclopentadiene-1,2,	53	446,203	226489
						4	Spiro[9,9']difluorene, 2,2'-(2,5,8-trioxanonane-1,9-	42	446,188	226486
						5	5-[3,5-Ditrifluoromethylphenoxy]-6-methoxy-4-meth	42	446,07	226117
						6	Rhodium, (.eta.5-2,4-cyclopentadien-1-yl)[(1,2,3,4-	36	446,067	226196
						7	Yangambin	9	446,194	226197
						8	Imidazole, 2,4,5-triiodo-	9	445,727	226491
						9	Silane, [[(17.beta.)-3-methoxyestra-1,3,5(10)-trien	7	446,267	226238
						10	Androsta-3,5-dien-17-one, 3,12-bis[(trimethylsilyl)o	7	446,267	226237
						11	Zirconium, [2-butene-2,3-diolato(2-)-O,O']bis[(1,2,3	7	446,176	226210
						12	Bis[4-[4-hydroxy]piperidino-3-aminophenyl]sulfone	7	446,199	226167
						13	1,3,5-Triazine-2,4,6-triamine, N,N-dihexyl-N',N''-dip	7	446,316	226297
						14	Acetic acid, trifluoro-, 1-[(1,2,3,6-tetrahydro-1,3-dir	3	446,066	226096
						15	Phthalazine, 1-(4-carbamylphenylamino)-4-(4-meth	2	447,137	226544
						16	16-Epi-estriol-3-TMS-phenylboronate	2	446,245	226296
						17	3-tert-Butyl-N'-(4-(dimethylamino)benzylidene)-1-ph	2	503,308	235643
						18	Silane, diphenyl(3-ethylphenoxy)nonyloxy-	2	446,264	226464
						19	Silane, [[(17.beta.)-2-methoxyestra-1,3,5(10)-trien	1	446,267	226241
						20	Phosphine, 1,3-phenylenebis[diphenyl-	1	446,135	226481
2,616	742	1080565	35570	38001	0,045	1	Nitrous oxide	5	44,001	84
						2	Nitrous oxide	5	44,001	83
						3	Carbon dioxide	3	43,99	82
						4	Carbon dioxide	3	43,99	81
						5	Ethyne, fluoro-	2	44,006	77
						6	Ethyne, fluoro-	2	44,006	76
						7	Ethylene oxide	2	44,026	75
						8	Acetaldehyde	2	44,026	72
						9	Acetaldehyde	2	44,026	71
						10	Formaldehyde	2	30,011	23
						11	Formaldehyde	2	30,011	22
						12	Ethane	2	30,047	21
						13	Ethane	2	30,047	19
						14	Ethylene oxide	2	44,026	74
						15	Ethylene oxide	2	44,026	73
						16	Formaldehyde	2	30,011	24
						17	Ethane	2	30,047	20
						18	1,2-Propanediamine	2	74,084	791
						19	Propane	1	44,063	80
						20	Propane	1	44,063	79
12,608	3675	493353	16494	17376	0,042	1	1,3-Dimethyl-4-amino-4,5(1H)-dihydro-1,2,4-triazole	28	128,07	12006
						2	2H-Azepin-2-one, hexahydro-4-methyl-	9	127,1	11857
						3	2-Azacyclooctanone	9	127,1	11811
						4	3-[1,1,3,3-Tetramethylbutyl]-2-oxazolidinone	9	199,157	60388
						5	2H-Azepin-2-one, hexahydro-6-methyl-	7	127,1	11859
						6	5-Isothiazolecarboxamide	7	128,004	11999
						7	6-Amino-hex-2-en-1-ol	7	115,1	7811
						8	Cyclopentanemethanamine, 2-amino-	7	114,116	7380
						9	2H-Azepin-2-one, hexahydro-5-methyl-	5	127,1	11858
						10	1H-Azonine, octahydro-	4	127,136	11887
						11	2-(2-Thienyl)ethylamine	2	127,046	11788
						12	1H-Azonine, octahydro-	2	127,136	11888
						13	2-Azacyclooctanone	2	127,1	11812
						14	1-Methyl-2,4,5-trioxoimidazolidine	1	128,022	11991
						15	2-Buten-1-amine, N-butyl-, (Z)-	1	127,136	11915
						16	2-Hydroxyethyl 2,2,2-trifluoroacetate	1	158,019	29771
						17	6,7-Dioxabicyclo[3.2.2]nonane	1	128,084	12239
						18	2-Azacyclooctanone	1	127,1	11808
						19	1,8-Diaminooctane	1	144,163	21052
						20	1-Tridecanamine	1	199,23	60553
14,035	4094	115114	7615	8319	0,023	1	2,5-Dimethyl-1-pyrroline	33	97,089	2987
						2	(1R,2R)-(-)-1,2-Diaminocyclohexane	33	114,116	7388
						3	Cyclopentaneethanol, .beta.,2,3-trimethyl-	27	156,151	28351
						4	Cyclopentane, propyl-	25	112,125	6700
						5	1-Pentene, 5-butoxy-	25	142,136	19965
						6	1-Undecene, 8-methyl-	25	168,188	36770
						7	7-Oxabicyclo[4.1.0]heptane, 3-methyl-	17	112,089	6608
						8	3-Penten-2-one, (E)-	10	84,058	1412
						9	1-Pentene, 3,3-dimethyl-	10	98,11	3368
						10	1-Pentene, 2-methyl-	10	84,094	1478
						11	5-Amino-3-methylpyrazole	10	97,064	2947
						12	1-Pyrroline, 3-ethyl-	10	97,089	2986
						13	Cyclopentane, 1,1-dimethyl-	10	98,11	3390
						14	Cyclobutane, 1,2-diethyl-	9	112,125	6737
						15	1-Pentene, 2-methyl-	9	84,094	1487
						16	4-Piperidinemethanamine	9	114,116	7350
						17	1-Azabicyclo[2.2.2]octan-3-one	8	125,084	10851
						18	1,7-Heptanediol	8	132,115	14421
						19	1-Hexene	7	84,094	1453
						20	6-(2-propynyloxy)-1-hexanol	7	156,115	28990
14,986	4373	231337	16414	17149	0,023	1	Ethanol, 2-(2-butoxyethoxy)-, acetate	90	204,136	63715
						2	Ethanol, 2-(2-butoxyethoxy)-, acetate	90	204,136	63714
						3	Ethanol, 2-(2-butoxyethoxy)-, acetate	78	204,136	63716
						4	2-[2-[2-(2-Butoxyethoxy)ethoxy]ethoxy]ethyl aceta	59	292,189	137492
						5	2-[2-(2-Methoxyethoxy)ethoxy]ethyl acet	50	250,142	101809
						6	2-Isobutoxyethyl acetate	42	160,11	31229
						7	2-Propanol, 1-(2-methylpropoxy)-	40	132,115	14458
						8	1,2-Butanediol, 3,3-dimethyl-	39	118,099	8859
						9	2-[2-[2-(2-Hydroxyethoxy)ethoxy]ethoxy]ethyl acet	38	236,126	90119
						10	2-Butanol, 3-bromo-, acetate	38	193,994	56600
						11	5-Hexen-3-ol, 2,2,4-trimethyl-	36	142,136	20028
						12	1,3-Dioxane, 2-methyl-	33	102,068	4265
						13	2-[2-[2-[2-[2-(2-Acetyloxyethoxy)ethoxy]ethox	28	454,241	227856
						14	Acetamide, N-ethyl-	25	87,068	1881
						15	Ethanol, 2-(1-methylethoxy)-, acetate	23	146,094	21968
						16	2-Butoxyethyl acetate	16	160,11	31221
						17	1,3-Dioxolane-2-acetic acid, 2-methyl-	16	146,058	21840
						18	2-[2-(2-Butoxyethoxy)ethoxy]ethyl acetate	12	248,162	100321
						19	2-[2-[2-[2-(2-Butoxyethoxy)ethoxy]ethoxy]ethoxy]e	10	336,215	173702
						20	2-Butoxyethyl acetate	10	160,11	31225
15,374	4487	253125	19415	20275	0,021	1	9-Octadecene, (E)-	80	252,282	104181
						2	Cyclopentane, 1,1,3-trimethyl-	52	112,125	6786
						3	Cyclopentane, (2-methylpropyl)-	52	126,141	11606
						4	1-Hexene, 3-methyl-	43	98,11	3320

						#	Compound			
						5	Cyclopentane, 1,1-dimethyl-	43	98,11	3390
						6	1-Nonene	43	126,141	11502
						7	1-Hexene, 3-methyl-	38	98,11	3328
						8	3-Nonene	30	126,141	11499
						9	trans-1,3-Diethylcyclopentane	25	126,141	11579
						10	trans-1,2-Diethyl cyclopentane	25	126,141	11601
						11	1-Pentene, 2,3-dimethyl-	22	98,11	3361
						12	Cyclopentane, 1,2-dimethyl-, trans-	22	98,11	3418
						13	Cyclopentane, 1,2-dimethyl-, cis-	22	98,11	3408
						14	1-Hexene, 3-methyl-	22	98,11	3327
						15	1-Pentene, 3-methyl-	18	84,094	1477
						16	Isopropylcyclobutane	18	98,11	3336
						17	1-Pentene, 3-methyl-	14	84,094	1486
						18	Cyclohexane, 1-ethyl-2-methyl-, cis-	14	126,141	11620
						19	Cyclopentane, 1,3-dimethyl-	11	98,11	3392
						20	3-Penten-2-one	11	84,058	1403
16,638	4858	307362	18116	19145	0,026	1	Cyclopentane, (2-methylpropyl)-	46	126,141	11607
						2	Cyclohexane, 1,2,3-trimethyl-, (1.alpha.,2.alpha.,3	46	126,141	11634
						3	11-Dodecen-1-ol, 2,4,6-trimethyl-, (R,R,R)-	46	226,23	82983
						4	4-Hepten-3-one, 4-methyl-	43	126,104	11374
						5	2-Methyl-Z-7,8-epoxyhexadecane	43	254,261	105866
						6	Cyclohexene, 1,1,2,3-tetramethyl-	38	140,157	18043
						7	6-Tridecene, 7-methyl-	38	196,219	58307
						8	3-Octene, 2,2-dimethyl-	30	140,157	17993
						9	Cycloheptanone, 3-methyl-, (R)-	30	126,104	11437
						10	Cyclohexane, 1-methyl-2-propyl-	30	140,157	18037
						11	Oxacycloheptadecan-2-one	25	254,225	105680
						12	Disparlure	22	282,292	129456
						13	2-Propanamine, N,N'-methanetetraylbis-	18	126,116	11249
						14	Cyclopropane, 1,1-dimethyl-2-pentyl-	18	140,157	18056
						15	1,19-Eicosadiene	18	278,297	126193
						16	trans-1,3-Diethylcyclopentane	11	126,141	11579
						17	Disparlure	10	282,292	129459
						18	11-Hexadecen-1-ol, acetate, (Z)-	10	282,256	129367
						19	Z-7-Tetradecenoic acid	10	226,193	82767
						20	1,15-Hexadecadiene	10	222,235	79558
16,727	4884	94523	7713	8669	0,02	1	Heptadecane	64	240,282	94346
						2	Oxalic acid, 6-ethyloct-3-yl ethyl ester	59	258,183	108899
						3	3-Ethyl-3-methylheptane	53	142,172	19201
						4	Sulfurous acid, hexyl octyl ester	53	278,192	125655
						5	Sulfurous acid, hexyl pentyl ester	50	236,145	90252
						6	Oxalic acid, 6-ethyloct-3-yl heptyl ester	45	328,261	167606
						7	Hexane, 3,3-dimethyl-	45	114,141	7634
						8	Sulfurous acid, hexyl heptyl ester	43	264,176	113722
						9	Octadecane	40	254,297	105884
						10	Sulfurous acid, hexyl 2-pentyl ester	40	236,145	90254
						11	Oxalic acid, 6-ethyloct-3-yl isobutyl ester	39	286,214	132800
						12	Oxalic acid, butyl 6-ethyloct-3-yl ester	39	286,214	132773
						13	4,4-Dimethyl octane	38	142,172	19177
						14	2-(2-Bromoethyl)-3-methyl-oxirane	38	163,984	33875
						15	Hexane, 2,4,4-trimethyl-	35	128,157	12725
						16	4-Heptanone, 3-methyl-	35	128,12	12545
						17	Heptane, 3,3-dimethyl-	35	128,157	12688
						18	Sulfurous acid, 2-ethylhexyl hexyl ester	33	278,192	125660
						19	2-Hexen-1-ol, 2-ethyl-	25	128,12	12518
						20	Octane, 2-bromo-	16	192,051	54933
17,738	5181	1294283	40267	41521	0,046	1	Diethyl Phthalate	91	222,089	78786
						2	Phthalic acid, cyclobutyl ethyl ester	83	248,105	100550
						3	Diethyl Phthalate	83	222,089	78784
						4	Phthalic acid, 2-ethoxyethyl ethyl ester	78	266,115	115325
						5	Phthalic acid, ethyl tridec-2-yn-1-yl ester	78	372,23	198346
						6	Phthalic acid, monoamide, N-ethyl-N-(3-methylphe	78	311,152	153790
						7	Phthalic acid, ethyl 2-(2-nitrophenyl)ethyl ester	64	343,106	179006
						8	2-((Pent-4-enyloxy)carbonyl)benzoic acid	59	234,089	88876
						9	2-((4-Methylpentyloxy)carbonyl)benzoic acid	59	250,121	102181
						10	1,2-Benzenedicarboxylic acid, monobutyl ester	59	222,089	78839
						11	1,2-Benzenedicarboxylic acid, butyl 2-ethylhexyl e	59	334,214	172655
						12	1,2-Benzenedicarboxylic acid, mono(2-ethylhexyl)	59	278,152	125890
						13	2-Acetylbenzoic acid	59	164,047	34235
						14	2-(Pentyloxycarbonyl)benzoic acid	59	236,105	90420
						15	2-(Nonyloxycarbonyl)benzoic acid	59	292,167	137725
						16	2-(sec-Butoxycarbonyl)benzoic acid	59	222,089	78810
						17	Benzothiazole, 2-methyl-	53	149,03	23561
						18	2-(Octyloxycarbonyl)benzoic acid	53	278,152	125795
						19	2-(Heptyloxycarbonyl)benzoic acid	53	264,136	113875
						20	2H-1,3-Benzimidazol-2-one, 5-amino-1,3-dihydro-	50	149,059	23499
17,864	5218	409229	20193	21327	0,029	1	Cyclohexane, 1,1-dimethyl-	38	112,125	6750
						2	1,2-Dodecanediol	35	202,193	62617
						3	11-Dodecen-1-ol, 2,4,6-trimethyl-, (R,R,R)-	27	226,23	82983
						4	Cycloheptanone, 3-methyl-, (R)-	25	126,104	11437
						5	Silane, [(11-chloroundecyl)oxy]trimethyl-	22	278,183	125668
						6	Sulfurous acid, cyclohexylmethyl nonyl ester	22	304,207	147844
						7	3-Hexene, 2-methyl-, (Z)-	18	98,11	3379
						8	3-Hexene, 2-methyl-, (E)-	18	98,11	3378
						9	2-Hexene, 2-methyl-	14	98,11	3334
						10	3-Hexene, 3-methyl-, (E)-	14	98,11	3377
						11	2-Hexene, 2-methyl-	14	98,11	3324
						12	3-Hexene, 2-methyl-, (E)-	14	98,11	3382
						13	Methanone, dicyclopropyl-	11	110,073	5824
						14	Cyclopentanecarboxaldehyde	11	98,073	3251
						15	1-Hexadecanol	10	242,261	95980
						16	Methanone, dicyclopropyl-	10	110,073	5820
						17	1H-Imidazole, 4,5-dihydro-2-(1-methylethyl)-	10	112,1	6330
						18	2-(Pentyloxycarbonyl)benzoic acid	10	236,105	90420
						19	Cyclohexane, 1-ethyl-2-methyl-, trans-	10	126,141	11624
						20	Methanone, dicyclopropyl-	10	110,073	5822
18,011	5261	1415666	70064	71057	0,031	1	Diethyl Phthalate	93	222,089	78783
						2	Phthalic, 5-methylhex-2-yl ethyl ester	78	292,167	137799
						3	Phthalic acid, 8-chlorooctyl ethyl ester	78	340,144	176546
						4	Phthalic acid, ethyl pentadecyl ester	72	404,293	213828
						5	Phthalic acid, 2-chloropropyl ethyl ester	72	270,066	118676
						6	Phthalic, cyclobutyl ethyl ester	72	248,105	100550
						7	Phthalic acid, ethyl 2-pentyl ester	72	264,136	113877
						8	Phthalic, monoamide, N-ethyl-N-(3-methylphe	72	311,152	153790
						9	Phthalic acid, ethyl 4-methylhept-3-yl ester	72	306,183	149648
						10	Phthalic acid, cyclohexylmethyl ethyl ester	64	290,152	136195

						#	Compound			
						11	Diethyl Phthalate	64	222,089	78785
						12	Phthalic acid, ethyl pentyl ester	64	264,136	113876
						13	Diethyl Phthalate	62	222,089	78782
						14	Diethyl Phthalate	60	222,089	78784
						15	Diethyl Phthalate	60	222,089	78786
						16	1,2-Benzenedicarboxylic acid, dipropyl ester	59	250,121	102186
						17	Phthalic acid, 4,4-dimethylpent-2-yl propyl ester	59	306,183	149702
						18	1,2-Benzenedicarboxylic acid, dipropyl ester	59	250,121	102184
						19	2-((4-Methylpentyloxy)carbonyl)benzoic acid	59	250,121	102181
						20	1,2-Benzenedicarboxylic acid, monobutyl ester	58	222,089	78837
19,231	5619	165352	9101	9913	0,028	1	Cyclohexane, 1,1-dimethyl-	50	112,125	6749
						2	Cycloheptane, methyl-	50	112,125	6689
						3	1,19-Eicosadiene	38	278,297	126193
						4	4-Ethyl-2-hydroxycyclopent-2-en-1-one	38	126,068	11197
						5	2-Pentene, 3-ethyl-4,4-dimethyl-	38	126,141	11611
						6	2,5-Dimethyl-1-pyrroline	35	97,089	2987
						7	Cyclopentane, 2-isopropyl-1,3-dimethyl-	35	140,157	18060
						8	Cyclohexane, 1,2-dimethyl- (cis/trans)	32	112,125	6828
						9	1-Hexadecanol	30	242,261	95980
						10	1-Tridecene	27	182,203	47267
						11	Cyclotetradecane	27	196,219	58279
						12	Oxalic acid, cyclobutyl hexadecyl ester	25	368,293	195550
						13	Cyclopentane, 1-ethyl-3-methyl-, trans-	22	112,125	6831
						14	Cyclopentane, 1-ethyl-3-methyl-	22	112,125	6794
						15	Cyclohexane, 1-ethyl-4-methyl-, cis-	22	126,141	11622
						16	Cyclopentane, 1-ethyl-3-methyl-, cis-	22	112,125	6825
						17	(S)-(+)-5-Methyl-1-heptanol	22	130,136	13745
						18	Oxalic acid, cyclobutyl pentadecyl ester	16	354,277	186678
						19	Oxalic acid, cyclobutyl heptadecyl ester	16	382,308	203491
						20	Oxalic acid, cyclobutyl octadecyl ester	16	396,324	210293
21,574	6307	246786	7985	8200	0,051	1	1,1,1,5,7,7,7-Heptamethyl-3,3-bis(trimethylsiloxy)te	37	444,149	225661
						2	Morphinan, 7,8-didehydro-4,5-epoxy-17-methyl-3,(	27	429,216	221936
						3	7-Chloro-10-ethyl-1-[[2-[(2-hydroxyethyl)amino]ethy	25	503,159	235615
						4	Morphinan, 7,8-didehydro-4,5-epoxy-17-methyl-3,(	22	429,216	221935
						5	2-[4-Acetamidophenylsulfonyl]-1,4-naphthoquinon	16	355,051	187154
						6	3-(4-N,N-Dimethylaminophenyl)propenoic acid, 2-(	10	355,155	187147
						7	Heptasiloxane, 1,1,3,3,5,5,7,7,9,9,11,11,13-te	10	504,152	235668
						8	Codeine-propionyl	9	355,178	187332
						9	Glaucine	9	355,178	187330
						10	3-Pyrroline-3-carboxylic acid, 2-(4-bromophenyl)-4-	9	429,058	221893
						11	3-Amino-2-phenazinol ditms	9	355,154	187185
						12	8-Furan-2-yl-3,3-dimethyl-6-morpholin-4-yl-3,4-dihy	9	355,135	187222
						13	Pyrazolo[3,4-b]pyridin-3(2H)-one, 4-trifluoromethyl-	9	355,093	187194
						14	Norcodeine di-TMS derivative	9	429,216	221934
						15	5-Hydroxy-1-(3-isopropoxy-propyl)-2-methyl-1H-ber	9	355,178	187363
						16	1,3,5,7,9,11-Hexaethylbicyclo[5.5.1]hexasiloxane	9	458,092	228686
						17	Pregn-5-en-20-one, 3-[(tripropylsilyl)oxy]-, (3.beta.)	9	472,374	231435
						18	Benzoic acid, 2,4-bis[(trimethylsilyl)oxy]-, trimethyls	9	370,145	196470
						19	3.beta.-Acetoxy-16-isothiocyanatopregn-5-en-20-c	9	415,218	217601
						20	1,3,5,7,9-Pentaethyl-1,9-dibutoxypentasiloxane	9	500,23	235210
23,21	6787	240529	9609	9693	0,039	1	Tetradecanenitrile	23	209,214	68717
						2	1,3-Cyclohexanedione, 2-(2-propenyl)-	18	152,084	26038
						3	Thiazolidin-4-one, 5-(2-furfurylidene)-2-imino-	16	194,015	56855
						4	Diethyl selenide	9	137,995	17073
						5	Pyridine, 2-acetamido-6-hydroxy-	9	152,059	25726
						6	2H-Pyran-2-one, 3,4,5,6-tetramethyl-	9	152,084	26034
						7	Aziridine, 1-(2-methyl-1-propenyl)-	9	97,089	3004
						8	Phenol, 3-ethoxy-	9	138,068	17275
						9	3-Cyclohexen-1-one, 2-isopropyl-5-methyl-	9	152,12	25239
						10	Phenol, 3-ethoxy-	9	138,068	17276
						11	1,8(2H,5H)-Naphthalenedione, hexahydro-8a-meth	9	180,115	45516
						12	2-Cyclohexen-1-one, 3,4,4-trimethyl-	9	138,104	17605
						13	Phenol, 4-ethoxy-	9	138,068	17277
						14	2-Cyclohexen-1-one, 4,4-dimethyl-	9	124,089	10553
						15	2-Cyclohexen-1-one, 3-methyl-6-(1-methylethyl)-	9	152,12	25293
						16	2-Cyclohexen-1-one, 4,4,6-trimethyl-	9	138,104	17604
						17	2-Pyrrolidinone, 3-[(1,4,5,6-tetrahydro-3-pyridinyl)c	9	194,106	55845
						18	Phenol, 2-ethoxy-	9	138,068	17274
						19	Phenol, 4-ethoxy-	9	138,068	17279
						20	3,4,5,6,7,8-Hexahydro-2H-chromene	9	138,104	17579
24,327	7115	7180427	177834	178437	0,057	1	n-Hexadecanoic acid	94	256,24	107549
						2	Tridecanoic acid	93	214,193	72647
						3	Tridecanoic acid	86	214,193	72648
						4	n-Hexadecanoic acid	72	256,24	107548
						5	Tridecanoic acid	70	214,193	72646
						6	Pentadecanoic acid	59	242,225	95851
						7	Isopropyl palmitate	53	298,287	143137
						8	Dodecanoic acid	50	200,178	61121
						9	Dodecanoic acid	50	200,178	61122
						10	Tetradecanoic acid	50	228,209	84455
						11	n-Decanoic acid	47	172,146	39474
						12	n-Hexadecanoic acid	41	256,24	107547
						13	Nonanoic acid	35	158,131	30180
						14	Pentadecanoic acid	35	242,225	95855
						15	Tridecanoic acid	25	214,193	72643
						16	n-Decyl .alpha.-d-2-deoxyglucoside	14	304,225	147845
						17	3,7-Dimethyl-8-oxo-1,5-dioxa-spiro[5.5]undecane-:	11	256,131	107006
						18	Dodecanoic acid, trimethylsilyl ester	11	272,217	120973
						19	Isotridecyl alcohol, trimethylsilyl derivative	10	272,254	121171
						20	Chlorpropham	10	213,056	71700
25,4	7430	340587	15141	16318	0,035	1	Bicyclo[4.1.0]heptane, 7-butyl-	64	152,157	25441
						2	cis-11-Tetradecen-1-ol	64	212,214	71325
						3	11-Tetradecen-1-ol, acetate, (Z)-	58	254,225	105724
						4	2-Cyclopenten-1-one, 2-pentyl-	43	152,12	25171
						5	2-Cyclopenten-1-one, 2-pentyl-	38	152,12	25166
						6	Cyclopentane, 1,2-dimethyl-3-(1-methylethenyl)-	38	138,141	17001
						7	trans-Decalin, 2-methyl-	35	152,157	25429
						8	1,1'-Bicyclopentyl	30	138,141	16868
						9	Spiro[3.5]nonan-1-one, 5-methyl-, trans-	30	152,12	25235
						10	Cyclodecene, 1-methyl-	30	152,157	25420
						11	Naphthalene, decahydro-, cis-	25	138,141	16913
						12	o-Menth-8-ene	25	138,141	16856
						13	1H-Imidazole-4-propanamine	22	125,095	10771
						14	Bicyclo[3.1.0]hexan-2-one, 5-(1-methylethyl)-	22	138,104	17639
						15	cis-Decalin, 2-syn-methyl-	22	152,157	25433
						16	Hexahydro-1-oxa-cyclopropa[d]inden-2-one	18	152,084	26062

						#	Compound			
						17	Cyclohexene, 1-pentyl-	18	152,157	25425
						18	Cyclohexene, 3,5,5-trimethyl-	18	124,125	10684
						19	Bicyclo[2.2.1]heptane, 2,2,3-trimethyl-, endo-	11	138,141	16996
						20	Spiro[4.5]decan-2-one	11	152,12	25118
26,708	7814	654890	26380	28072	0,037	1	Octadecanenitrile	91	265,277	114922
						2	Heptadecanenitrile	83	251,261	103254
						3	Tetradecanenitrile	50	209,214	68714
						4	Cyclohexane, 1-(cyclohexylmethyl)-4-methyl-, cis-	38	194,203	56516
						5	1,1'-Bicyclohexyl, 2-methyl-, trans-	25	180,188	45737
						6	Cyclohexane, 1-methyl-4-(1-methylethyl)-, cis-	18	140,157	18076
						7	1-Methyl-4-(1-methylethyl)-cyclohexane	18	140,157	18058
						8	m-Menthane, (1S,3S)-(+)-	18	140,157	18004
						9	m-Menthane, (1S,3R)-(+)-	18	140,157	18003
						10	Cyclohexane, 1-methyl-4-(1-methylethyl)-, cis-	18	140,157	18075
						11	Cyclohexane, 1-methyl-4-(1-methylethyl)-, trans-	18	140,157	18078
						12	1H-Imidazol, 1-methyl-2-amino-	18	97,064	2953
						13	1-Methyl-4-(1-methylethyl)-cyclohexane	18	140,157	18059
						14	Cyclohexane, 1-methyl-4-(1-methylethyl)-, trans-	14	140,157	18080
						15	Cyclohexane, 1-ethyl-4-methyl-, cis-	11	126,141	11622
						16	2-Aziridinone, 1-tert-butyl-3-(1-methylcyclohexyl)-	11	209,178	68666
						17	Cyclohexanone, 3-butyl-	11	154,136	26707
						18	3,5-Dimethyl-3-heptene	11	126,141	11547
						19	4-Octen-3-one	11	126,104	11329
						20	Cyclohexane, 1-ethyl-4-methyl-, cis-	11	126,141	11621
27,448	8031	6429702	167962	172909	0,053	1	Octadecanoic acid	93	284,272	131260
						2	Octadecanoic acid	93	284,272	131261
						3	Octadecanoic acid	92	284,272	131259
						4	Octadecanoic acid	91	284,272	131258
						5	Pentadecanoic acid	89	242,225	95855
						6	Octadecanoic acid	89	284,272	131262
						7	Octadecanoic acid, 2-(2-hydroxyethoxy)ethyl ester	80	372,324	198268
						8	Pentadecanoic acid	70	242,225	95854
						9	n-Hexadecanoic acid	64	256,24	107547
						10	n-Hexadecanoic acid	60	256,24	107548
						11	Tetradecanoic acid	58	228,209	84453
						12	Tetradecanoic acid	58	228,209	84452
						13	Tridecanoic acid	49	214,193	72647
						14	Tridecanoic acid	49	214,193	72646
						15	Undecanoic acid	43	186,162	50052
						16	n-Decanoic acid	43	172,146	39472
						17	n-Decanoic acid	38	172,146	39471
						18	n-Decanoic acid	38	172,146	39470
						19	n-Decanoic acid	38	172,146	39473
						20	Nonanoic acid	35	158,131	30180
27,724	8112	1532169	40424	46513	0,053	1	Hexadecanamide	83	255,256	106565
						2	Tetradecanamide	80	227,225	83608
						3	Tetradecanamide	72	227,225	83609
						4	9-Octadecenamide, (Z)-	72	281,272	128443
						5	Decanamide-	59	171,162	38977
						6	Octadecanamide	59	283,288	130204
						7	Dodecanamide	53	199,194	60440
						8	9-Octadecenamide, (Z)-	50	281,272	128445
						9	Nonadecanamide	45	297,303	142051
						10	Octadecanamide	45	283,288	130205
						11	Silane, hexyl-	43	116,102	8287
						12	Octanamide	42	143,131	20317
						13	Benzeneethanamine, 2-fluoro-.beta.,3,4-trihydroxy	42	229,111	85011
						14	Tetradecanamide	38	227,225	83610
						15	Hexadecanamide	35	255,256	106564
						16	2-Hydroxy-2-methylhept-6-en-3-one	25	142,099	19767
						17	Undecanamide, 11-bromo-	22	263,088	112862
						18	Oxetane, 2,2,3-trimethyl-	16	100,089	3905
						19	o-Menthan-8-ol	16	156,151	28238
						20	Pentadecanamide, 15-bromo-	16	319,151	160272
30,923	9051	606125	18665	19532	0,049	1	Tetradecanamide	72	227,225	83608
						2	Dodecanamide	59	199,194	60439
						3	Tetradecanamide	56	227,225	83610
						4	Decanamide-	56	171,162	38977
						5	Tetradecanamide	53	227,225	83609
						6	9-Octadecenamide, (Z)-	50	281,272	128445
						7	Pentadecanamide, 15-bromo-	45	319,151	160272
						8	Benzeneethanamine, 2-fluoro-.beta.,3,4-trihydroxy	39	229,111	85011
						9	Dodecanamide	38	199,194	60440
						10	7-Nonenamide	38	155,131	28131
						11	Propanol, [(butoxymethylethoxy)methylethoxy]-	37	248,199	100493
						12	Nonanamide	36	157,147	29478
						13	4-Cyclohexylbutyramide	33	169,147	37471
						14	Hexadecanamide	32	255,256	106565
						15	Cyclohexanemethanol, .alpha.,.alpha.,4-trimethyl-	32	156,151	28362
						16	Silane, octyl-	25	144,133	21082
						17	2,3-Dimethyl-4-penten-2-ol	23	114,104	7567
						18	3,5-Dihydroxycyclohexanamine	10	131,095	13899
						19	Octanoic acid, 2-ethoxyethyl ester	10	216,173	74069
						20	3-Piperidinamine, 1-ethyl-	10	128,131	12367

RT (min)	Scan number (#)	Area (Ab*s)	Baseline Heigth (Ab	Absolute Heigth (Ab	Peak Width 50% (min	Hit Number	Hit Name	Quality	Mol Weight	Entry Number Library
2,626	745	1152600	42736	43388	0,04	1	Nitrous oxide	5	44,001	84
						2	Nitrous oxide	5	44,001	83
						3	Carbon dioxide	4	43,99	81
						4	Ethylene oxide	3	44,026	75
						5	Carbon dioxide	3	43,99	82
						6	Ethylene oxide	3	44,026	73
						7	Ethyne, fluoro-	2	44,006	77
						8	Ethyne, fluoro-	2	44,006	76
						9	Acetaldehyde	2	44,026	72
						10	Acetaldehyde	2	44,026	71
						11	Ethane	2	30,047	21
						12	Ethane	2	30,047	19
						13	Ethylene oxide	2	44,026	74
						14	Formaldehyde	2	30,011	24
						15	Formaldehyde	2	30,011	23
						16	Formaldehyde	2	30,011	22
						17	Ethane	2	30,047	20
						18	1,2-Propanediamine	2	74,084	791
						19	Carbamic acid, monoammonium salt	2	78,043	1029
						20	Propane	1	44,063	80
2,742	779	338484	7549	8824	0,064	1	Acetaldehyde	7	44,026	72
						2	Propane	7	44,063	79
						3	Ethylene oxide	5	44,026	75
						4	Ethylene oxide	5	44,026	74
						5	Propane	4	44,063	80
						6	Propane	4	44,063	78
						7	Acetaldehyde	4	44,026	71
						8	Dimethylamine	4	45,058	87
						9	Ethylene oxide	4	44,026	73
						10	1-Propanol, 2-amino-, (S)-	2	75,068	902
						11	(R)-(-)-2-Amino-1-propanol	2	75,068	900
						12	1-Propanol, 2-amino-, (.+/-.)-	2	75,068	906
						13	1-Propanol, 2-amino-, (.+/-.)-	2	75,068	904
						14	2-Propanamine	2	59,073	250
						15	Cyclopropyl carbinol	2	72,058	693
						16	1-Propanol, 2-amino-, (S)-	2	75,068	901
						17	Cyclopropyl carbinol	2	72,058	692
						18	Oxiranemethanol, (S)-	2	74,037	815
						19	Oxiranemethanol, (R)-	2	74,037	814
						20	Nitrous oxide	2	44,001	84
14,992	4375	101031	7071	7328	0,034	1	Ethanol, 2-(2-butoxyethoxy)-, acetate	72	204,136	63715
						2	Ethanol, 2-(2-butoxyethoxy)-, acetate	47	204,136	63714
						3	Ethanol, 2-(2-butoxyethoxy)-, acetate	40	204,136	63716
						4	1,3-Dioxane, 2-methyl-	28	102,068	4265
						5	4-Isopropoxy-2-butanone	23	130,099	13426
						6	Morpholine	9	87,068	1863
						7	2-Propanone, O-methyloxime	9	87,068	1895
						8	Morpholine	9	87,068	1865
						9	Acetamide, N-ethyl-	9	87,068	1881
						10	Acetamide, N-acetyl-N-methyl-	9	115,063	7757
						11	Thiocyanic acid, ethyl ester	9	87,014	1855
						12	Thiocyanic acid, ethyl ester	9	87,014	1856
						13	Acetamide, N-acetyl-N-methyl-	9	115,063	7755
						14	Thiocyanic acid, ethyl ester	9	87,014	1853
						15	cis-1-Nitro-1-propene	9	87,032	1846
						16	1,2-Butanediol, 3,3-dimethyl-	9	118,099	8859
						17	Dibutoxymethane	9	160,146	31402
						18	Decane, 2,5,6-trimethyl-	9	184,219	48889
						19	2-Butanol, 3-methyl-, acetate	9	130,099	13489
						20	1,2-Butanediol, 3,3-dimethyl-	9	118,099	8856
24,283	7102	1348700	41978	42915	0,048	1	n-Hexadecanoic acid	98	256,24	107549
						2	Pentadecanoic acid	74	242,225	95851
						3	Tetradecanoic acid	72	228,209	84452
						4	Tridecanoic acid	59	214,193	72648
						5	Tetradecanoic acid	59	228,209	84455
						6	Tridecanoic acid	59	214,193	72643
						7	Tetradecanoic acid	58	228,209	84453
						8	Pentadecanoic acid	50	242,225	95855
						9	Tridecanoic acid	50	214,193	72646
						10	n-Decanoic acid	47	172,146	39474
						11	n-Decanoic acid	43	172,146	39473
						12	Undecanoic acid	40	186,162	50051
						13	Ethanone, 1-(4,5-dihydro-2-thiazolyl)-	38	129,025	12836
						14	Undecanoic acid	38	186,162	50052
						15	n-Decanoic acid	38	172,146	39472
						16	Ethanone, 1-(4,5-dihydro-2-thiazolyl)-	38	129,025	12837
						17	Nonanoic acid	35	158,131	30180
						18	n-Hexadecanoic acid	27	256,24	107549
						19	Dodecanoic acid	14	200,178	61117
						20	n-PROPYL NONYL ETHER	11	186,198	50326
27,427	8025	817027	25605	28122	0,046	1	Octadecanoic acid	95	284,272	131261
						2	n-Hexadecanoic acid	68	256,24	107549
						3	Tetradecanoic acid	64	228,209	84452
						4	Tetradecanoic acid	64	228,209	84455
						5	Tetradecanoic acid	53	228,209	84453
						6	Pentadecanoic acid	50	242,225	95854
						7	n-Decanoic acid	47	172,146	39473
						8	n-Decanoic acid	47	172,146	39474
						9	n-Hexadecanoic acid	43	256,24	107547
						10	n-Decanoic acid	43	172,146	39470
						11	Decanoic acid, silver(1+) salt	38	278,044	125286
						12	n-Decanoic acid	38	172,146	39472
						13	Ethanone, 1-(4,5-dihydro-2-thiazolyl)-	35	129,025	12837
						14	Nonanoic acid	35	158,131	30178
						15	Lactose	27	342,116	177854
						16	d-Glucohexodialdose	22	178,048	44210
						17	Cyclohexanecarboxylic acid, tridecyl e	10	310,287	153155
						18	Oxalic acid, propyl tetradecyl ester	10	328,261	167553
						19	Cyclohexanecarboxylic acid, octyl este	10	240,209	94165
						20	Oxalic acid, dodecyl propyl ester	10	300,23	144569